Recent Advances in Random Media Scattering Towards Physical Model and AI Driven Microwave Data Analysis

Shurun Tan 谭述润

Zhejiang University/University of Illinois Urbana-Champaign Institute (ZJUI), Zhejiang University, Haining, China

浙江大学伊利诺伊大学厄巴纳香槟校区联合学院，浙江大学

June 11, 2025

International Campus of Zhejiang University

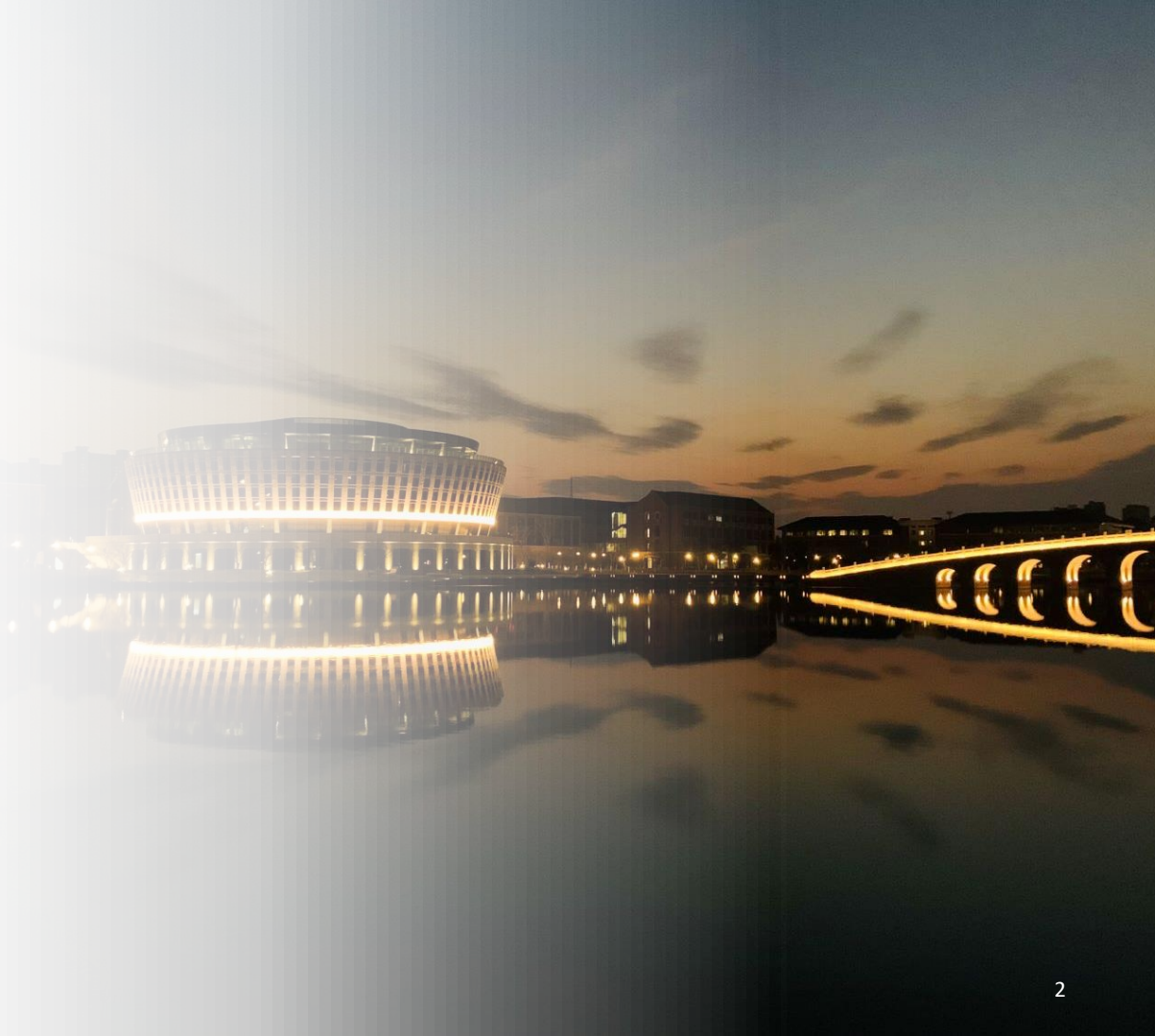

Microwave Remote Sensing of Environment Helps Address Key Challenges of Our Society

Images courtesy of iSWGR and SMAP

Ongoing Environmental Remote Sensing Satellite Missions

Name of the mission	Brief Description	Country, Region, Organization
LandSat 1to 8	The world's longest continuously acquired collection of space-based moderate-resolution land remote sensing data	USGS, NASA
Sentinel-1 to 6	Constellation of ~12 Satellites, the Copernicus Program, radar and multi-spectral imaging for land, ocean, and atmospheric monitoring	ESA
SMAP	L-band Active and Passive Mission for Global Soil Moisture Observation	NASA
CYGNSS	L-band, Signal of Opportunity, Cyclone Global Navigation Satellite System, for hurricane forecasting	NASA
NISAR	L- (US) and S- (Indian) band, InSAR, optimized for studying hazards and global environmental change	NASA/ ISRO
GCOM	Global Change Observation System Mission, for long-term observation of Earth environmental changes. GCOM-W1 carries AMSR-2 Radiometer, GCOM-C1 carries SGLI Imager.	JAXA
ALOS	The Advanced Land Observing Satellite for cartography, regional observation, disaster monitoring, and resource surveying. Instruments include PRISM, AVNIR-2 and PALSAR.	JAXA
CryoSat	ESA's Earth Explorer Mission dedicated to measuring the thickness of polar sea ice and monitoring changes in the ice sheets that blanket Greenland and Antarctica. Main payload is a Synthetic Aperture Interferometric Radar Altimeter (SIRAL).	ESA

Ongoing Environmental Remote Sensing Satellite Missions

Name of the mission	Brief Description	Country, Region, Organization
TerraSAR-X and TanDEM-X	X-band, TerraSAR-X and TanDEM-X are German radar satellites from DLR (the German Aerospace Center). TerraSAR-X launched in 2007 and was joined by TanDEM-X in 2010. Both satellites remain operational. The twin satellites feature a unique geometric accuracy that is unmatched by any other spaceborne sensor.	German, ESA
RADARSAT-Constellation	C-band, The RADARSAT Constellation Mission (RCM) is a three-satellite constellation, developed and operated by CSA (Canadian Space Agency). Launched on the 12th of June 2019 with an expected lifespan of 7 years.	Canada, CSA
TSMM	dual frequency (13.5/17.25 GHz) Ku-band, The Terrestrial Snow Mass Mission ('TSMM') will provide moderate resolution (500m) SAR measurements across all northern hemisphere snow covered areas every 7 days.	Canada, CSA, ECCC
CIMR	The CIMR mission would carry a wide-swath conically-scanning multi-frequency microwave radiometer to provide observations of sea-surface temperature, sea-ice concentration and sea-surface salinity. Uniquely, it would also observe a wide range of other sea-ice parameters.	ESA
Biomass	P-band synthetic aperture radar (SAR) launched in 2025. It will provide crucial data for monitoring the carbon cycle and climate change by delivering detailed 3D maps of the world's forests.	ESA
CryoRad	The mission would comprise a 0.4-2 GHz nadir-looking radiometer installed on a polar-orbit satellite, with a focus on sea ice, snow, and ice sheet properties, contributing to better understanding of cryosphere changes.	ESA Earth Explorer candidate

China Ongoing Environmental Remote Sensing Satellites

Name of the mission	Brief Description	Launch Time
高分5号02星	Equipped with hyperspectral equipment to dynamically monitor the air pollution situation in China	2021.9
陆探1号	L-band fully polarized InSAR; The total area of the SAR antenna carried on this satellite exceeds 33 square meters, making it the largest SAR satellite in orbit in China.	2022.1
海洋盐度探测卫星	Loading synthetic aperture radiometers (L-,C-,K- band) and L-band scatterometer to obtain physical parameters such as sea surface roughness, and sea surface temperature of the ocean surface	2024
陆地水资源探测卫星	L-band active and passive microwave imager; Used for water resource monitoring and management, drought monitoring, and soil and water conservation monitoring	/

Two Fundamental Problems in Microwave Remote Sensing

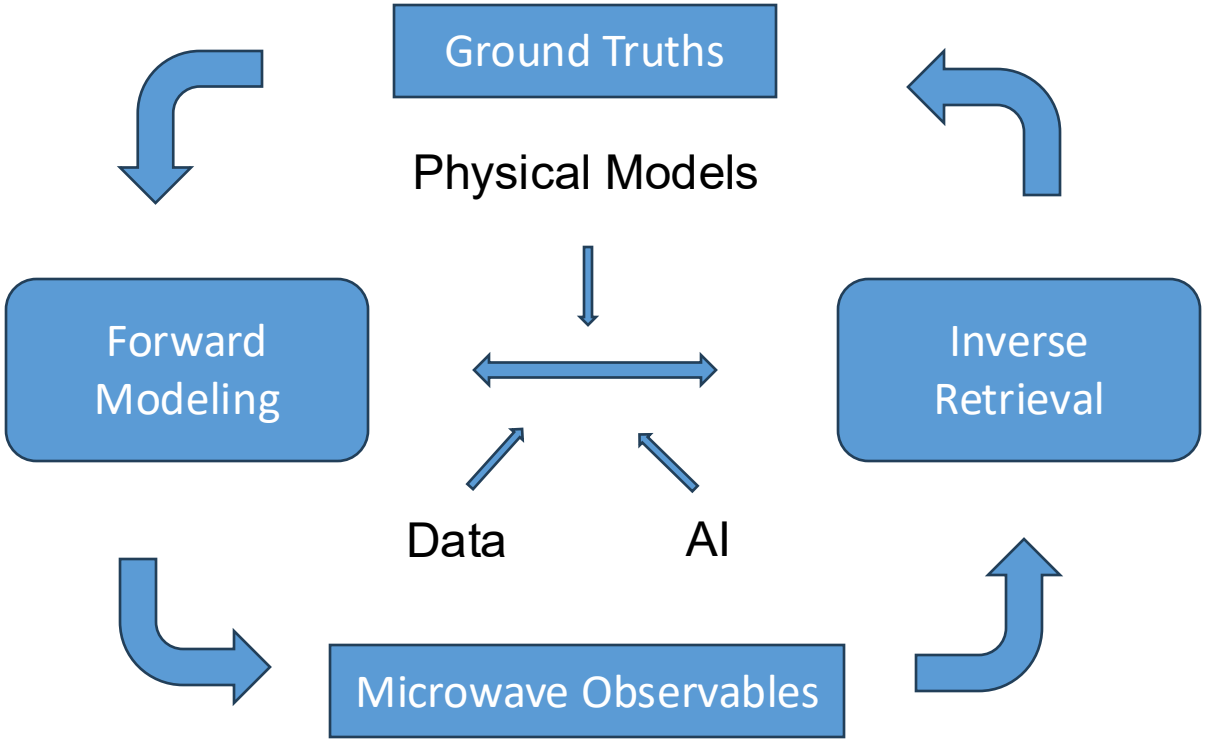

Covered in today's discussion

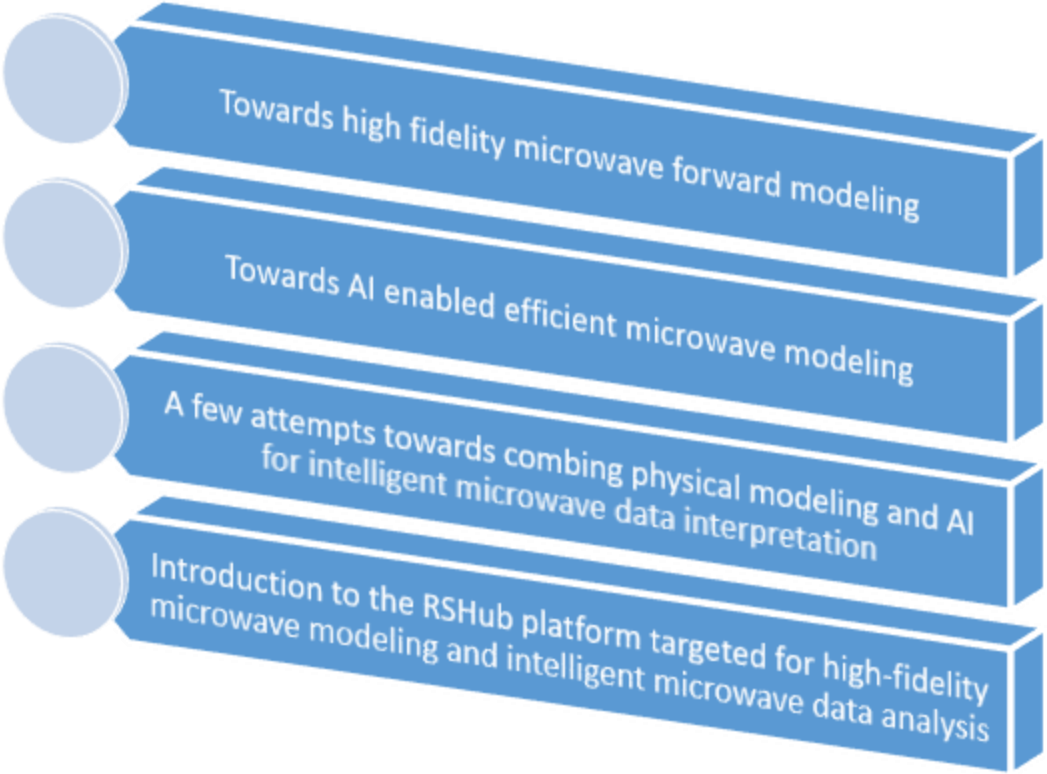

Fundamentals for Microwave Remote Sensing: Electromagnetic Wave Scattering of Random Media

Bare Soil

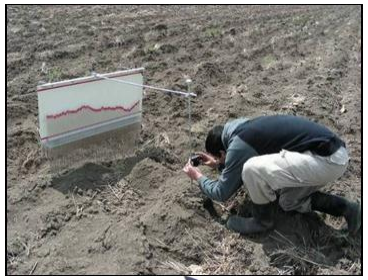

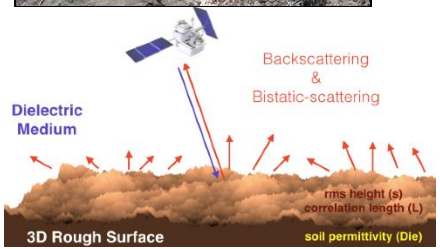

Random Rough Surfaces

Vegetation

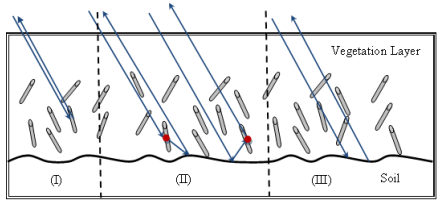

Sparse Random Volumes

Snowpack

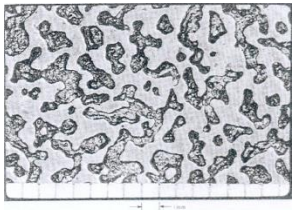

Dense Random Volumes

Scattering from Rough Surface & Bare Soil Remote Sensing: Vertical Heterogeneity

Rough surface representation

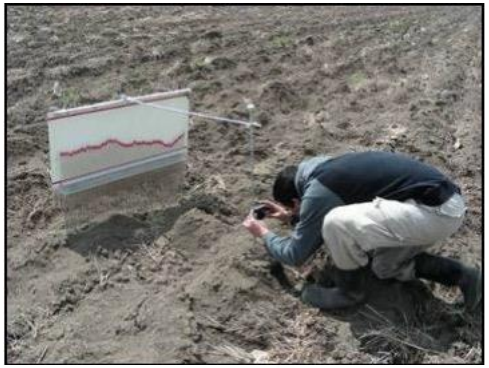

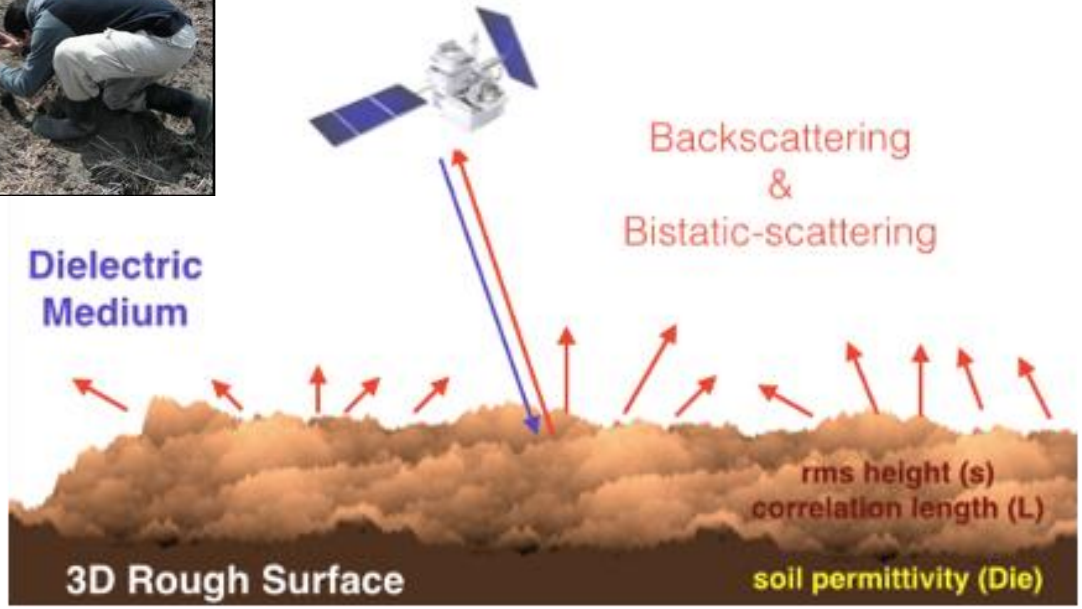

EM modeling of rough surface scattering

Maxwell's Eqn

$$\nabla \times \bar{E} = i\omega \bar{B}$$
$$\nabla \times \bar{H} = \bar{J} - i\omega \bar{D}$$
$$\nabla \cdot \bar{D} = \rho$$
$$\nabla \cdot \bar{B} = 0$$

Numerical Solutions

Based on Differential Form:
- FEM: HFSS, **Comsol**
- FDTD: CST

Based on Integral Equation (IE)
- SIE: NMM3D-SIE, Feko
- VIE: **Discrete Dipole Approximation (DDA)**

……

Constitutive Relations

$$\bar{D} = \varepsilon(\bar{r})\bar{E}$$
$$\bar{B} = \mu \bar{H}$$

Analytical Approximations

Kirchhoff approximation (KA)

Small Perturbation Method(SPM)

Advanced IEM (AIEM)

……

Geometry and material complexities are expressed in $\varepsilon(\bar{r})$.

NMM3D-SIE

Tapered incident wave in the wave vector domain

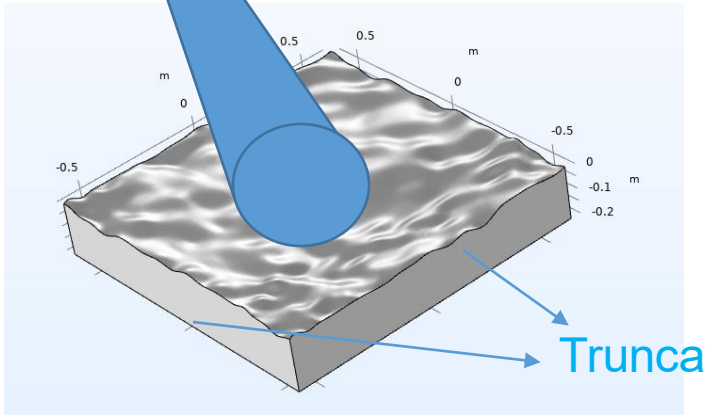

Only surface segmentation is required

Only applicable for homogenenous rough soil.

NMM3D-DDA

Plane wave excitation with periodic boundary conditions to truncate the computing domain

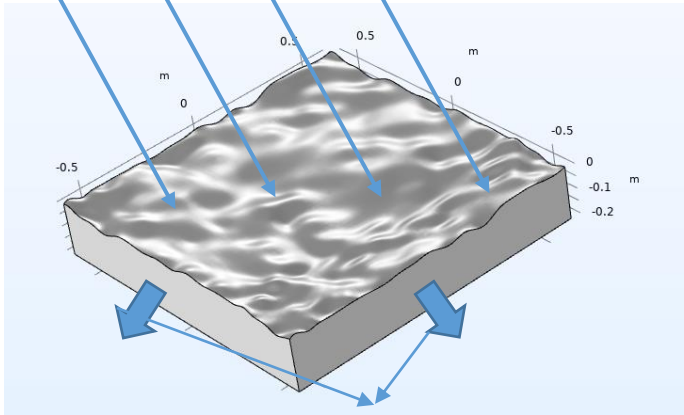

Volume segmentation is required

Applicable to inhomogeneous soils with arbitrary texture distributions and layering.

NMM3D-SIE on a homogeneous soil/air interface

SIE in PMCHW form

$$\overline{E}^{\text{inc}}(\overline{r})_{\tan} = (L_1 + L_2)\overline{J}(\overline{r})_{\tan} - (K_1 + K_2)\overline{M}(\overline{r})_{\tan}$$

$$\overline{H}^{\text{inc}}(\overline{r})_{\tan} = (K_1 + K_2)\overline{J}(\overline{r})_{\tan} + \left(\frac{1}{\eta_1^2}L_1 + \frac{1}{\eta_2^2}L_2\right)\overline{M}(\overline{r})_{\tan}$$

The operators:

$$L_{1,2}\overline{X}(\overline{r}) = \int_S ds' \left[-i\omega\mu_{1,2}\overline{X}(\overline{r}') + \frac{-i}{\omega\varepsilon_{1,2}}\nabla\nabla'\cdot\overline{X}(\overline{r}') \right] G_{1,2}(\overline{r},\overline{r}')$$

$$K_{1,2}\overline{X}(\overline{r}) = \int_S ds' \overline{X}(\overline{r}') \times \nabla G_{1,2}(\overline{r},\overline{r}')$$

- Surface size: $16\lambda \times 16\lambda$; $64\lambda \times 64\lambda$; or larger
- Shorter wavelength in the soil region

Large number of unknowns

Acceleration Algorithms

SMCG; UV; PBTG

NMM3D-VIE-DDA Approach for Layered Rough Surface Scattering Characterization

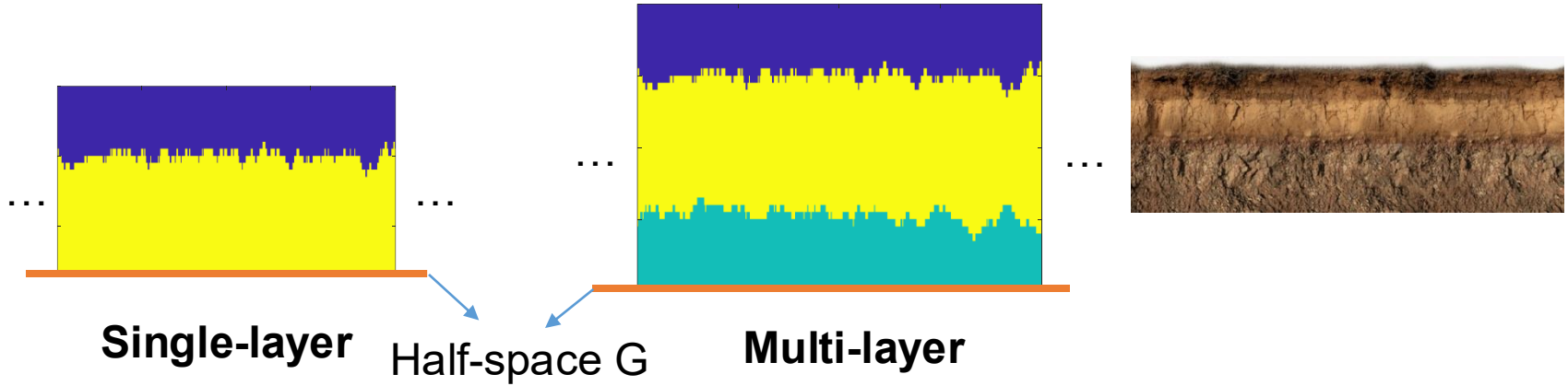

VIE-DDA:

$$\bar{p}_i = \bar{\bar{\alpha}}_i \left[\bar{E}_{inc}(\bar{r}_i) + \frac{k^2}{\varepsilon} \sum_{j \neq i} \bar{\bar{G}}_P^0 (\bar{r}_i, \bar{r}_j; \bar{k}_{i\rho}) \bar{p}_j + \frac{k^2}{\varepsilon} \sum_j \bar{\bar{G}}_P^R (\bar{r}_i, \bar{r}_j; \bar{k}_{i\rho}) \bar{p}_j \right]$$

- horizontal: truncated by periodic boundary condition, ~ $10\lambda \times 10\lambda$
- bottom layer: represented by the half-space Green's function
- need to discretize the inhomogeneous soil volume

Single-Layer Validation – Backscattering Coefficient and Emissivity

- **Soil parameters :**

Case	Site	RMSH	CL	m_v	ϵ_r	
1-1	XYP	1.30 cm	18 cm	0.129	6.69+j0.63	Wet
1-2				0.015	2.78+j0.14	Dry

Case 1-1 Wet soil

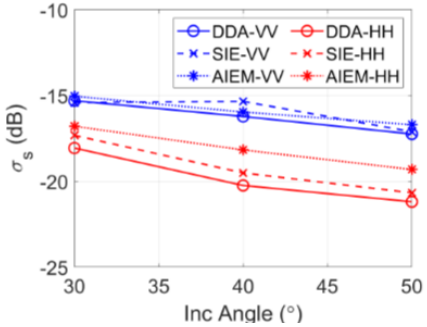

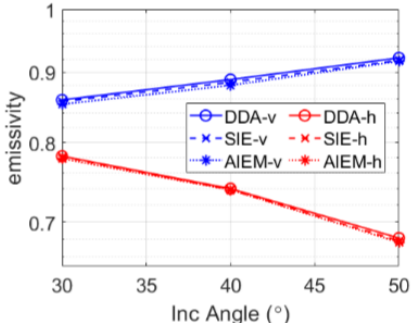

Case 1-2 Dry soil

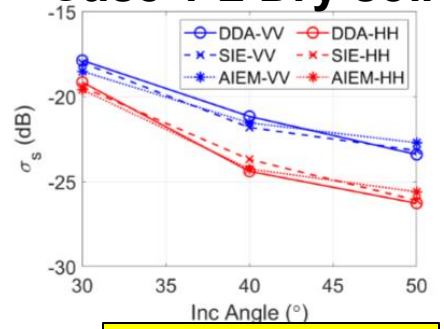

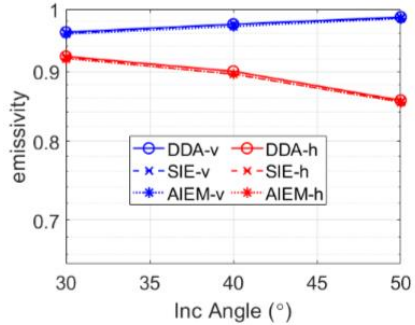

Backscattering coefficient

Emissivity

Three Methods:

Full-wave – NMM3D-VIE; NMM3D-SIE

Approximate – AIEM

- Overall consistent.
- For backscattering, higher consistency is observed for dry soils.
- The proposed VIE-DDA method agrees well with SIE under various angles, polarizations, and soil moisture levels.

Single-Layer Validation – Bistatic Scattering Coefficient for Cross-Polarization in the Incidence Plane

Case	Site	RMSH	CL	m_v	ϵ_r
1-1	XYP	1.30 cm	18 cm	0.129	6.69+j0.63
1-2				0.015	2.78+j0.14

Wet
Dry

Incident angle=40 °

Case 1-1
Wet soil

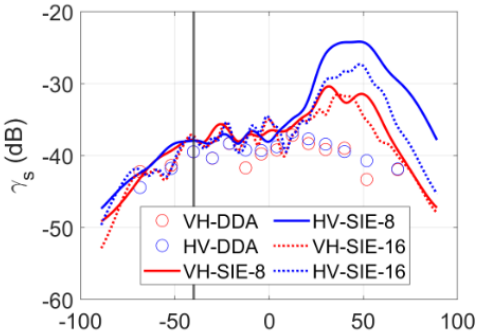

Case 1-2
Dry soil

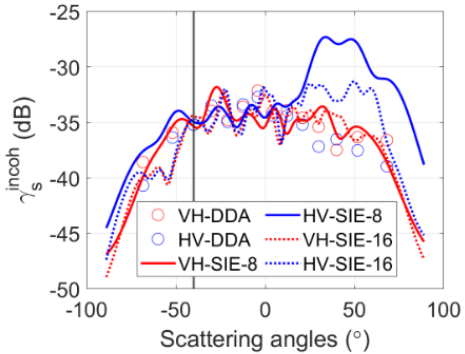

- SIE requires larger surface truncation to ensure convergence in the specular direction.
- The VIE-DDA method is shown to be accurate and effective.

Single-Layer Validation – Bistatic Scattering Coefficient in the Upper Half-Space

Case	Site	RMSH	CL	m_v	ϵ_r
1-1	XYP	1.30 cm	18 cm	0.129	6.69+j0.63
1-2				0.015	2.78+j0.14

Wet

Incident angle=40 °

VIE

SIE

AIEM

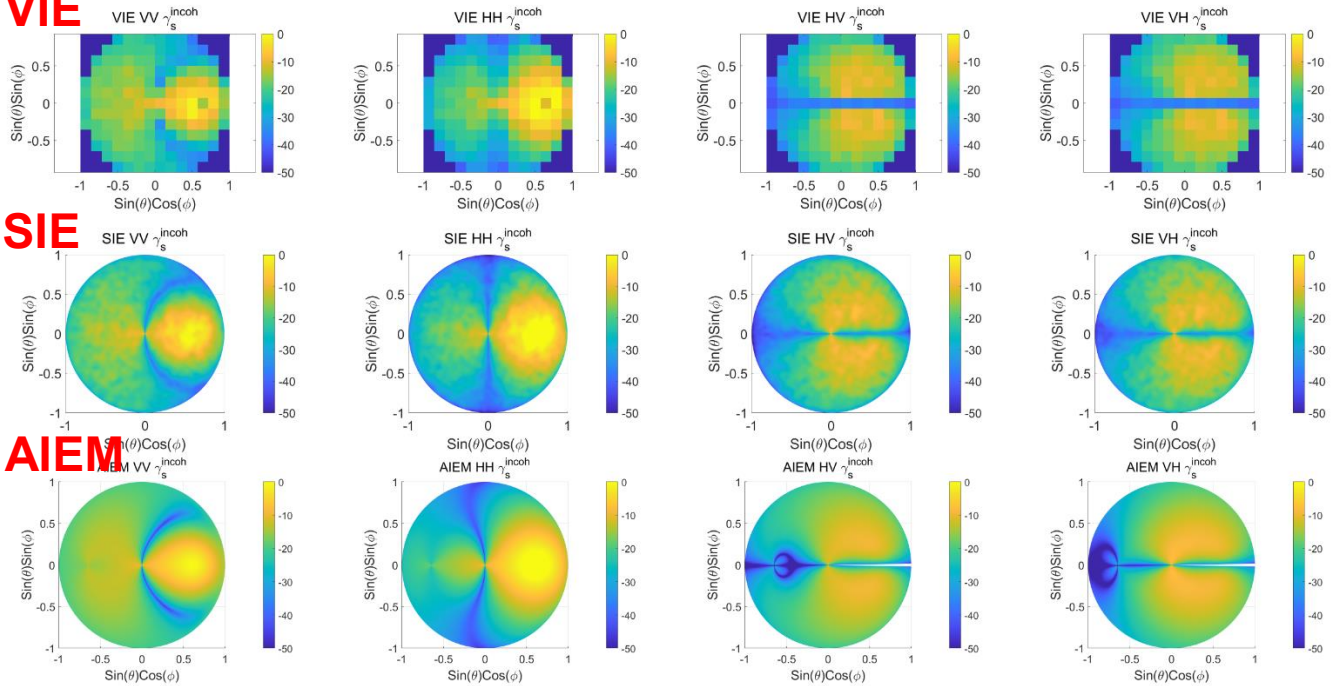

VV HH HV VH

- Good overall consistency: Co-pol strong in the specular direction within the incidence plane; Cross-pol stronger in the specular direction inclined out of the incidence plane.
- Due to the infinite-surface treatment, the VIE method yields relatively smaller incoherent bistatic scattering coefficients near the specular direction.

Single layer verification - a rougher soil

Comparison of scattering coefficients between two incident surfaces:

Parameters

RMSH	CL	m_v	ε_r
1.78 cm	8.3 cm	0.047	3.61+j0.24

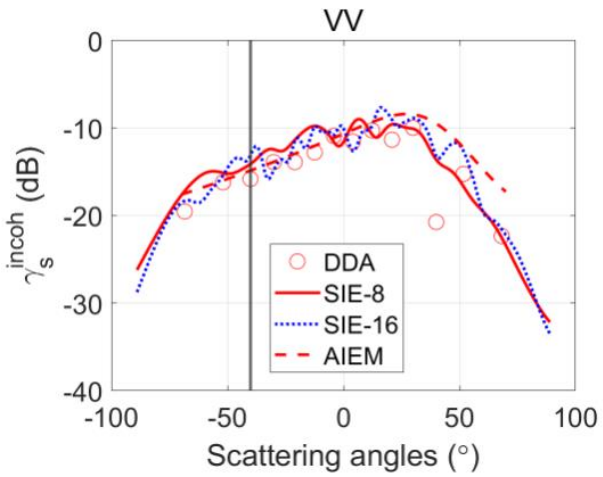

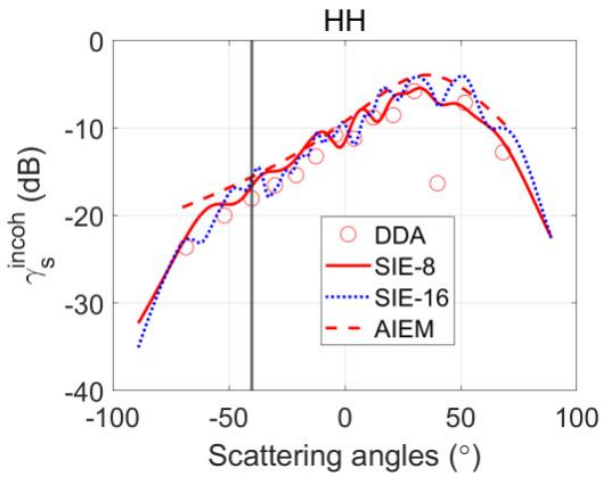

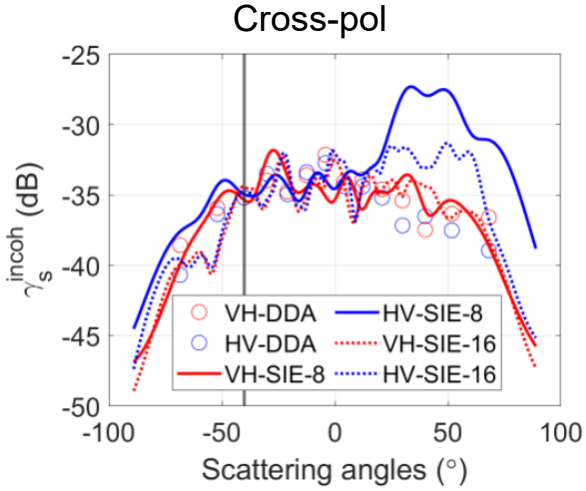

- **The overall consistency among the three methods remains good.**
- **SIE** shows **reduced convergence**, increased computation time, and requires **more Monte Carlo simulations**.
- **AIEM**, especially under **HH polarization**, exhibits **noticeable differences** compared to the other two methods.
- The **VIE-DDA** method maintains **stable computational efficiency** and matches well with the SIE results.

The multi-layer cases

Four scenarios:

Single layer

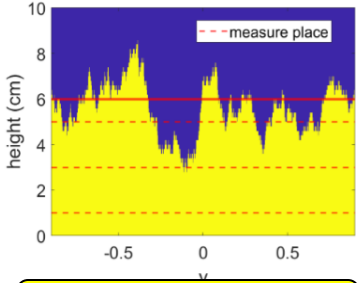

Flat discrete

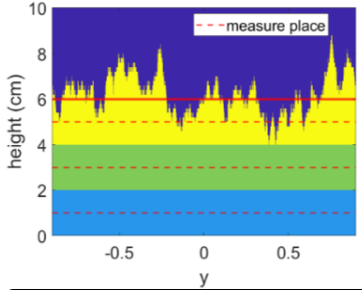

Rough discrete

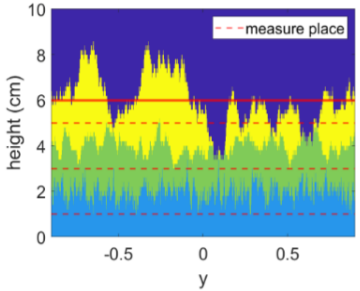

Continuous profile

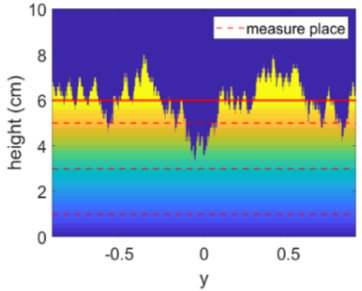

Ground truth ref: Xinyuan Pasture

Depth (cm)	1	3	5
m_v (m^3/m^3)	0.007	0.079	0.083

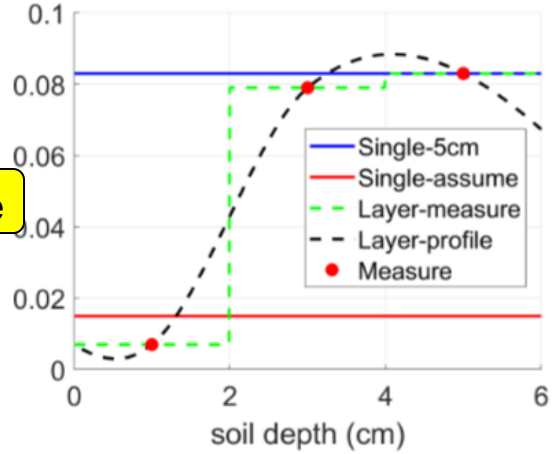

Five mv configurations:

L1-1 Single layer -- 5cm
L1-2 Single layer assumed between 1cm and 3cm

L2 Flat discrete layer
L3 Rough discrete layer
L4 Continuous profile

Scattering from layered soil

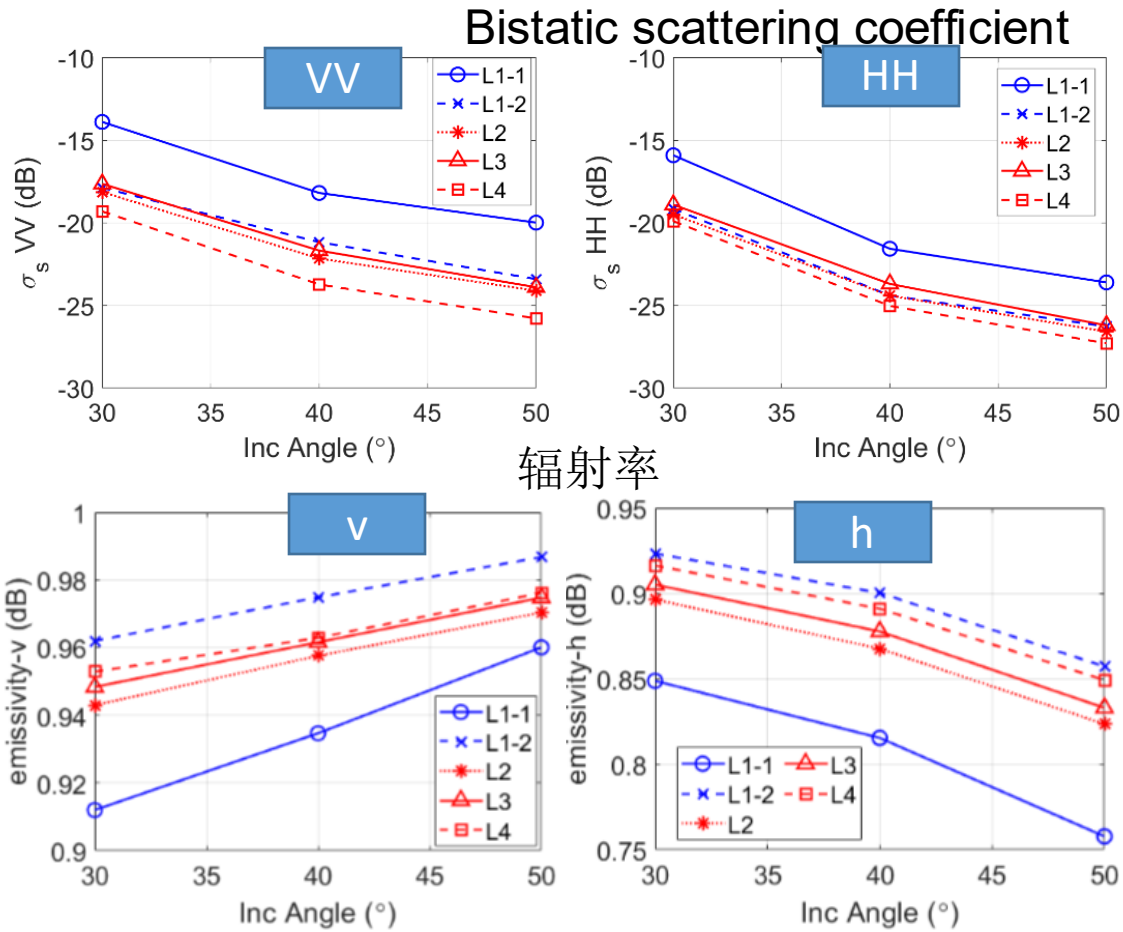

Conclusions:

- Single v.s. Multi: Single-layer equivalent moisture can match microwave observations of rough layered surfaces to a certain extent.

- Compare between Multi: little difference between internally rough and internally flat layering, while continuous profile layering is associated with relatively lower backscattering and higher emissivity.

Scattering from layered soil

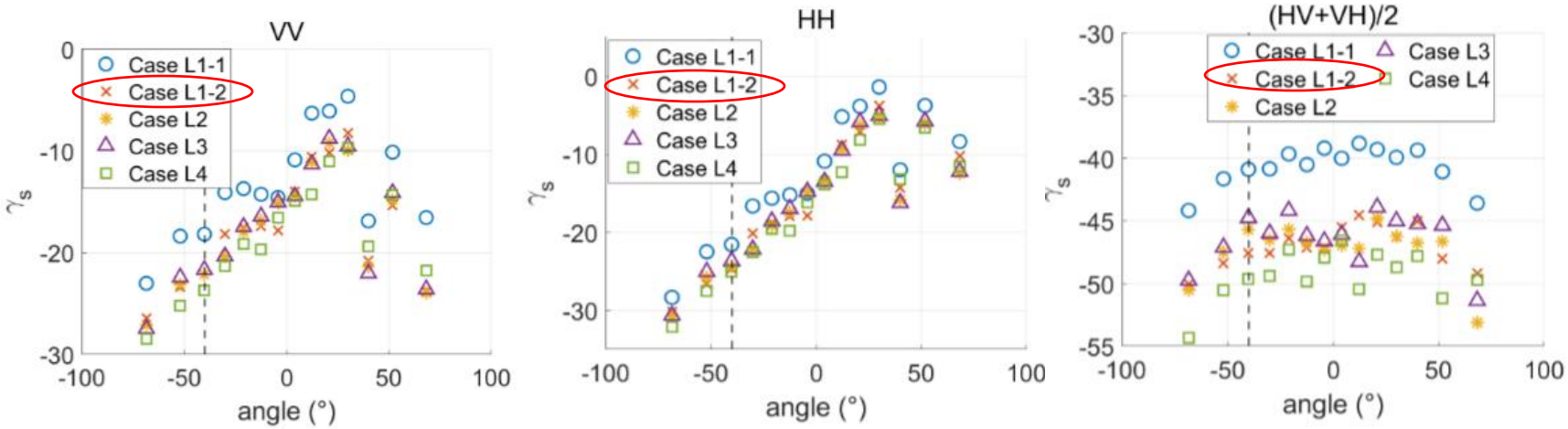

L1-1 L1-2 L2 L3 L4 Biscattered coefficient in the incidence plane –40 ° incidence

Conclusion：

- Single v.s. Multi： Single-layer equivalent moisture matches microwave observations of rough layered surfaces (L1-2 matchesL3/L4/L5).
- Compare between Multi： little difference between internally rough and flat layering; continuous profile layering features lower backscattering.

Scattering from layered soil

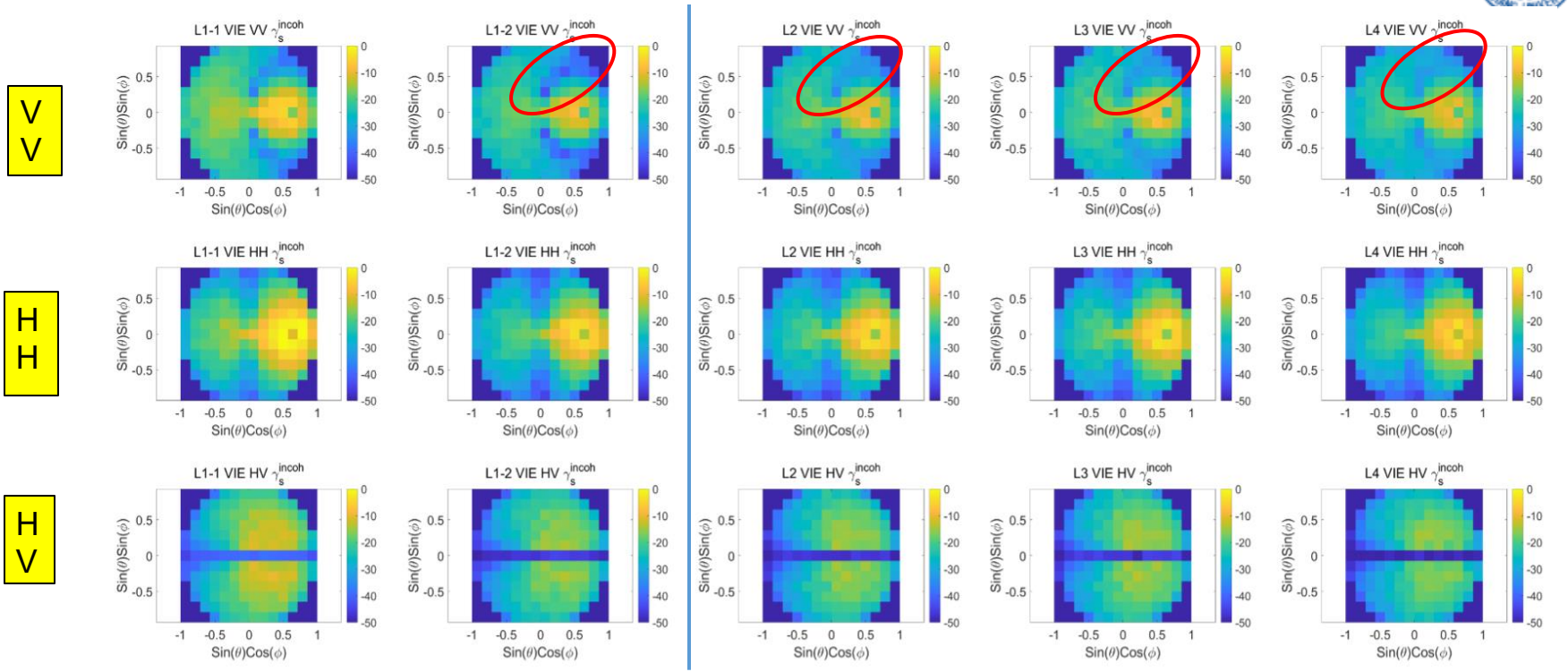

- For HH HV VH, L1-2 matches the layered cases
- For VV, in the direction perpendicular to the incidence plane, they are different;
- Layering enhances the VV scattering component toward that direction.

Summary of Soil Scattering

- The VIE-DDA approach effectively handles scattering from soil with vertical heterogeneity, illustrating sensitivities of microwave observables to certain soil profile configurations.

- The VIE-DDA approach in general agrees with the SIE approach for homogeneous soil scattering while with advantages in convergence for large rms or large permittivity contrast.

Scattering from Vegetated Land Surfaces: Scattering from Structured Sparse Random Media & Coupling Vegetation / Soil Scattering Interactions

Remote Sensing of Vegetated Land Surface is Critical to Food Security, Carbon Cycle, and Water Cycle

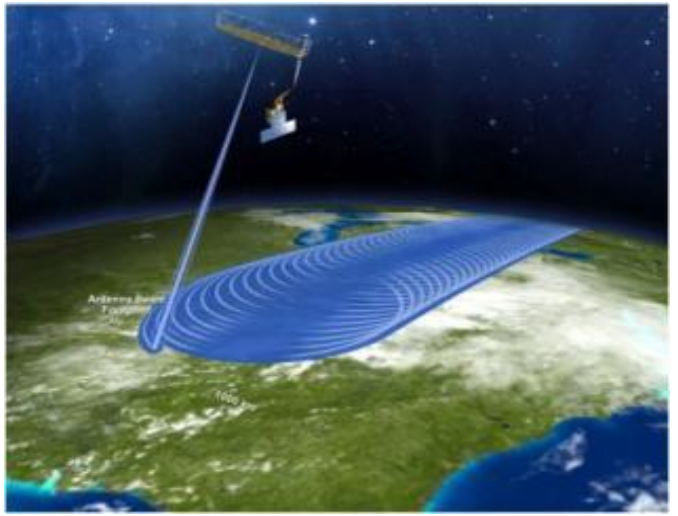

- Retrieve vegetation parameters (e.g. biomass)
- Retrieve vegetated surface physical parameters (e.g. soil moisture)

-> Assess crop yields

->Understand the global carbon cycle, water cycle and climate change

Hybrid wave approach and Radiative Transfer theory overview

Hybrid wave approach

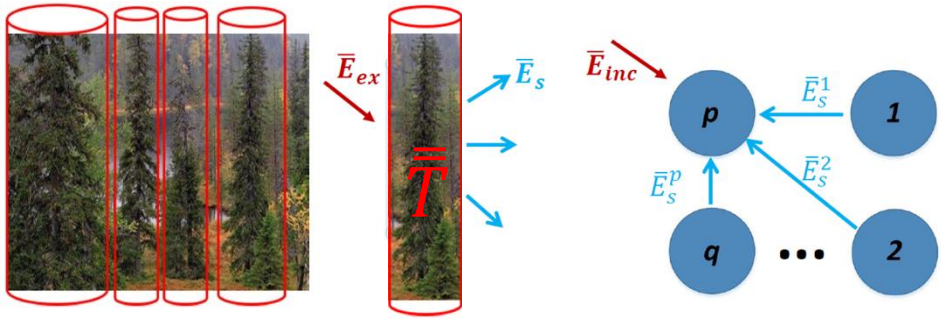

Geometry of trees | Single tree T-matrix | Foldy-Lax multiple scattering equations

$$\psi_l^E = \psi_{inc} + \sum_{\substack{j=1 \\ j\neq l}}^{N} G_0 T_j \psi_j^E$$

- Characterization of realistic vegetation structure
- Considering coherent wave interactions
- Computing intensive

[1] Huang H, Tsang L, Colliander A, et al. Propagation of waves in randomly distributed cylinders using three-dimensional vector cylindrical wave expansions in Foldy–Lax equations[J]. IEEE Journal on Multiscale and Multiphysics Computational Techniques, 2019, 4: 214-226.

Radiative Transfer (RT) theory

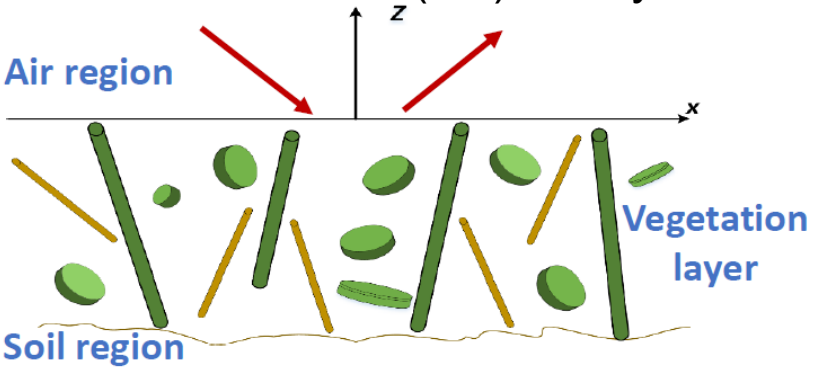

$$\cos\theta \frac{d\bar{I}_u(\theta,\phi,z)}{dz} = -\bar{\bar{\kappa}}_e(\theta,z)\bar{I}_u(\theta,\phi,z) + \bar{S}(\theta,\phi,z)$$

$$-\cos\theta \frac{d\bar{I}_d(\theta,\phi,z)}{dz} = -\bar{\bar{\kappa}}_e(\pi-\theta,z)\bar{I}_d(\theta,\phi,z) + \bar{W}(\theta,\phi,z)$$

- Assuming uniform distribution of scatterers: homogenization
- Considering multiple incoherent wave interactions through numerical iterative approach
- Relatively higher computational efficiency

RT model driven by realistic vegetation structure

Hybrid approach

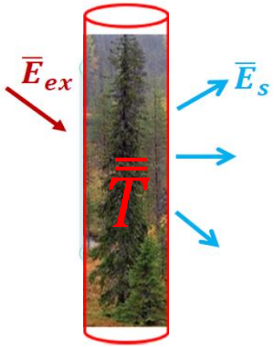

Geometric structures of vegetation reflected in the T-matrix

Radiative Transfer (RT) theory

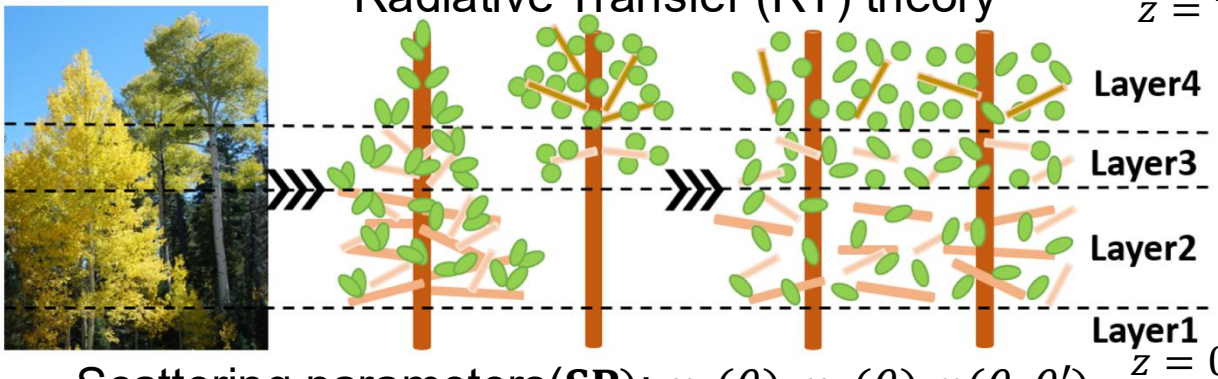

Scattering parameters(**SP**): $\kappa_e(\theta), \kappa_a(\theta), p(\theta, \theta')$

At each height (z), the total SP is acquired by independent scattering assumption and incoherent summation over all scatterers. **The vertical structure of vegetation is reflected in SP(z).**

The **Passive Radiative Transfer Equation** (RTE) Considering Vertical Heterogeneity:

$$\cos\theta \frac{dI(z,\theta)}{dz} = -\kappa_e(\theta, z) I(z,\theta) + \kappa_a(\theta, z) \frac{K_B T}{\lambda^2} + \int_0^{\pi} p(\theta; \theta', z) I(z, \theta') \sin\theta' d\theta'$$

Chen K, Tan S. A multiple-scattering microwave radiative transfer model for land emission with vertically heterogeneous vegetation coverage[J]. IEEE Transactions on Geoscience and Remote Sensing, 2024.

Microwave scattering model driven by vegetation fine structure

Lidar360 software

Lidar Point cloud data of a forest

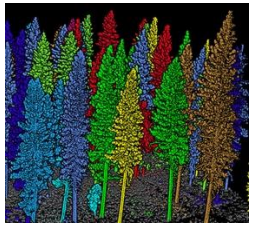

Single tree Segmentation

Single tree point cloud

Forest parameters

Tree species,
Tree height,
Tree distribution

AdQSM
(quantitative structure model)

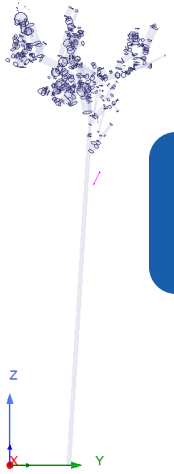

Structure approximated by cylinders

PolSARproSIM
(software developed by ESA)

Virtual tree structures

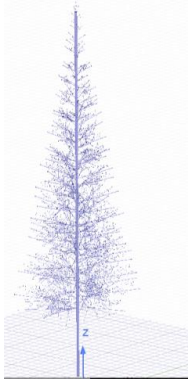

Extract RT model inputs from the tree structure

Scheme1:

- High quality requirements on point clouds
- Lack of moisture content information

The spatial locations, dimensions, orientation angles, moisture content of tree trunks, branches, and leaves. Canopy structure parameters

Microwave scattering model driven by vegetation fine structure

For trunks, primary branches and secondary branches:

$$P(\theta,\phi;\theta',\phi';z)=\left\langle\sum_{i=1}^{N_i} n_0^{(i)}(z)\left|f^{(i)}(\theta,\phi;\theta',\phi')\right|^2\right\rangle_{\text{tree species}}$$

$$n_0^{(i)}(z)=\begin{cases}\dfrac{N_A^{\text{tree}}}{L^{(i)}\cos\theta^{(i)}} & ,\text{for } z_0^{(i)}\le z\le z_0^{(i)}+L^{(i)}\cos\theta^{(i)}\\ 0 & ,\text{otherwise}\end{cases}.$$

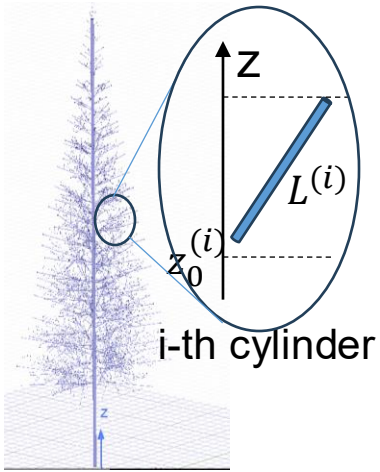

N_i is total number of cylinders on a tree.

$\langle.\rangle_{\text{tree species}}$ represents average for different tree species.

$z_0^{(i)}$ is the starting height of the i-th cylinder.

$n_0^{(i)}(z)$ is the number density of i-th cylinder per unit volume;

N_A^{tree} is the number density of the tree per area

For tertiary branches and leaves:

$$P(\theta,\phi;\theta',\phi';z)=\left\langle\sum_{s=1}^{N_s} n_0^{(s)}(z)\left\langle\left|f^{(s)}(\theta,\phi;\theta',\phi')\right|^2\right\rangle\right\rangle_{\text{tree species}}$$

$$n_0^{(s)}(z)=\frac{N^{(s)}N_A^{\text{tree}}S(z)}{V_{\text{crown}}}$$

$\langle.\rangle$ represents orientation average, $\langle.\rangle_{\text{tree species}}$ represents average for different tree species.

N_s is the number of scatterer species and $N^{(s)}$ is the number of the s-th specie per tree.

$S(z)$ is the height-dependent canopy sectional area and V_{crown} is the total canopy volume.

$n_0^{(s)}(z)$ is the number density per unit volume of the s-th specie (tertiary branch and leaf).

Passive RT model incorporating volume-surface coupling by introducing incoherent bistatic scattering coefficients into boundary conditions

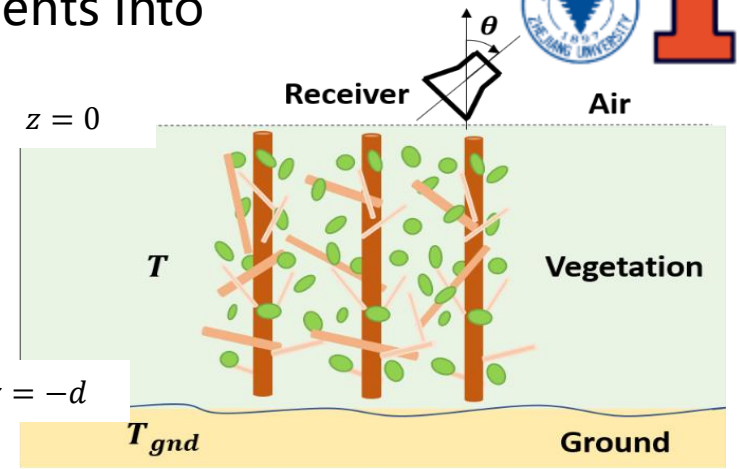

Boundary conditions for RT model:

$$T_d(\theta, z=0) = 0$$

$$T_u(\theta, z=-d) = (1-r(\theta))T_{gnd} + T_d(\theta, z=-d)r^{coh}(\theta) + \int_0^{\pi/2} d\theta' \sin\theta' \gamma^{incoh}(\theta,\theta') T_d(\theta', z=-d)$$

Features:

- Use total reflectivity to suppress the upward emission from the soil
- Fully consider rough surface/vegetation interactions

Numerical iterative approach is applied to solve the RT equation with boundary conditions.

Virtual tree structure generated by PolSARproSIM

Coniferous tree with a truncated ellipsoidal canopy

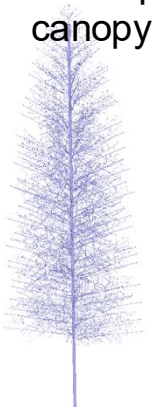

18.7

Coniferous tree with a conical canopy

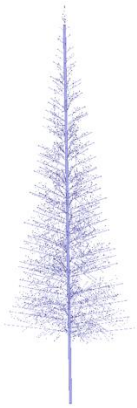

13.3

Broadleaf tree with a truncated ellipsoidal canopy

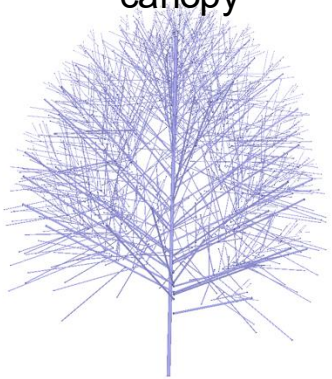

119.7

Tree Height ~ N(8.45m,0.45m)

Water Content (*kg/tree*)

(averaged over tree species)

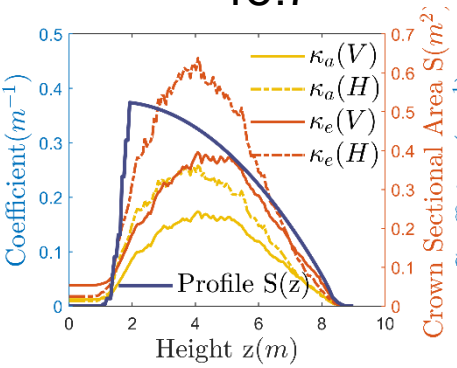

Case1

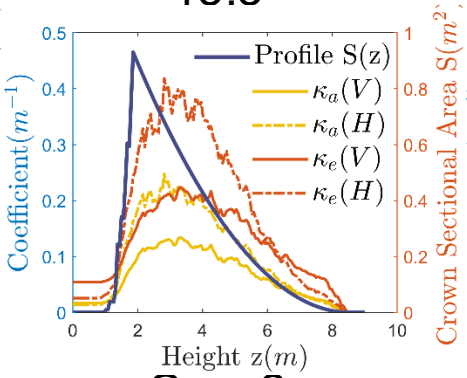

Case2

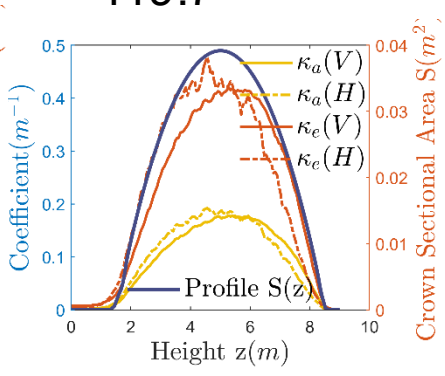

Case3

The vertical structure of vegetation is reflected in the scattering parameters that vary with height.

Influence of vegetation vertical structure on brightness temperatures and transmissivities: same VWC =5kg/m^2

Simulation settings:
Frequency:1.41GHz
Vegetation temperature=300K

Soil temperature=300K
rms height=1cm
Correlation length=10cm

Considered volume/surface scattering coupling.

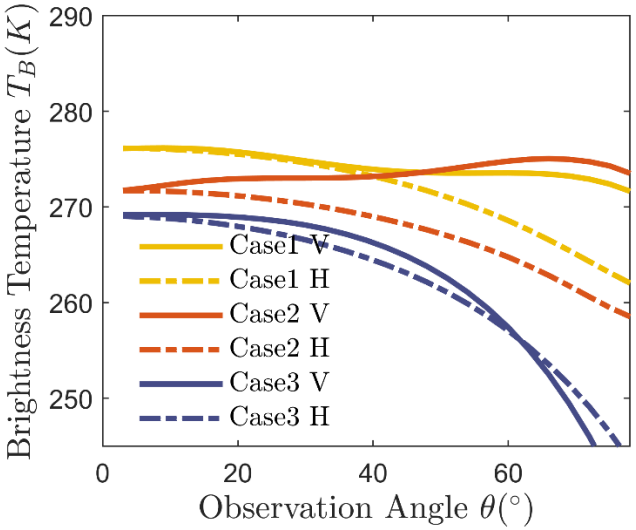

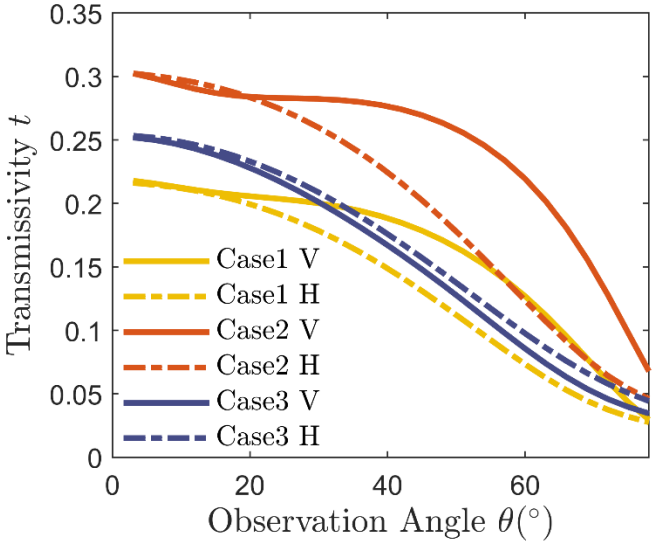

- Vegetation structure has a significant impact on TB, particularly at large observation angles.

- The transmissivity varies notably with different vegetation structures, and the difference tends to diminish as the observation angle increases.

Active RT Model Incorporating Volume-Surface Coupling

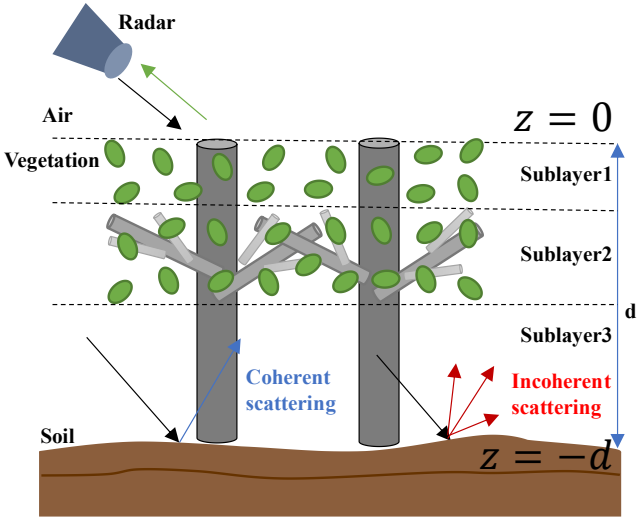

Active vector RT equation

$$\cos\theta \frac{d\bar{I}_u(\theta,\phi,z)}{dz} = -\bar{\bar{\kappa}}_e(\theta,z)\bar{I}_u(\theta,\phi,z) + \bar{S}(\theta,\phi,z)$$

$$-\cos\theta \frac{d\bar{I}_d(\theta,\phi,z)}{dz} = -\bar{\bar{\kappa}}_e(\pi-\theta,z)\bar{I}_d(\theta,\phi,z) + \bar{W}(\theta,\phi,z)$$

Boundary conditions

$$\bar{I}_d(\theta,\phi,z=0) = \bar{I}_0\delta(\cos\theta - \cos\theta_0)\delta(\phi-\phi_0)$$

$$\bar{I}_u(\theta,\phi,z=-d) = \bar{\bar{r}}_{coh}(\theta)\bar{I}_d(\theta,\phi,-d) + \int_0^{2\pi} d\phi' \int_0^{\frac{\pi}{2}} d\theta' sin\theta' \bar{\bar{\gamma}}(\theta,\phi;\theta',\phi')\bar{I}_d(\theta',\phi',-d)$$

coherent

incoherent

Surface scattering characterization:

KA

NMM3D/AIEM

RT Equation Solved by Numerical Iterative Method

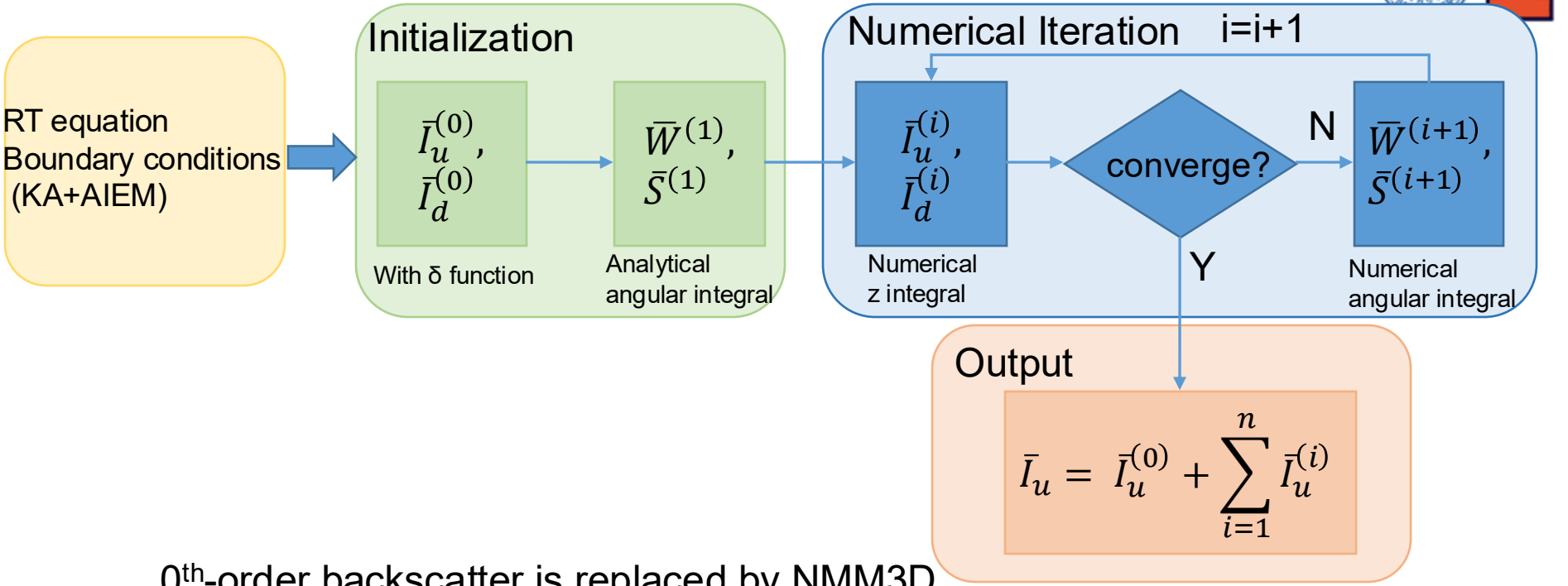

0th-order backscatter is replaced by NMM3D

$$\bar{I}_u^{(0)}(\theta_0, \phi_0 + \pi, 0) = \bar{\bar{D}}\left(-\sec\theta_0 \int_{-d}^{0} \kappa_e(\theta, z)dz\right) \bar{\bar{\gamma}}_{NMM3D} \bar{\bar{D}}\left(-\sec\theta \int_{-d}^{0} \kappa_e(\pi - \theta, z)dz\right) \bar{I}_0$$

Backscattering Enhancement Through Cyclical Correction

First-order Scattering Paths

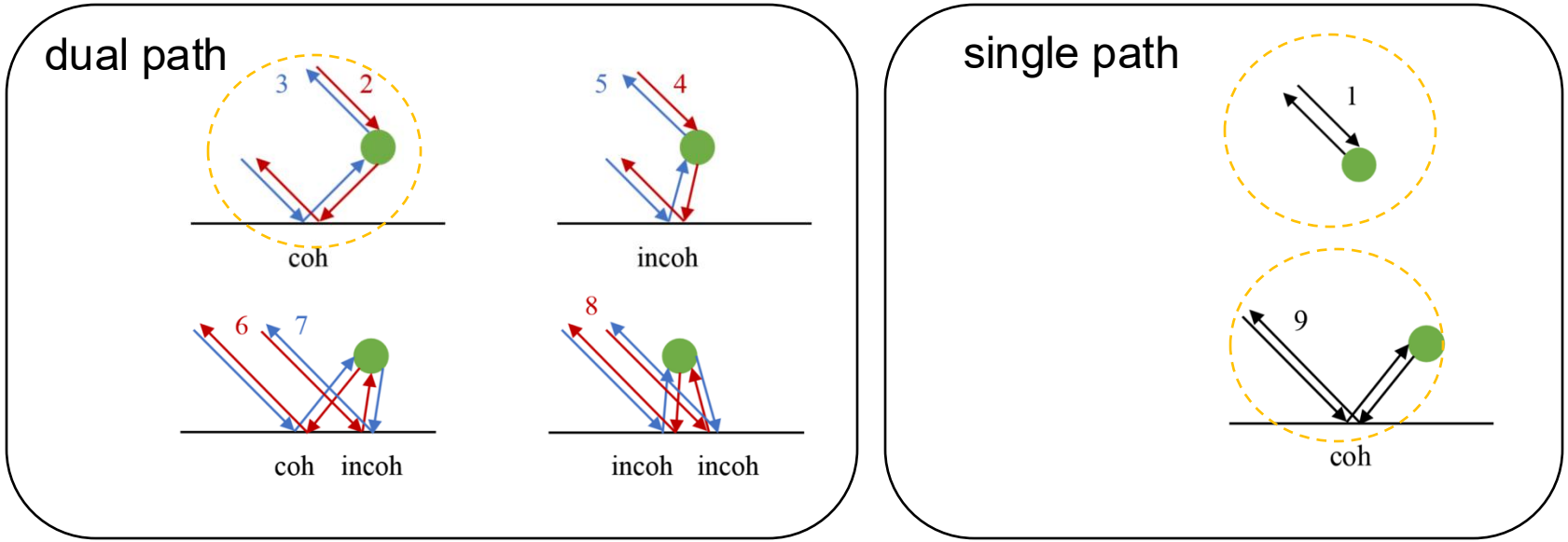

Cyclical correction:

$$I = I_{\text{dual}} + I_{\text{single}}$$

$$I_{cor} = 2I_{dual} + I_{single} = 2I - I_{single}$$

Effects of Multiple Scattering and Incoherent Surface Scattering

Cumulative contributions to backscattering before and after incorporating incoherent bistatic surface scattering

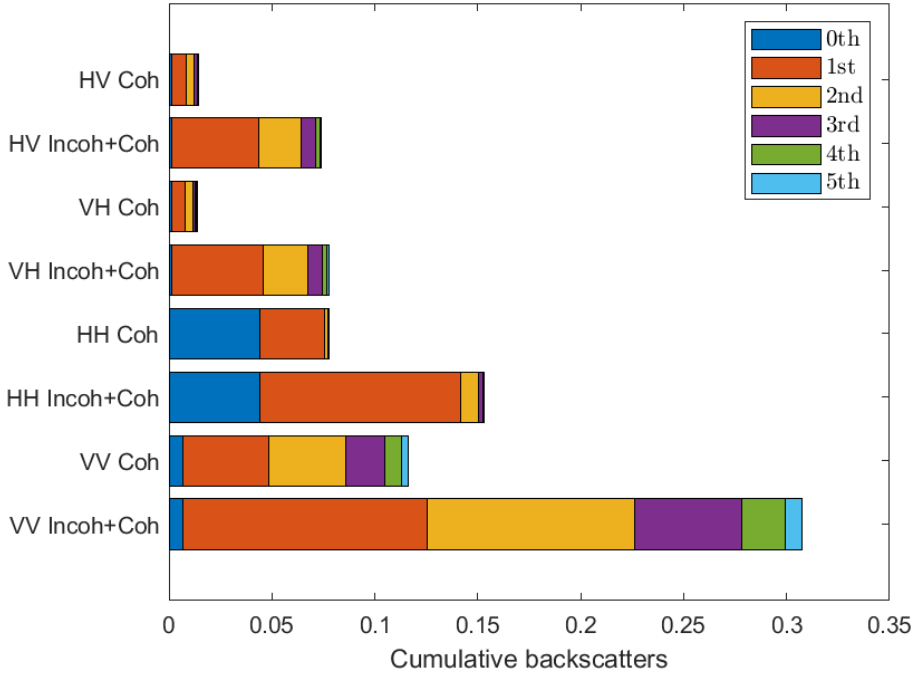

- Significant multiple scattering and bistatic surface/volume scattering coupling effects.
- High order scattering contributions double or triple due to bistatic surface/volume scattering coupling.

The Bistatic Coefficients of Different Scenes

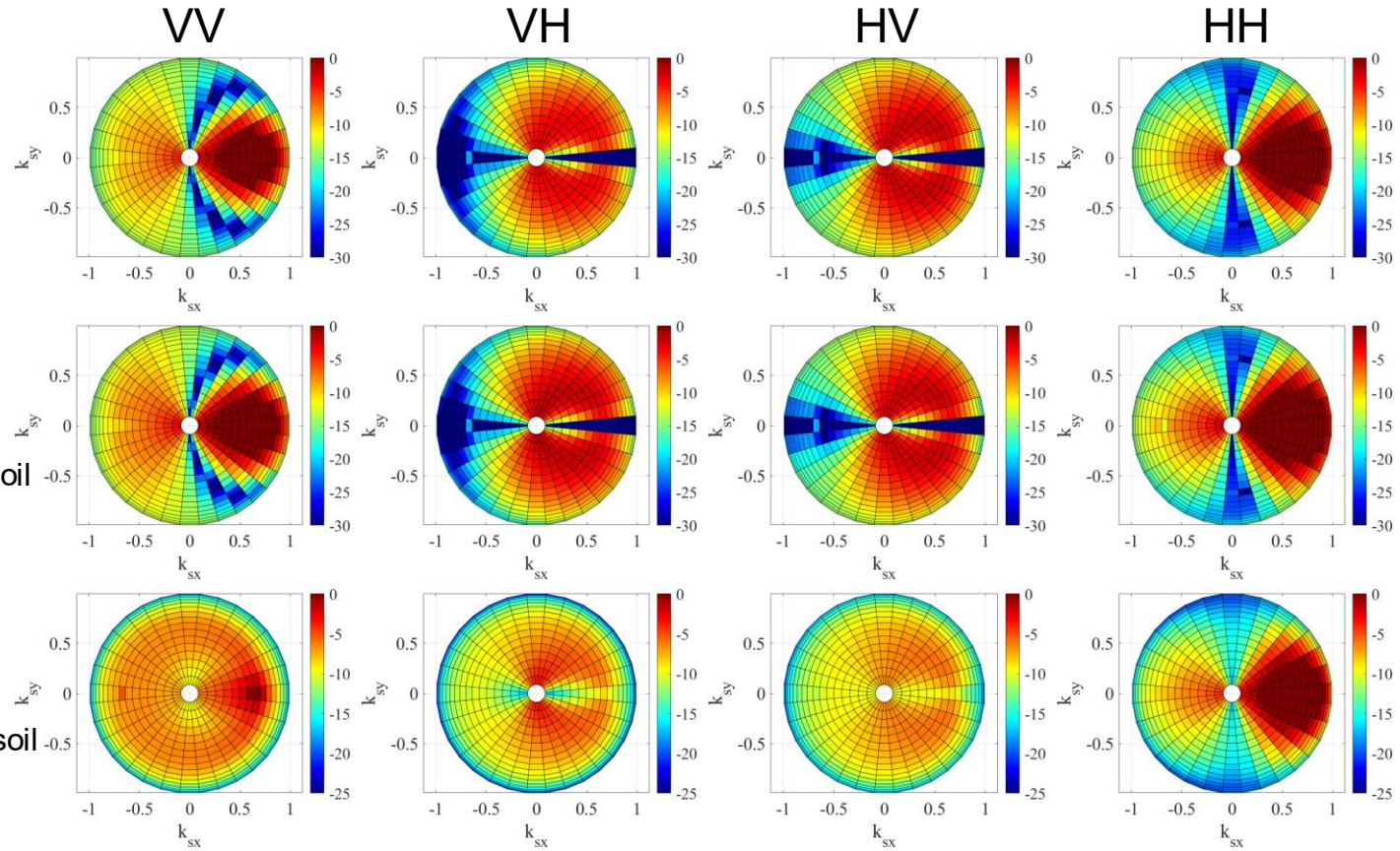

The bistatic coefficients of bare soil and very sparsely vegetated soil are similar.
Moderate vegetation coverage redistributes the bistatic coefficients in the upper hemi-sphere.

Simultaneous Active and Passive RT Model Validation

SMAPVEX12
Forest site F5
High VWC: 14.1kg/m^2
Low soil roughness:
0.78cm (RMS height)

Active

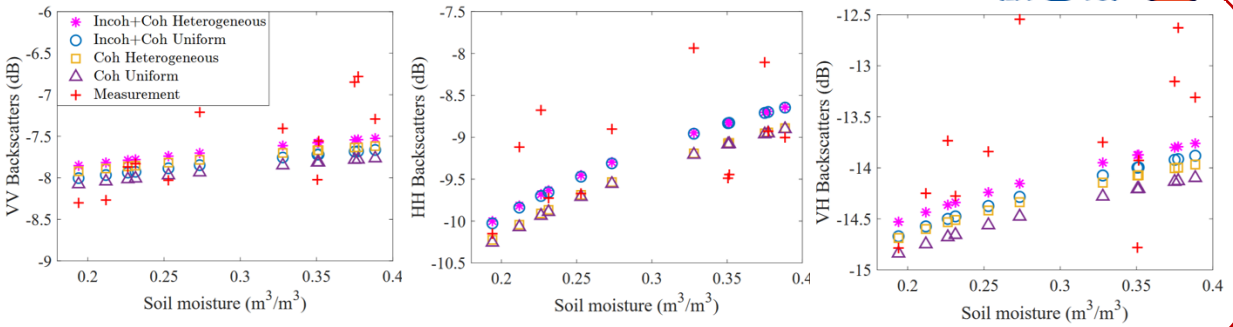

RMSE Comparison Between Simulated and Measured Data

Bistatic scattering	Vertical heterogeneity	Co-pol (dB) VV	Co-pol (dB) HH	Cross-pol (dB) VH	Cross-pol (dB) HV	Brightness Temp. (K) TBV	Brightness Temp. (K) TBH
yes	yes	0.42	0.59	0.71	0.65	5.0	3.8
yes	no	0.45	0.58	0.78	0.73	7.3	4.2
no	yes	0.44	0.67	0.82	0.75	6.5	4.8
no	no	0.51	0.92	0.86	0.86	8.9	5.6

Passive

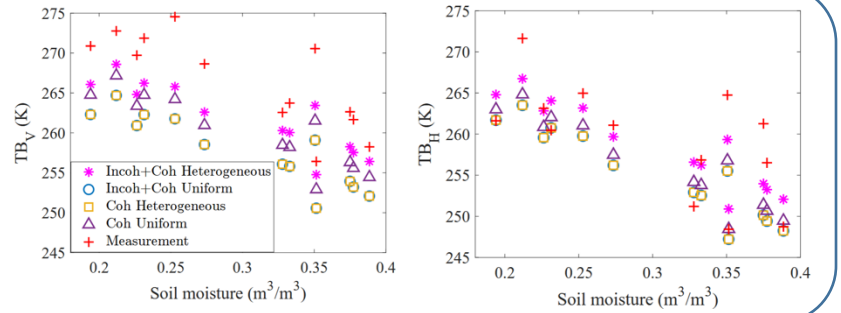

In this site with high VWC and low soil roughness,

- The effect of surface bistatic scattering is relatively weak especially when the veg vertical structure heterogeneity is accounted.
- Meanwhile the vertical vegetation structure heterogeneity affects Tb more than backscatter.

Simultaneous Active and Passive RT Model Validation

SMAPVEX12
Forest site F3
Low VWC: 7.3kg/m^2
High soil roughness:
1.93cm(RMS height)

Active

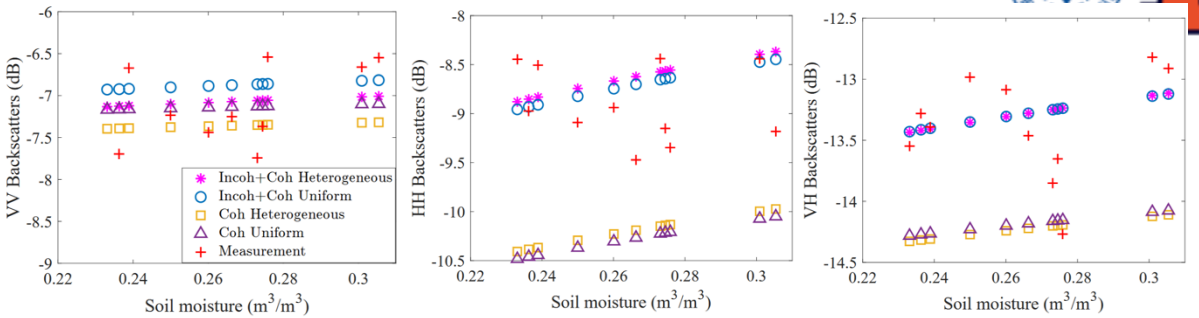

RMSE Comparison Between Simulated and Measured Data

Bistatic scattering	Vertical heterogeneity	Backscatter (dB) VV	Backscatter (dB) HH	Cross-pol (dB) VH	Cross-pol (dB) HV	Brightness Temp. (K) TBV	Brightness Temp. (K) TBH
yes	yes	0.54	0.51	0.42	0.40	5.2	2.9
yes	no	0.55	0.47	0.42	0.40	8.4	2.9
no	yes	0.64	1.36	0.94	0.90	11.7	12.5
no	no	0.55	1.44	0.90	0.87	14.8	12.5

Passive

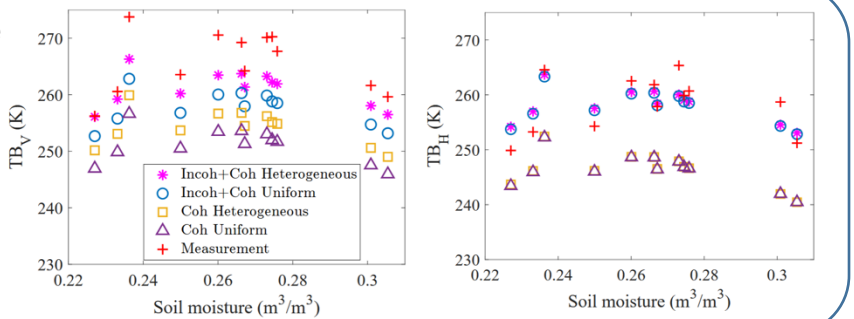

In this site with low VWC and high soil roughness,

- The effect of surface bistatic scattering is significant in both active and passive models;
- Meanwhile, the vertical vegetation structure heterogeneity weakly affects the results other than Tbv especially when the surface bistatic scattering is accounted.

Driving Questions: RT Approach vs. Hybrid Approach

Transmissivity of a layer of vertical cylinders: RT (0-order) vs. Hybrid

Transmission	RTE/DBA	Hybrid Method
Case 1	0.35	0.66
Case 2	0.089	0.45

[1] Huang H, Tsang L, Colliander A, et al. Propagation of Waves in Randomly Distributed Cylinders Using Three-Dimensional Vector Cylindrical Wave Expansions in Foldy–Lax Equations[J]. IEEE Journal on Multiscale and Multiphysics Computational Techniques, 2019, 4: 214-226.

Exploring the applicability of the RT theory in realistic vegetated land scenarios :

1) Transmissivity of **a layer of uniformly distributed vertical cylinders**:
   RT (multiple scattering) vs. Hybrid?
2) Transmissivity of **a layer of uniformly distributed trees**:
   RT (multiple scattering + vertical structure) vs. Hybrid?
3) Transmission through **a layer of non-uniformly distributed trees**:
   RT (multiple scattering + vertical structure) vs. Hybrid?

Transmissivity calculation through RT approach

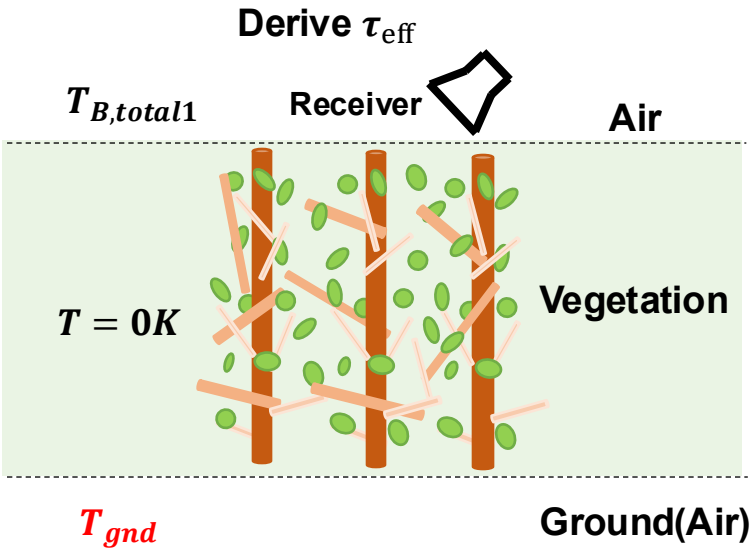

The transmissivity is related to $\gamma_t(\theta, \theta')$ by definition

$$\mathrm{t}(\theta) = \int_0^{\frac{\pi}{2}} \gamma_t(\theta, \theta') \sin(\theta') d\theta'$$

$$T_{B,\text{total1}}(\theta) = \int_0^{\frac{\pi}{2}} \gamma_t(\theta, \theta')\, T_{\text{gnd}} \sin(\theta') d\theta'$$
$$= T_{\text{gnd}} t(\theta) = T_{\text{gnd}} \exp(-\tau_{\text{eff}} \sec\theta)$$

Thus

$$\mathrm{t}(\theta) = \frac{T_B(\theta)}{T_{\text{gnd}}} = \exp(-\tau_{\text{eff}} \sec\theta)$$

Transmissivity calculation through RT approach in heterogeneous scenarios

① By averaging scattering parameters (SP)

Scattering parameters(**SP**): $\kappa_e(\theta,z), \kappa_a(\theta,z), p(\theta,\theta',z)$

The vertical structure of vegetation and horizontal distribution of vegetation are reflected in SP.

$$SP = \sum_{i=1}^{N} w_i SP_i \qquad \mathrm{t} = \frac{T_B(SP)}{T_{\mathrm{gnd}}}$$

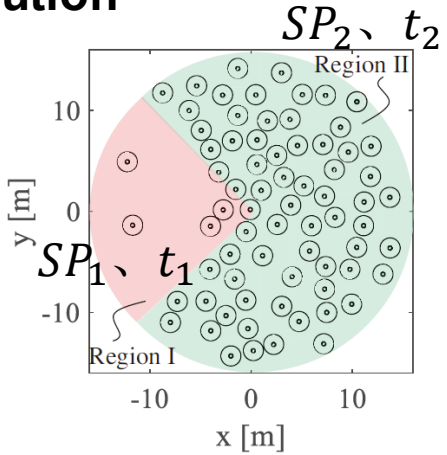

w_i and SP_i are proportion and SP of i-th region, respectively.

② By averaging transmissivity (t)

$$t = \sum_{i=1}^{N} w_i t_i$$

t_i is the transmissivity of i-th region

Hybrid approach and transmissivity calculation

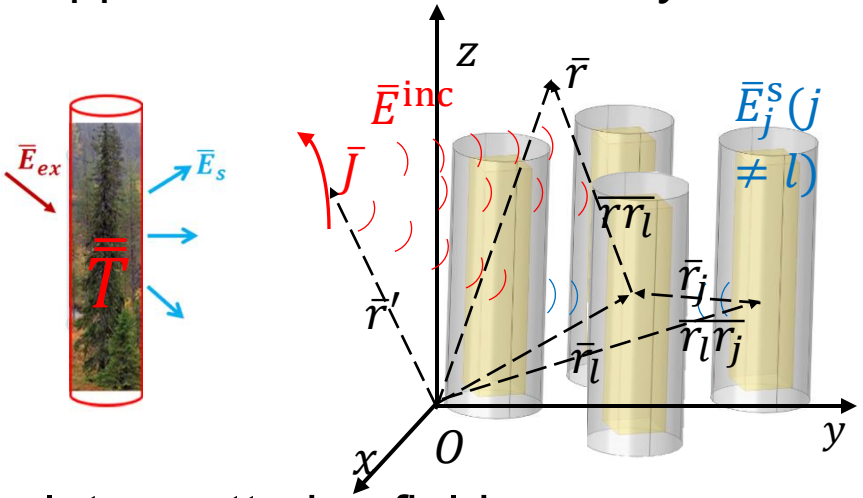

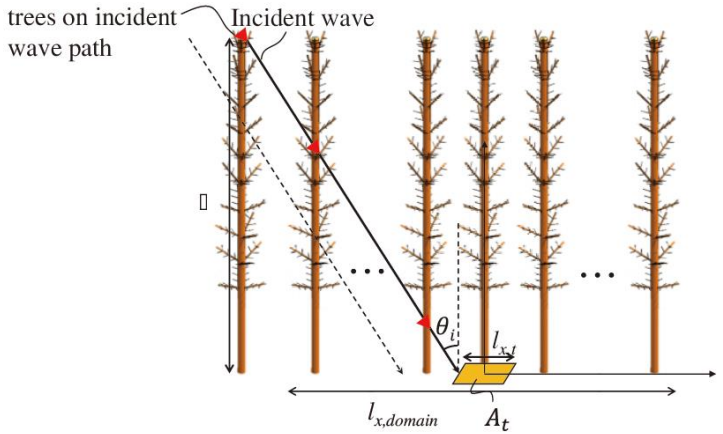

Calculate scattering field:

①Calculate the **T-matrix** coefficients in 3-D vector cylindrical wave expansions (capture multiple scattering within a realistic single plant)

②Calculate the scattering field using the **Foldy-Lax multiple scattering theory** (incorporate multiple scattering among plants)

Calculate transmissivity:

①Compute the transmissivity from the Poynting vector on the bottom plane.

$$T = \frac{1}{A_t} \iint_{A_t} \frac{\bar{S}^{tot} \cdot (-\hat{z})}{\bar{S}^{inc} \cdot (-\hat{z})} d\bar{r}.$$

②Perform Monte Carlo simulations involving **averaging** the transmissivities.

$$t = \frac{1}{N} \sum_{n=1}^{N} T_n$$

The transmissivities derived from the RT theory are similar to those derived from the hybrid method for **a layer of uniformly distributed trees**

Number and dimensions of a trunk and branches setting in hybrid approach[1]

	Trunk	Primary Branch	Secondary Branch
Number	1	30 (18)	180 (108)
Length [m]	13 (8)	1	0.3
Radius [cm]	12.5	2	0.5

(): 8 m tree

Orientation: 0~5° 30° ~80° 30° ~80°

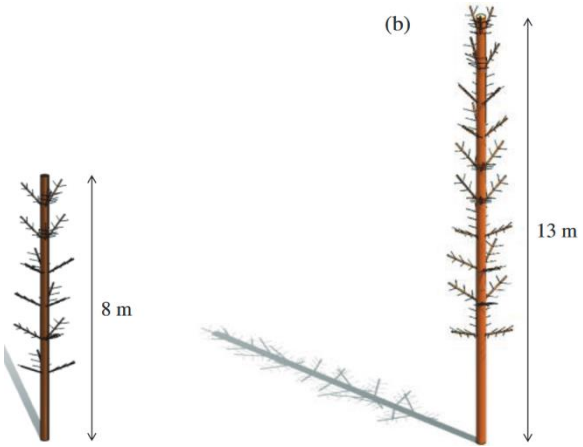

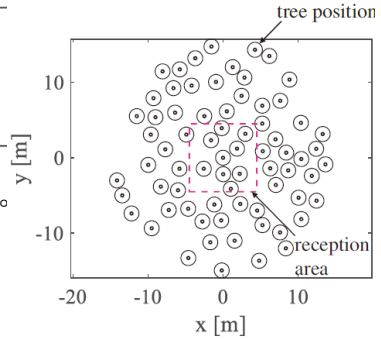

geometric configurations for uniformly distributed trees

Tree	Polarization	Transmissivity ($\theta = 40°$)	
		RT Model	Hybrid Method[1]
8m tree	V-pol	0.710 ≈	0.686
	H-pol	0.696	0.660
8m and 13m tree mixed (1:1)	V-pol	0.617 (SP) 0.636 (t)	0.624
	H-pol	0.605 (SP) ≈ 0.626 (t)	0.598
13m tree	V-pol	0.563	0.559
	H-pol	0.556 ≈	0.536

[1] Jeong, Jongwoo, et al. "Full-wave electromagnetic simulations of forests at L-band by using Fast Hybrid Method." *Progress In Electromagnetics Research* 178 (2023): 111-127.

The RT model produces comparable transmissivity estimates for both **uniformly and non-uniformly distributed trees**, while the hybrid approach reveals a markedly higher transmissivity under non-uniform vegetation distribution.

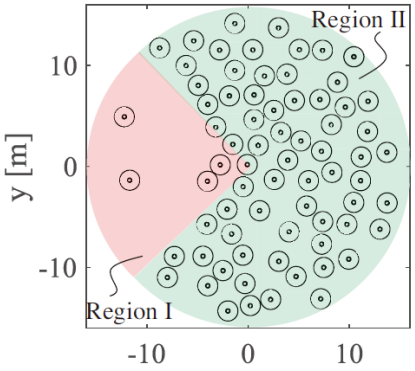

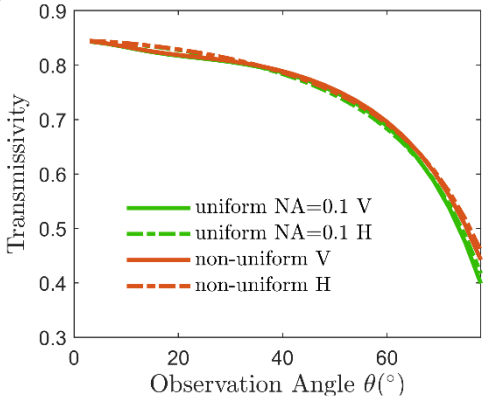

Transmissivity calculation in RT model:

$$t_{\text{uniform}} = t_{\text{total region}} \quad \text{(Adjust tree density)}$$

$$t_{\text{non-uniform}} = \frac{1}{4} t_{\text{region}I} + \frac{3}{4} t_{\text{region}II}$$

	Region I	Region II	Total Region
Tree densities	0.0224 trees/m^2	0.127 trees/m^2	0.1 trees/m^2
Proportion of area	1/4	3/4	1

Tree height = 8m	Polarization	Transmissivity($\theta = 40°$)		
		RT Model		Hybrid Method
Non-Uniform (t)	V-pol	0.793	$<$	0.875
	H-pol	0.791	$\approx$	$<$
Uniform (SP)	V-pol	0.785	$\approx$	0.755
	H-pol	0.783		

Jeong, Jongwoo, et al. "Full-wave electromagnetic simulations of forests at L-band by using Fast Hybrid Method." *Progress In Electromagnetics Research* 178 (2023): 111-127.

Summary of Vegetated Land Surface Scattering

- **Hybrid full wave approach and RT model inter-comparison**: In scenarios where vegetation is uniformly distributed, the transmissivity predicted by the radiative transfer model closely matches that obtained from full-wave simulations. However, discrepancies arise between the two approaches when vegetation distribution is non-uniform.
- **Realistic vegetation structure modeling and its effects**: Realistic vegetation structures are accounted in both models, demonstrating effects on transmissivity and active/ passive microwave observables of vegetated land surfaces.
- **RT framework and validation**: Active and passive models for vegetated land surfaces considering **multiple scattering** effects, **bistatic surface volume scattering coupling**, and **backscattering enhancement** are proposed and compares well with experimental data from SMAPVEX12.

Image courtesy of iSWGR

Scattering of Dense Random Media and Snow Remote Sensing: Wet Snow

Volume Scattering from Snowpack

Snow is ice grains embedded in air background

Volume fraction: 10% ~ 50%

Grain size: 0.2~3 mm

These ice grains interact with microwave

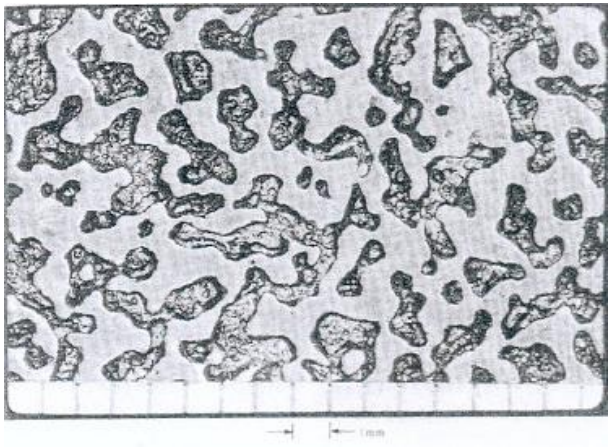

The Partially Coherent Approach: Dense Media Radiative Transfer (DMRT)

Coherent near / intermediate field interaction, exact

Incoherent far field, volume / surface interact, intensity, approximation

Phase info lost

Solve Maxwell's Eq. over a block of computer snow (3~5λ) to homogenize the snowpack

Substitute the effective parameters into & Solve Radiative Transfer Eq.

Backscatter: σ

Bistatic scatter: γ

Brightness temperature: T_b

homogenization

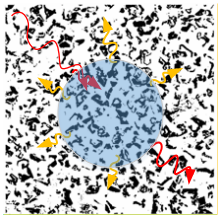

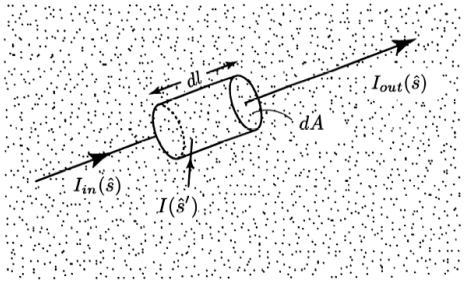

- Homogenization
- Efficient and stable
- Losing phase information

$$\frac{dI(\hat{s})}{ds} = -\kappa_e I(\hat{s}) + \int d\hat{s}' P(\hat{s}, \hat{s}') I(\hat{s}')$$

Quasi-Crystalline Approximation (QCA): Densely Packed Sticky Hard Spheres

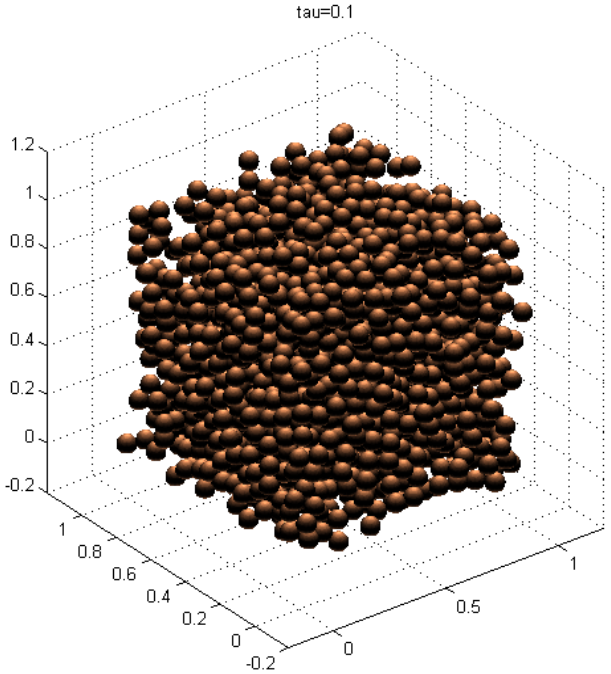

Simulated particles f_V = 40%

Sticky Hard Spheres:
- *non-penetrable, no overlap*
- *Sticky, tend to form clusters*

Parameters:
- Grain diameter
- Stickiness τ
- Volume fraction f_v

Bicontinuous Media: Computer Generation

$$S(\bar{r}) = \frac{1}{\sqrt{N}} \sum_{n=1}^{N} \cos(\bar{\zeta}_n \cdot \bar{r} + \delta_n)$$

$$p_G(\zeta) = \frac{b+1}{\Gamma(b+1)\langle\zeta\rangle}\left[(b+1)\frac{\zeta}{\langle\zeta\rangle}\right]^b \exp\left(-(b+1)\frac{\zeta}{\langle\zeta\rangle}\right)$$

$$\Theta_\alpha[S(\bar{r})] = \begin{cases} 1 \text{ (ice)}, & \text{if } S(\bar{r}) \geq \alpha \\ 0 \text{ (air)}, & \text{if } S(\bar{r}) < \alpha \end{cases}$$

real snow

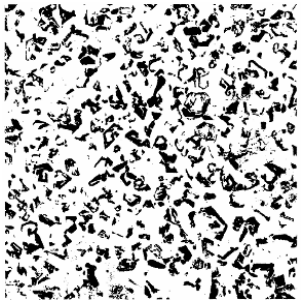

Depth Hoar (30%)
3 cm * 3 cm picture

A. Wiesmann, C. Mätzler, and T. Weise, "Radiometric and structural measurements of snow samples," *Radio Sci.*, vol. 33, pp. 273-289, 1998.

Bicontinuous media

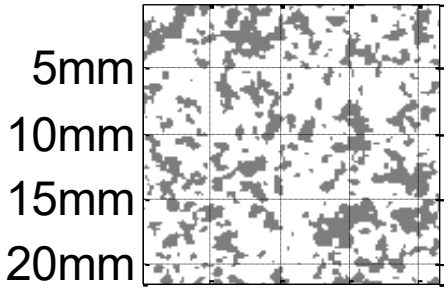

$f_V = 30\%$
$\langle\zeta\rangle = 4500[m^{-1}]$
$b = 1.5$

Ding, et al. (2010). TGRS 48(8): 3139-3151. Electromagnetic Scattering by Bicontinuous Random Microstructures with Discrete Permittivities.

- Controllable irregular microstructure
- Volume fraction: 0~100%
- Visually resembles snow
- Quantitatively compared in correlation function

Parameters:
- Size parameter $\langle\zeta\rangle$
- Shape parameter b
- Volume fraction f_v

Numerical Maxwell Solutions (NMM3D) over Spherical Samples of Bicontinuous Media

Discrete Dipole Approximation (DDA) with FFT

$$\bar{p}_i = \alpha_i \bar{E}_{inc} - \alpha_i \sum_{j=1, j\neq i}^{N} \left(-\frac{k^2}{\varepsilon}\right) \bar{\bar{G}}(\bar{r}, \bar{r}') \cdot \bar{p}_j$$

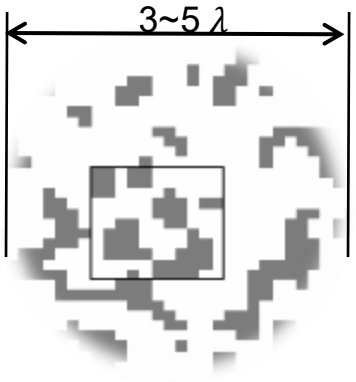

Coherent wave	Incoherent wave
$\langle \overline{E}_s(\theta_s, \varphi_s) \rangle = \frac{1}{N_r} \sum_{i=1}^{N_r} \overline{E_s^i}(\theta_s, \varphi_s)$	$\tilde{E}_s^i(\theta_s, \phi_s) = \overline{E}_s^i(\theta_s, \phi_s) - \langle \overline{E}_s(\theta_s, \phi_s) \rangle$

- Incoherent scattering power -> phase matrix and scattering coefficient
- Coherent scattering field -> effective permittivity
- Internal field -> absorption coefficient

Wet snow remote sensing

ZJUI

- Spatial-temporal distribution of SWE
- Snow melting process

Great impact

Climate change and hydrological processes

Key scientific challenge

Quantifying and describing their changing patterns

need

Wet snow microwave scattering models

Support/ improve the ability

Snow parameter retrieval (SWE/SD)

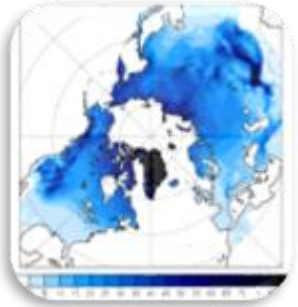

Methodology

1. Geometric characterization of the tri-continuous media

Accurately representing intricate internal composition of wet snow

- Generate three-phase tri-continuous media (air, ice, water)
- Microstructure of ice
- Water morphology (water film & droplets)

$$\begin{cases} ice & S(\vec{r}) > \alpha \\ water\ film & \beta < S(\vec{r}) < \alpha \\ water\ drop & S(\vec{r}) < \gamma \end{cases}$$

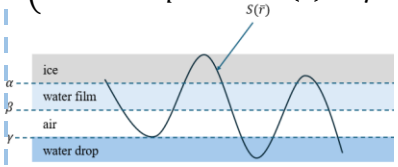

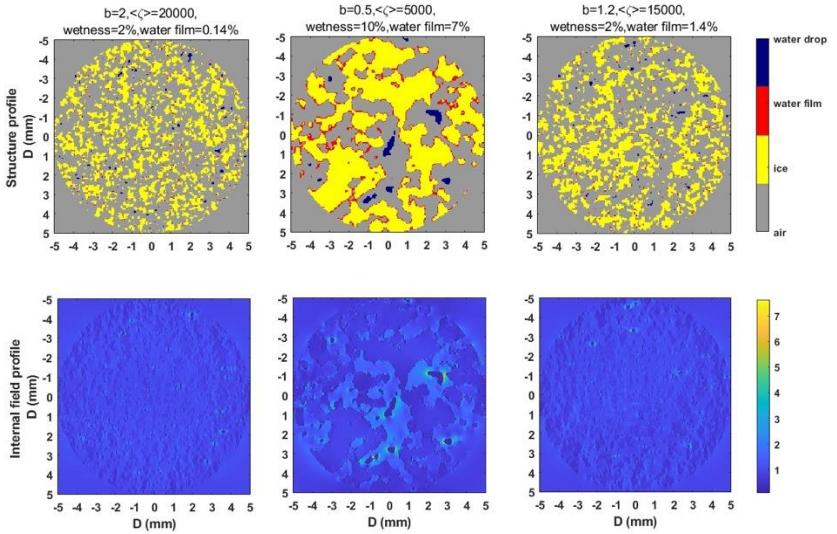

2. Electromagnetic scattering modelling of wet snow

Accurately calculating electromagnetic scattering properties

- The great difference of permittivity among air, ice and water, so that need increase the discretization density

DDA: Discrete Dipole Approximation

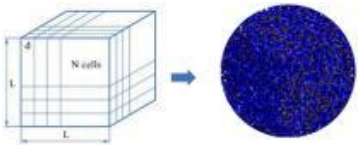

$$\bar{E}_{int}(\bar{r}_i) \rightarrow \kappa_a \rightarrow \kappa_a + \kappa_s = \kappa_e \rightarrow K'' = \kappa_e/2$$

$$\bar{E}_s(\bar{r}_i) \rightarrow \langle \bar{E}_s \rangle \xrightarrow{\text{Mie scattering matching}} \varepsilon_f \rightarrow K' = \mathrm{Re}\,(k\sqrt{\varepsilon_f})$$

$$\bar{E}_s(\bar{r}_i) \rightarrow \bar{E}_s^{inc} \rightarrow P \rightarrow \kappa_s$$

$$K = K' + iK''$$

$$\varepsilon_{eff} = (K/k)^2$$

Key results

1. The effect of microstructure parameter b (control the grain distribution) and $\langle \xi \rangle$ (inverse with grain size) on scattering properties

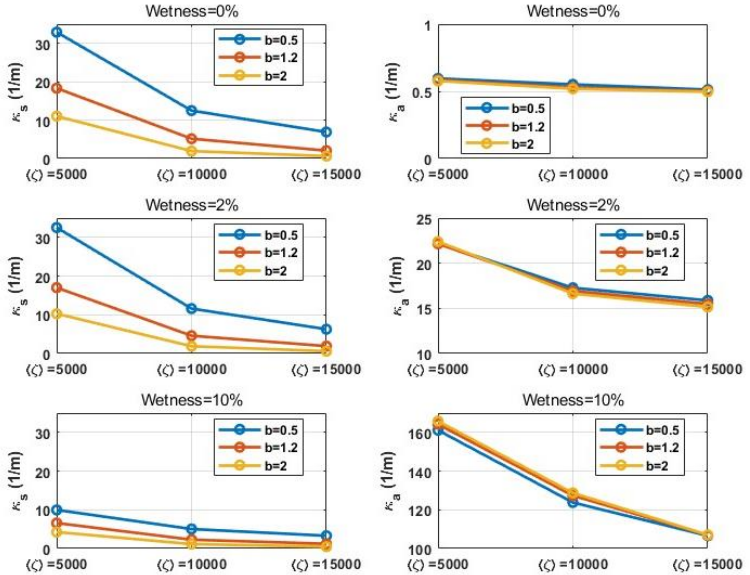

- Small grain size, less κ_a , κ_s and ε_f
- More uniform distribute, less κ_s, less affect κ_a

2. The effect of wetness and water morphology on scattering properties

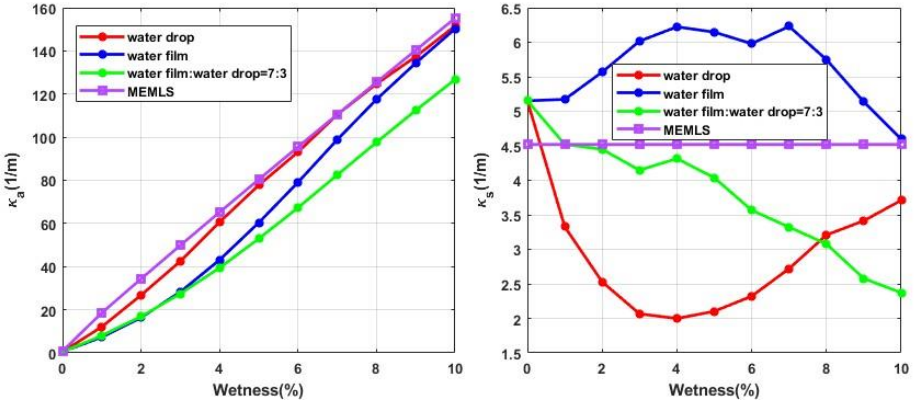

- Increase wetness, increase κ_a and ε_f
- Different water morphology affect the κ_s, but MEMLS not

Validation using tri-continuous model

Data from 2011.4.16 NoSREx

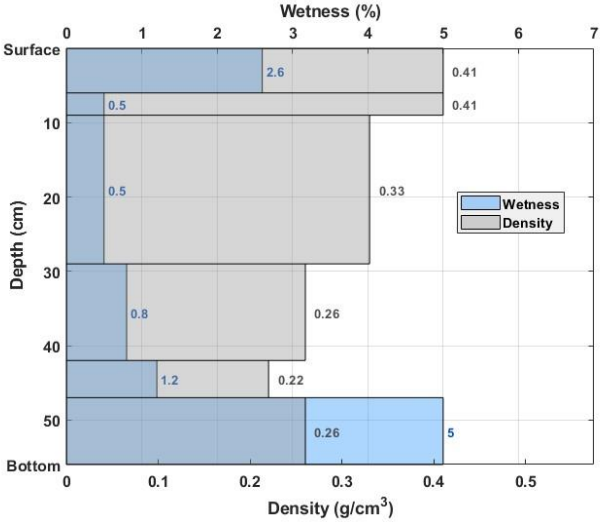

Vertical profiles of the original measured snow wetness and density for a stratified snow pit. Depth increases downward from the snow surface.

b=1.2, water morphology: water drop

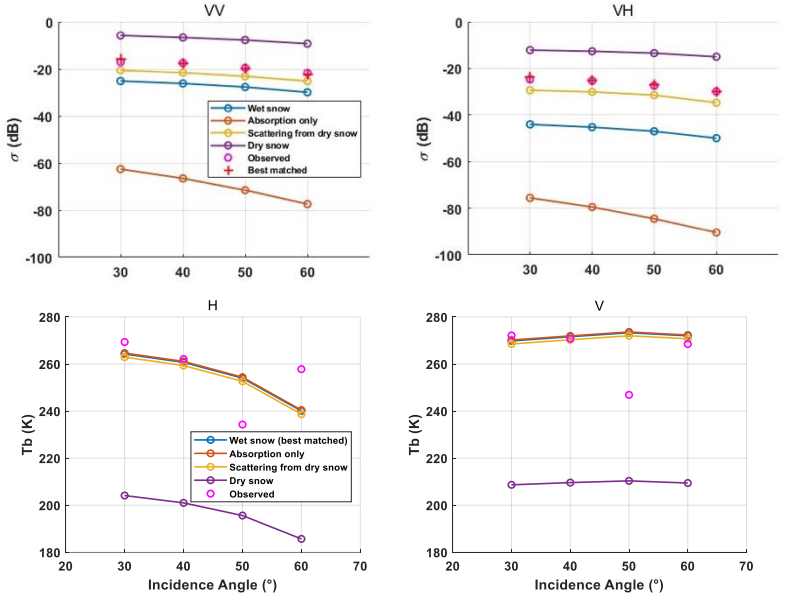

16.7GHz

37GHz

(i) the tri-continuous media results;
(ii) the scattering coefficients and phase matrix equal 0;
(iii) the scattering coefficients and phase matrix to be that of dry snow;
(iv) assume dry snow

TABLE III: Errors between simulated and observed microwave signals at 40° incidence angle

Passive (Tb)	H	V		
Error	1.88 K	0.58 K		
Active (σ)	VV	VH	HH	HV
Error	0.12 dB	0.09 dB	0.36 dB	0.62 dB

Altay campaign: Field area, devices and tools

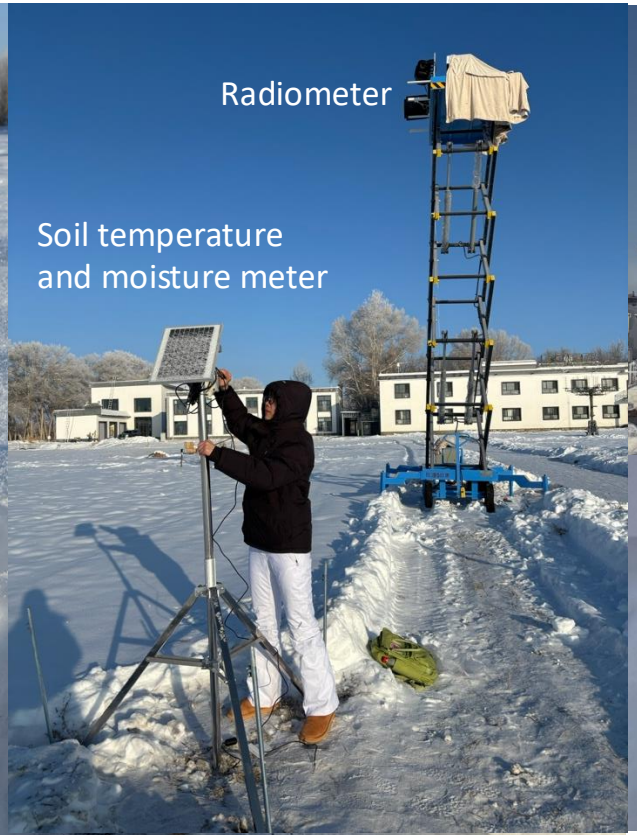

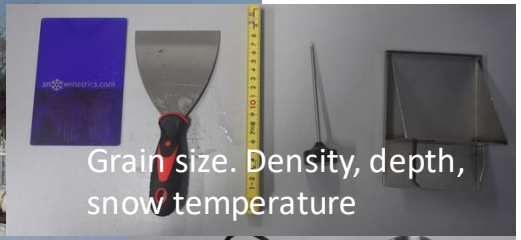

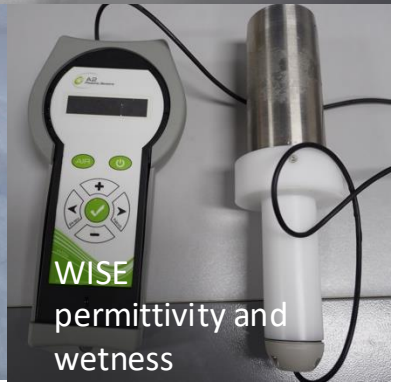

Pattern of SSA and density variation from dry to wet snow

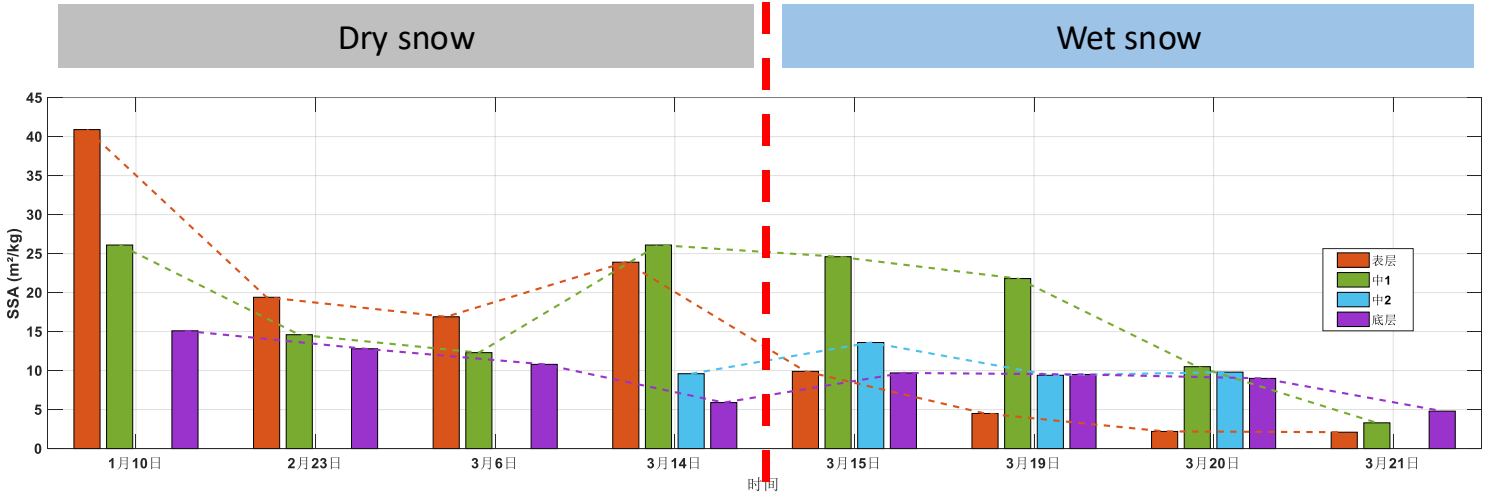

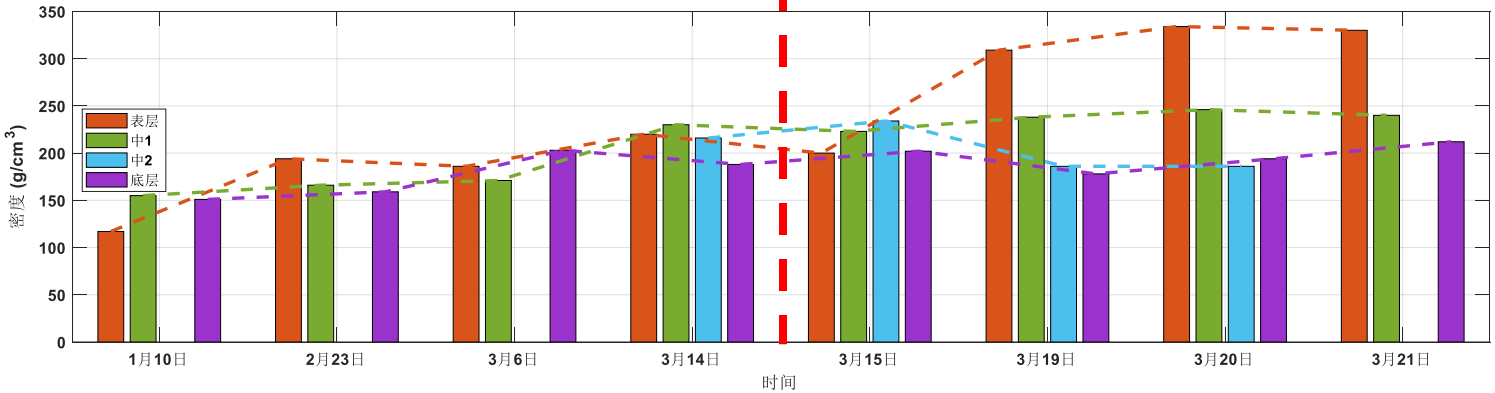

- In dry snow period, SSA (Specific Surface Area) of each snow layer decrease, a rise on Mar 14 due to the snowfall, surface layer has largest SSA.
- In wet snow period, overestimated grain size, surface SSA dropped sharply.

- During the dry snow period, the density of all layers showed an overall increasing trend.
- In the wet snow period, the surface layer density increased significantly over time, while the other layers showed little change.

Tb variation during the whole observed period

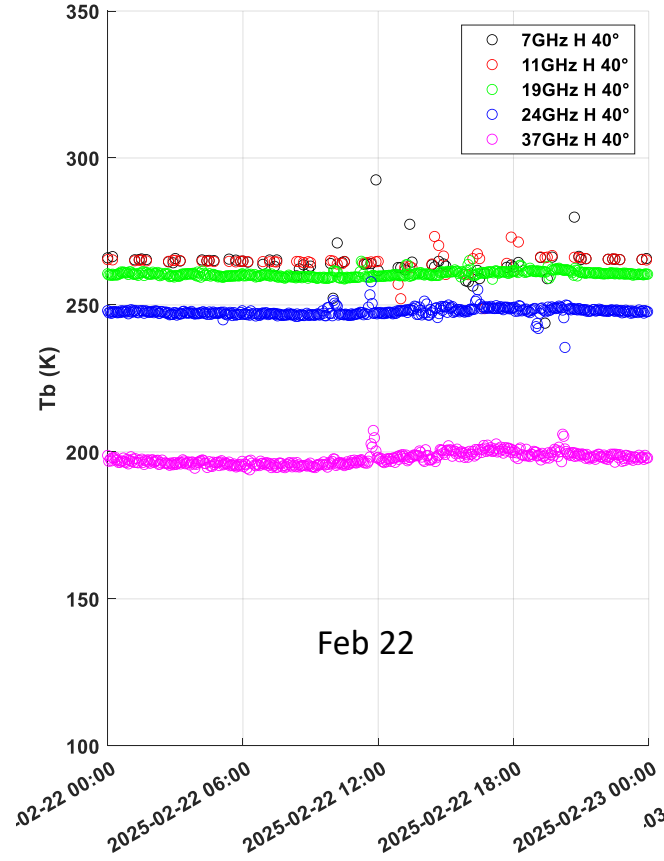

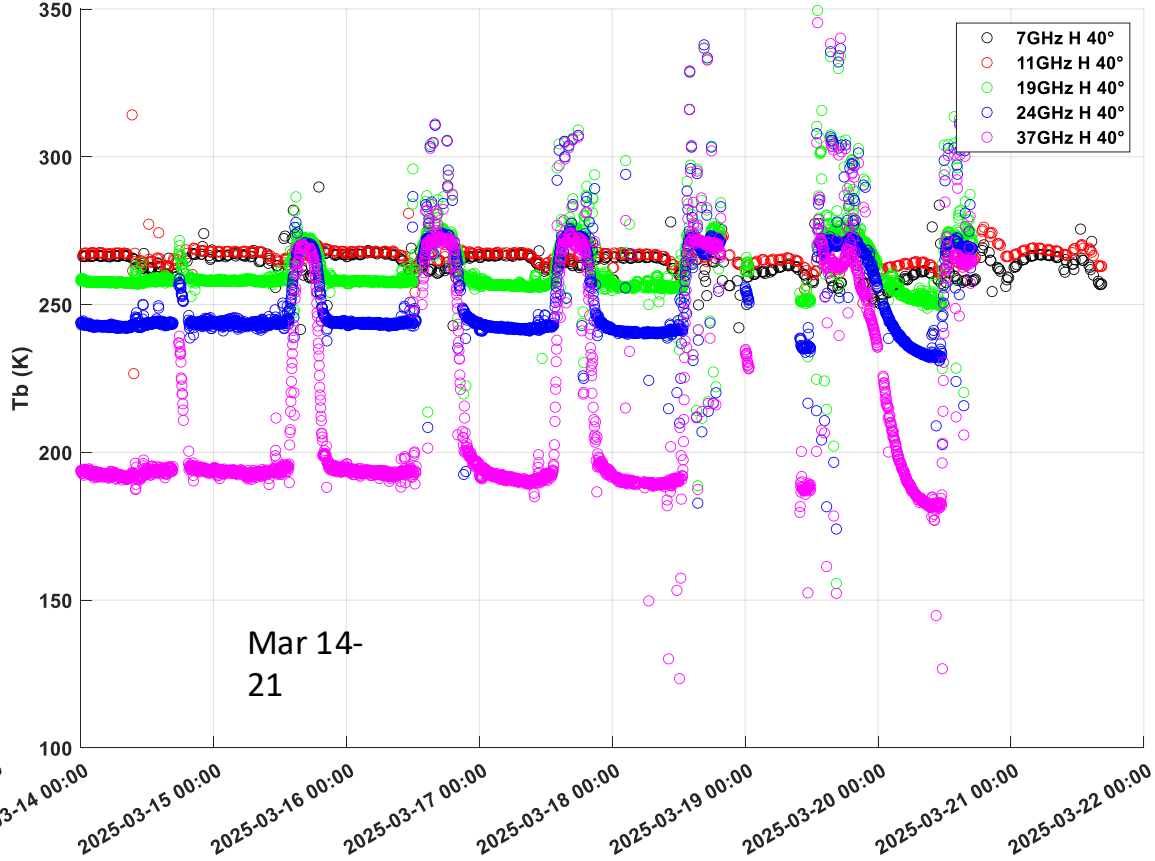

- During the dry snow period, the Tb remains stable throughout the day.
- During the wet snow period, melt-freeze cycles occur, and after refreezing, the minimum Tb at high frequencies is lower than that during the dry snow period.

Daily Tb variation during the wet snow period

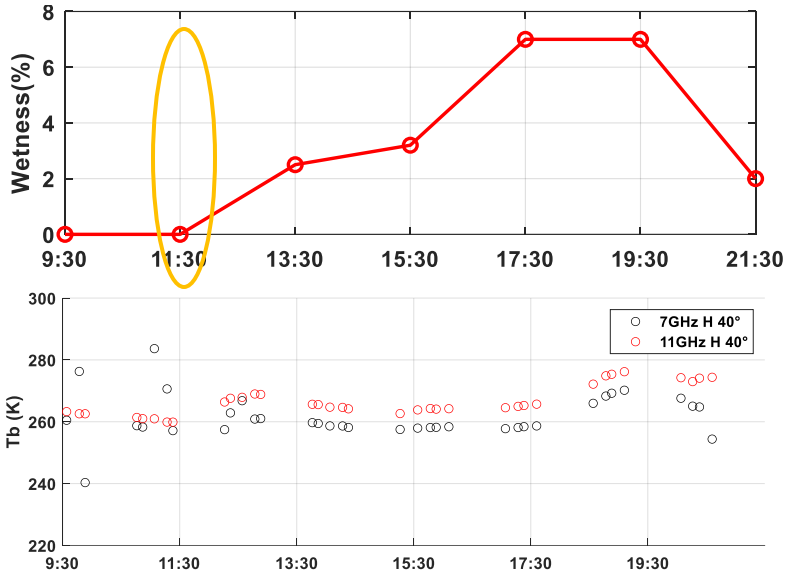

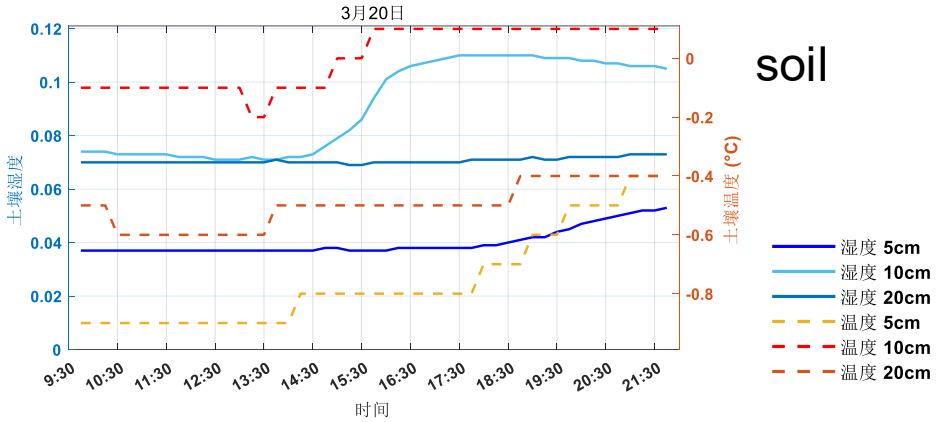

soil

- Tb are relatively sensitive during the transition from dry snow to the initial occurrence of wet snow (yellow circle).
- When the wetness continues to increase, Tb exhibit large fluctuations or even a decrease (red circle):
- Soil temperature began to rise from 13:30, with the temperature at 10 cm depth increasing the most. Soil moisture at 10 cm showed a significant increase after 15:00.

Summary of Microwave Scattering in Snowpack

- Partially Coherent Approach of QCA/DMRT, Bic/DMRT, Tri-cont./ DMRT: Homogenization
  - Calculate Phase Matrix, Extinction, Effective Permittivity for a Block of Snow, Substitute into RT equations

- Wet snow modeled with tri-continuous random media
  - Compares well with NoSREx data at Ku (σ) and Ka (Tb) bands

- Altay experiments show Tb sensitivity to snow wetness at earlier stages of snow melting with small wetness.
  - Signatures distinct for different frequencies.

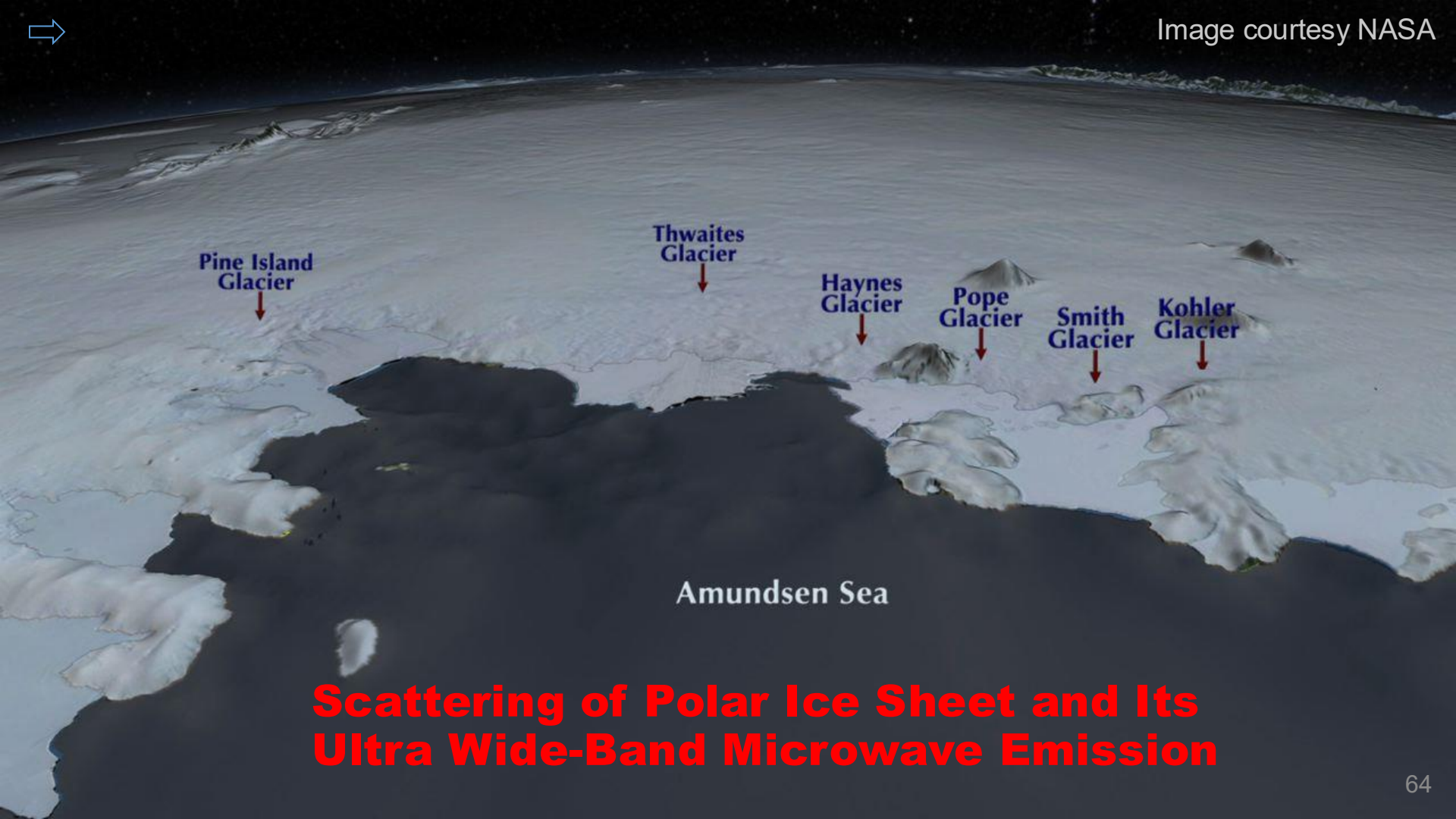

Scattering of Polar Ice Sheet and Its Ultra Wide-Band Microwave Emission

UWBRAD to Probe Ice Sheet Temperature Profile

- **0.5 - 2 GHz radiometry: lower frequency penetrates deeper**
- **Density fluctuation cause layering**
- **Kilometer thickness**

- **Negligible volume scattering**
- **Densely packed weak reflective layers**
- **Expect coherent layer effects**

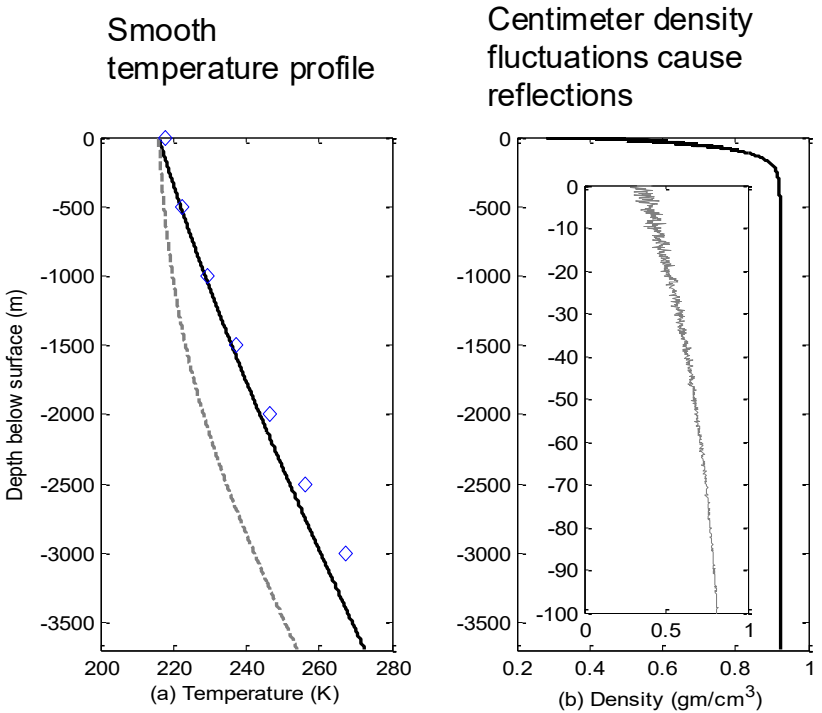

Temperature / density profile of Antarctica ice sheet

Incoherent & Coherent Models

❑ Incoherent model

- $r = |R_{01}|^2 + |R_{12}|^2$
- **Addition of intensities**
- **Solution of radiative transfer equation**
- **Model applied to thousands of layers**

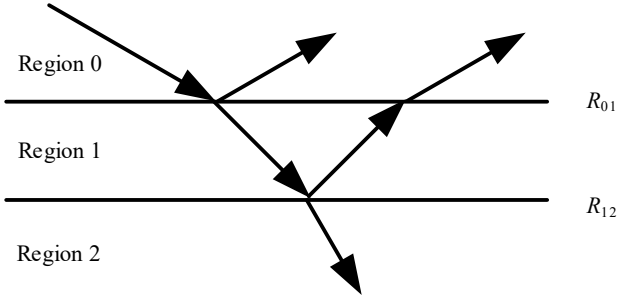

Apply to ice sheet with thousands of interfaces

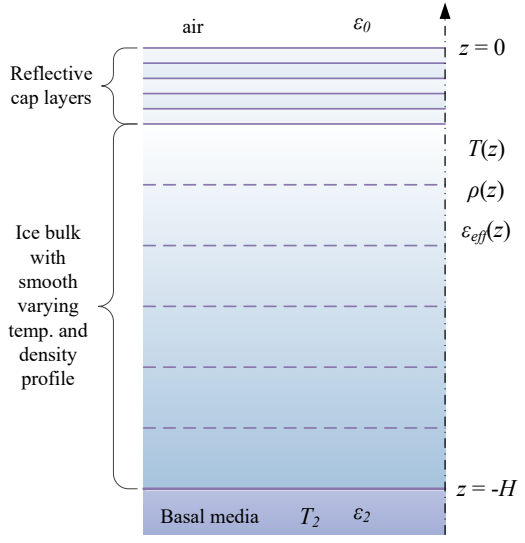

❑ Coherent model

- $r = \left|R_{01} + R_{12}e^{i2k_{1z}d}\right|^2 = |R_{01}|^2 + |R_{12}|^2 + 2\mathrm{Re}(R_{01}^* R_{12} e^{i2k_{1z}d})$
- **correlation term with phase**
- **Solution of Maxwell's Equation**
  - **Fluctuation dissipation theorem**
  - **Layered Medium dyadic Green's function**
- **Model applied to thousands of layers**

Coherent Model Compared with Incoherent Models: Frequency Dependence

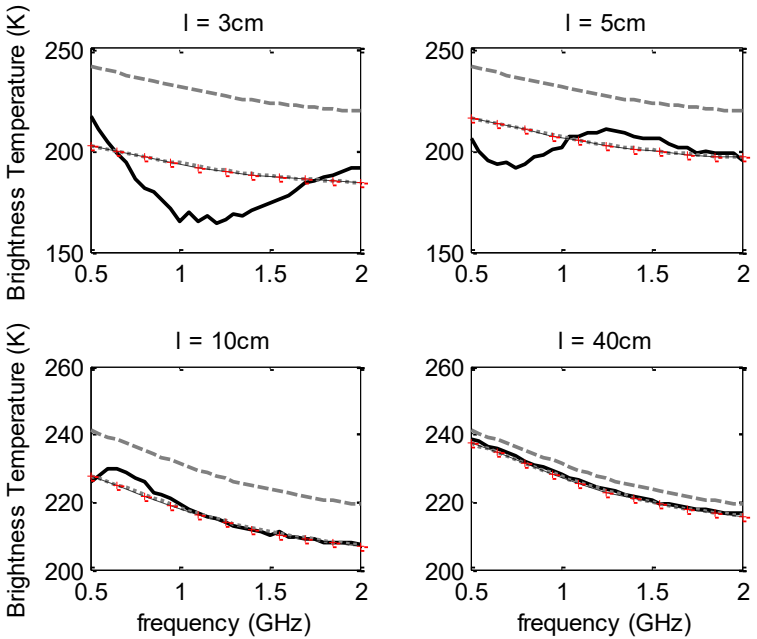

$\Delta = 0.040\text{g/cm}^3$; $\alpha = 30\text{m}$
$M = 0.01\text{m/yr}$; $T_s = 216\text{K}$
$H = 3700\text{m}$; water base

- Incoherent models: monotonic
- (Black) Coherent: resonance scattering for short correlation length
  - $l \sim \lambda/4$: maximum reflection
  - $l \sim \lambda/2$: minimum reflection

a) Cloud Model: grey dashed curve;
b) DMRT-ML: grey dotted;
c) MEMLS: black-dashed with red markers;
d) Coherent: black solid.

Tan et al., 2015. Physical models of layered polar firn brightness temperatures from 0.5-2 GHz. *IEEE J. Sel. Topics Applied Earth Observ. Remote Sens.*, vol. 8, pp. 3681-3691.

The Partially Coherent Model

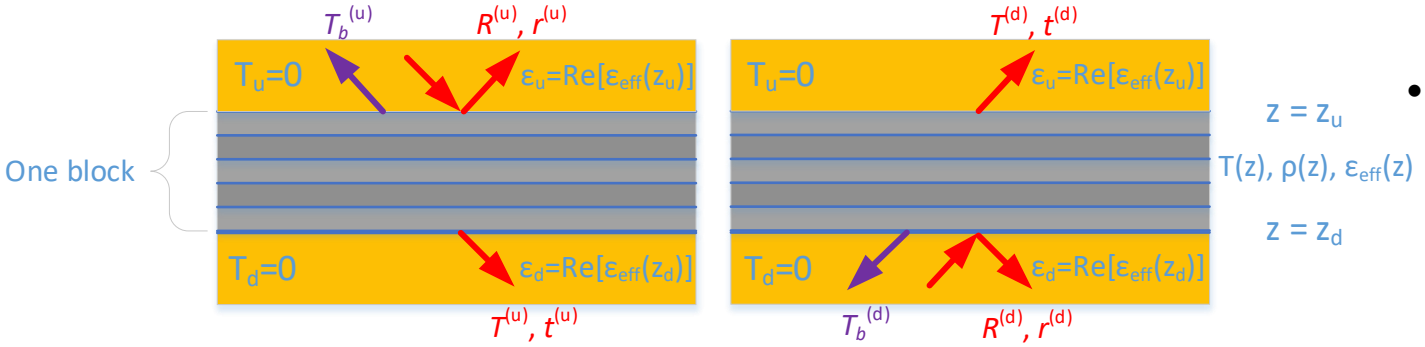

(a) excitation / observation from top (b) excitation / observation from bottom

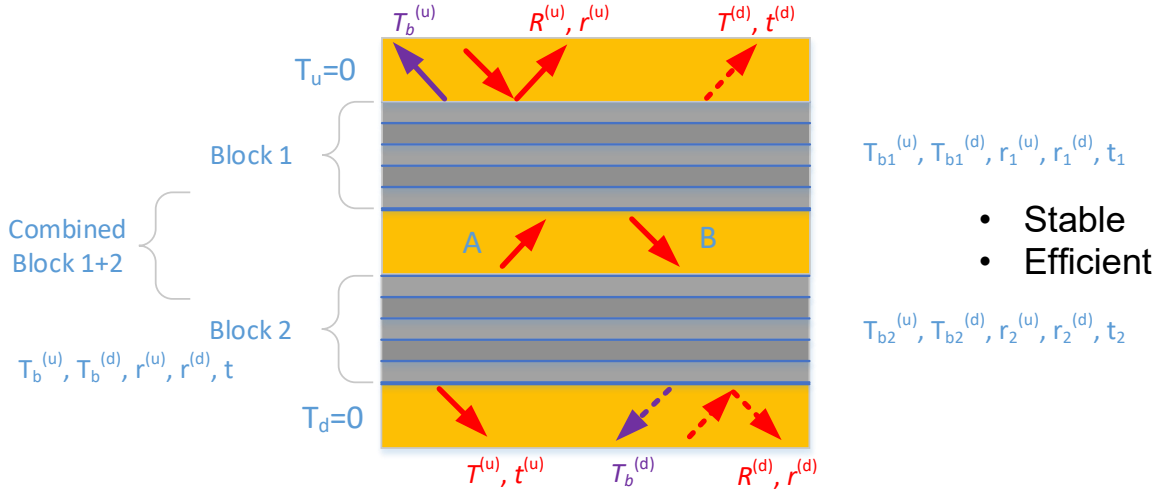

- Coherent interactions within a block: Maxwell Equations
- Incoherent interactions between blocks: Radiative Transfer Equation
  - Stable
  - Efficient

Results and CPU 6 times Speedup

$l = 3cm$

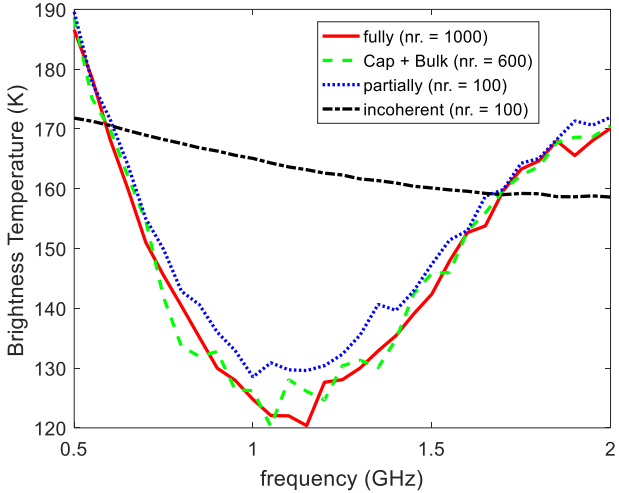

In partially coherent model, block size = $\max(10\lambda, 10l)$

$l = 3cm$	# real.	CPU per Freq.
Partially	100	10.4 sec
cap + bot.	600	44.8 sec
Fully	1000	60.3 sec

$l = 9cm$

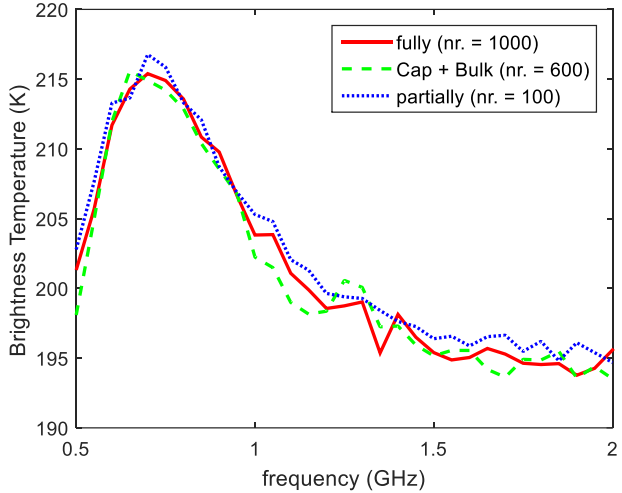

$l = 9cm$	# real.	CPU per Freq.
Partially	100	5.8 sec
cap + bot.	600	18.2 sec
Fully	1000	31.0 sec

- Partially coherent: Results agree with fully coherent approach.

Partially Coherent Model Applied to Greenland Summit Emission

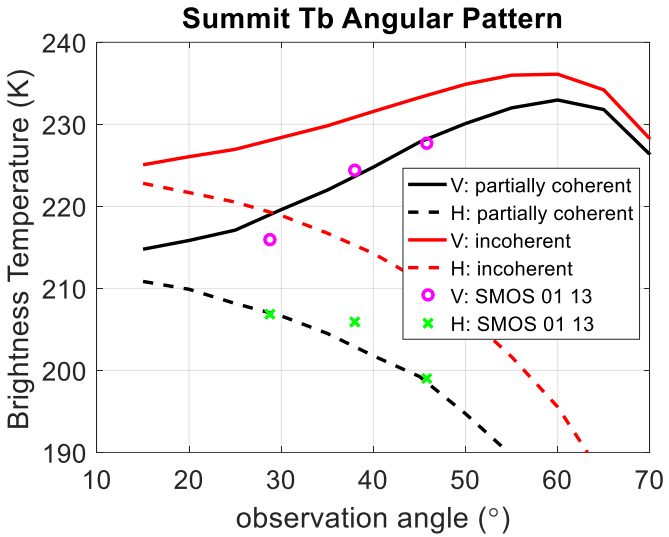

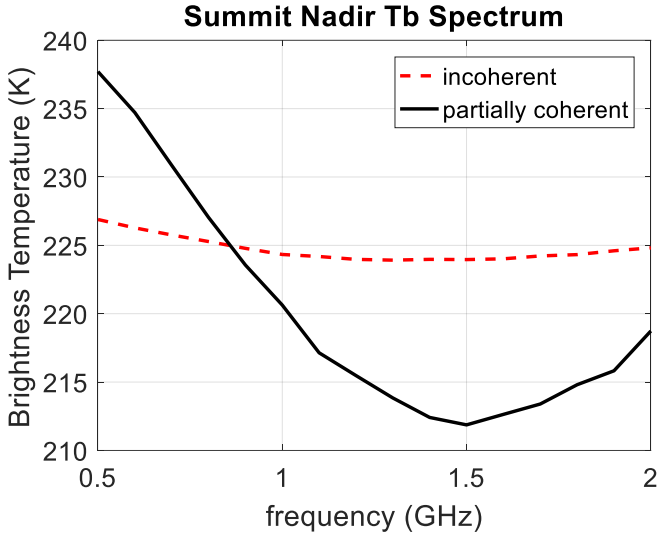

- Model driven by in-situ temperature & density profiles
- Results agree with L band SMOS data
- Coherent layer effects cause strong frequency dependent Tb spectrum

Tan, 2016. Multiple Volume Scattering in Random Media and Periodic Structures with Applications in Microwave Remote Sensing and Wave Functional Materials, Ph. D. dissertation, University of Michigan, Dec. 2016.

Multi-layer Roughness (hundreds of rough interfaces with weak permittivity contrasts)

- Density fluctuation introduces layers as well as rough interfaces
- Roughness introduces polarization and angular coupling
- Tb and emissivity prediction requires energy conservation
- 2nd order Small Perturbation Method (SPM2) conserves energy independent of roughness and layers

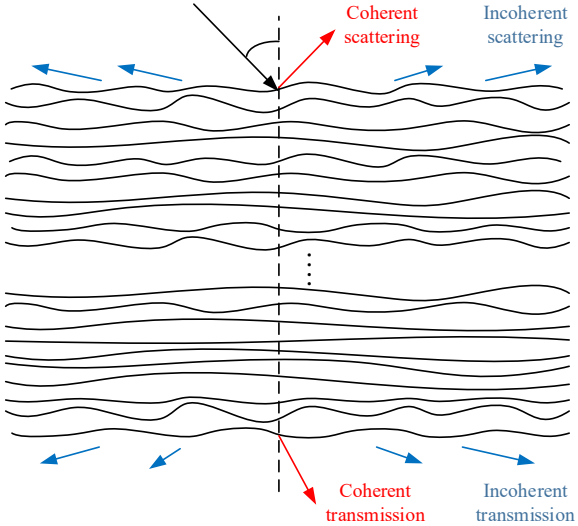

2m Snowpit @ Summit

Partially Coherent Approach Extended to Incorporate Multi-layer Roughness

- Energy conservation critical to brightness temperature predictions

- Partially coherent approach extended to include roughness
  - Coherent interactions within a block: SPM2 for Maxwell equations
  - Incoherent interactions between block: Radiative Transfer Equation

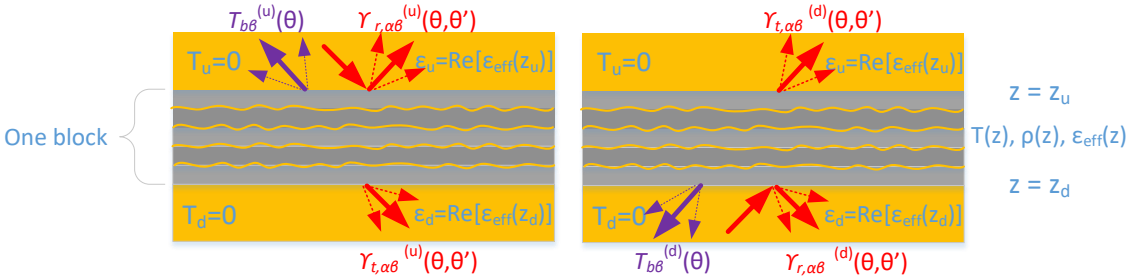

(a) excitation / observation from top (b) excitation / observation from bottom

Roughness: Model Compared with SMOS Data, Antarctica, Dome C

Without roughness

Use physical temperature profile, and thousands of interfaces

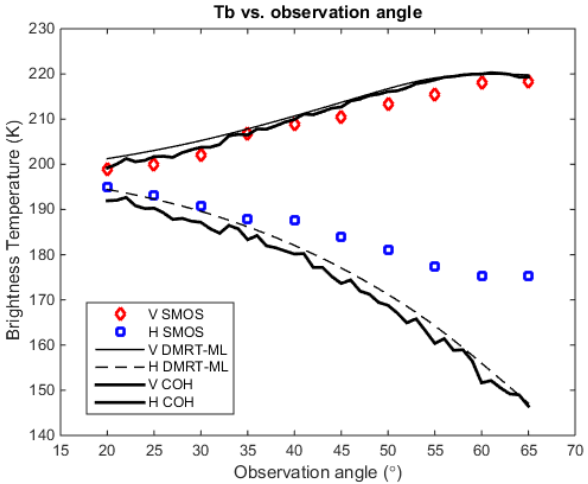

$\Delta = 0.04\text{gm/cc}$, $l = 9\text{cm}$, $\alpha = 70\text{m}$

1000 Monte Carlo simulations

With roughness

20 rough interfaces, Gaussian correlation

$h_{rms} = 1.5\text{cm}$, $l = 25\text{cm}$,

constant $T_0 = 228\ K$

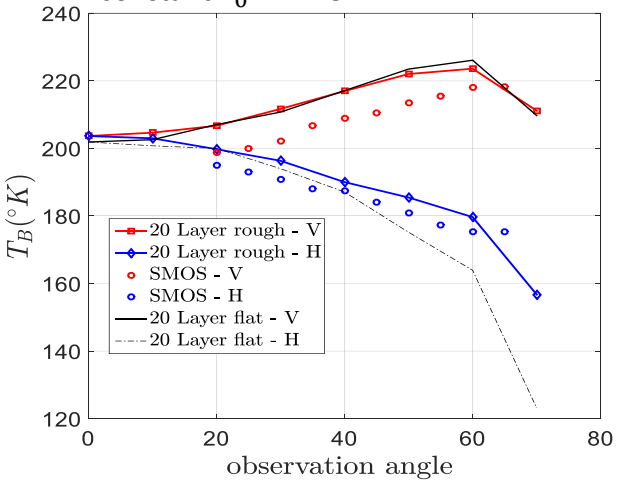

$\Delta = 0.18\text{gm/cc}$, $l = 9\text{cm}$, $\alpha = 3\text{m}$

400 realizations

- Roughness increases H-pol emissivity at large angles
- TE and TM emissivities agree at nadir.

Sanamzadeh et al., 2017, Scattering of Electromagnetic Waves from 3D Multi-layer Random Rough Surfaces Based on the Second Order Small Perturbation Method (SPM2): Energy Conservation, Reflectivity and Emissivity. JOSA A, vol. 34, pp395-409.

UWBRAD Greenland flight line (blue) of September 15, 2016 and ice sheet and sea ice flight of September 13-14, 2017

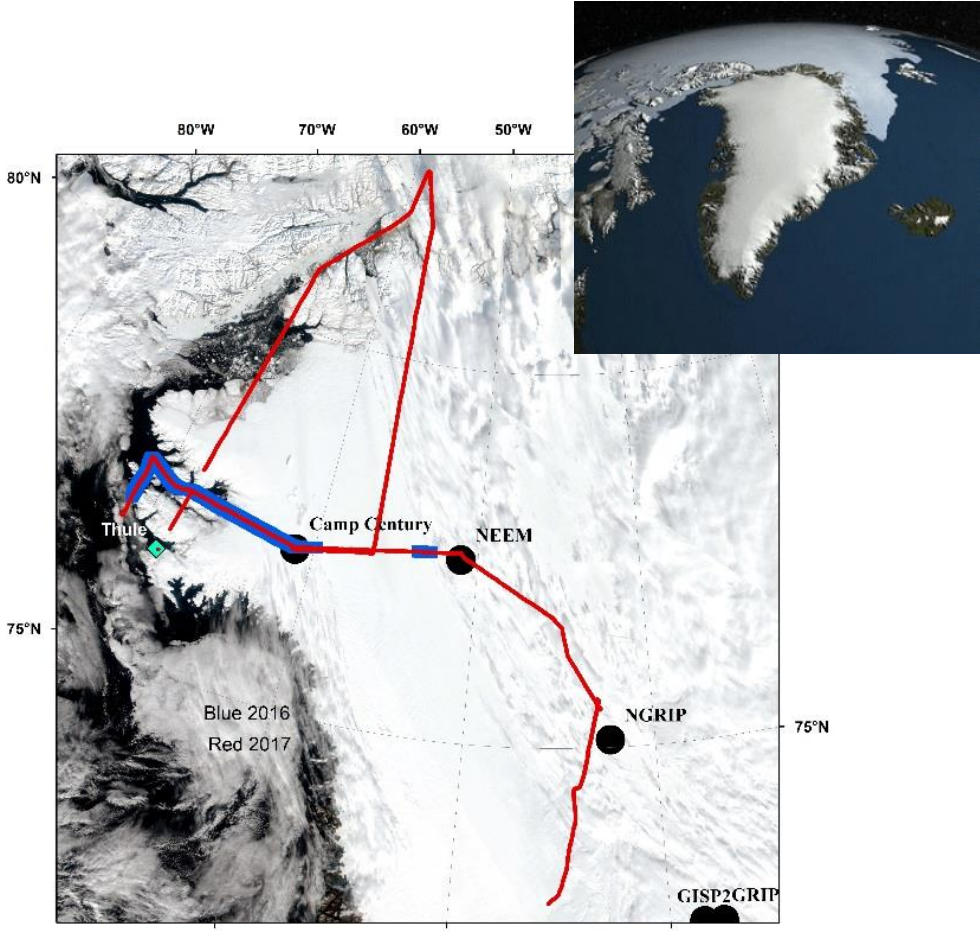

Greenland Sep 2016 Campaign Data Analysis

- Data collected over 3 different media of interest:
  - Ice free ocean
  - Snow covered land
  - Melt zones characteristic of the Greenland Ice Sheet

- Tb decreases rapidly as the flight proceeds onto the ice sheet before increasing as Camp Century is approached

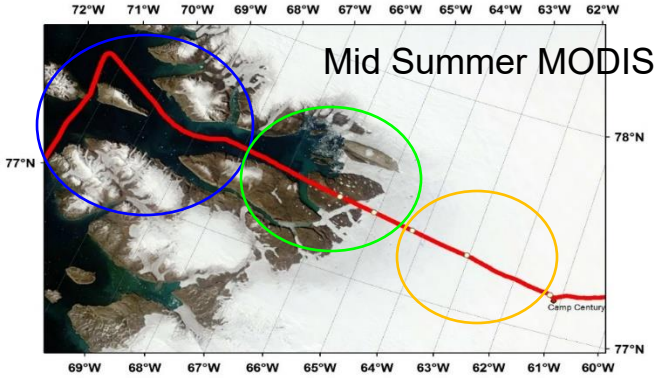

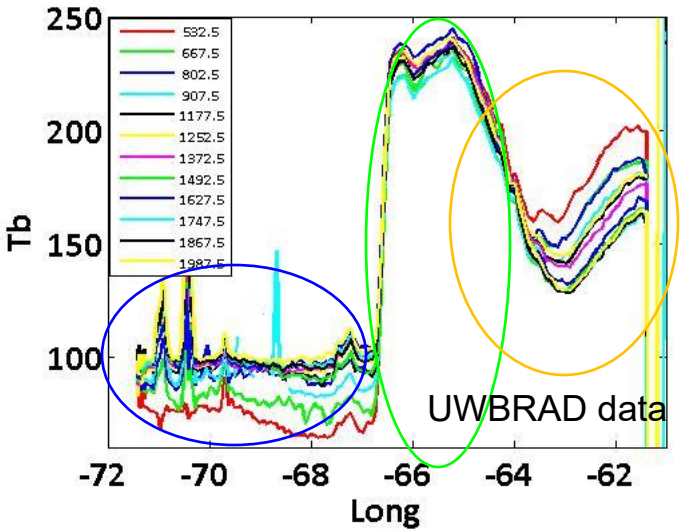

Spectra of Facies (2016 vs 2017)

- Rock and ablation facies spectra appear flat across the band
- 20 K-40K changes for percolation facies and also at the site near Camp Century
- Wet snow facies have a range of about 10 K
- Some systematic calibration effects apparent but signatures seem reasonable

(2016 - thin vs 2017 - heavy)

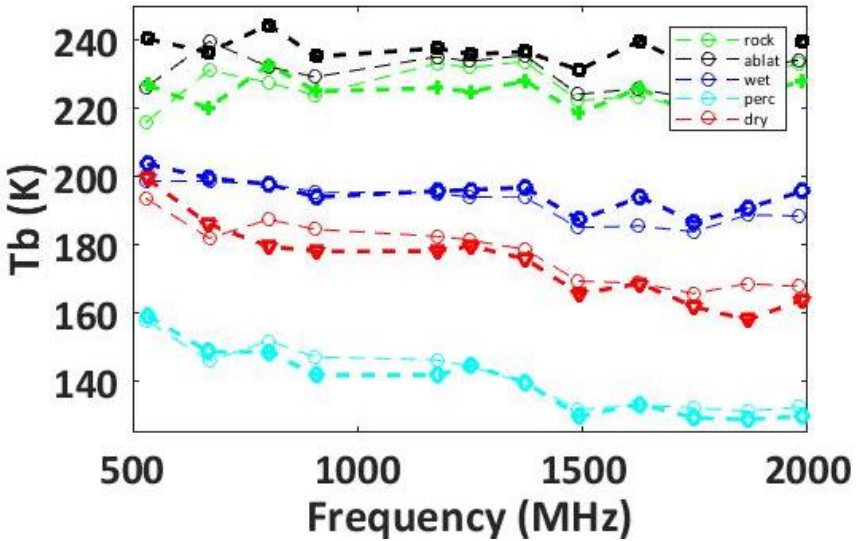

UWBRAB Data Spatial Variation & Correlation with L-band PALSAR Backscatter

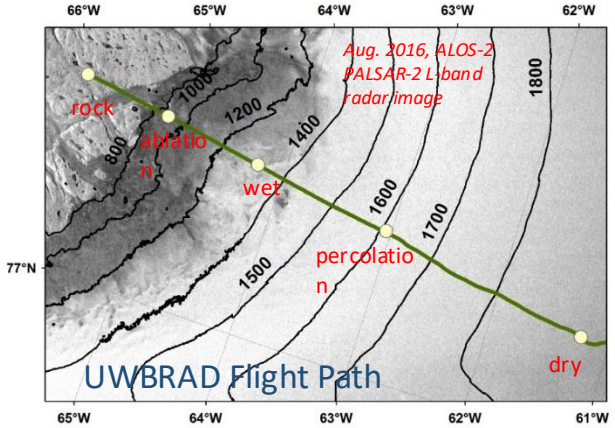

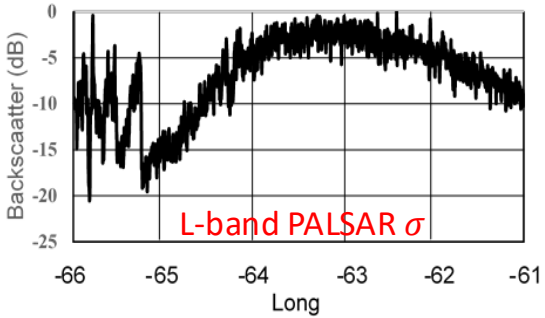

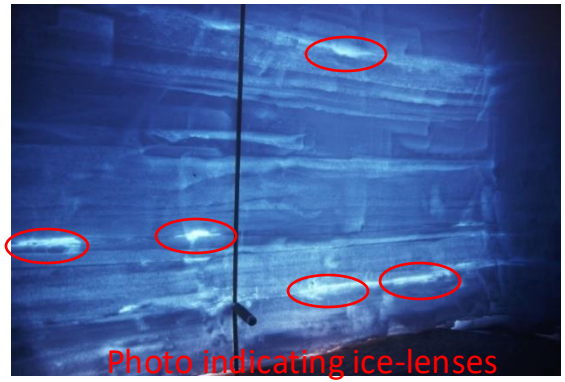

UWBRAD T_b

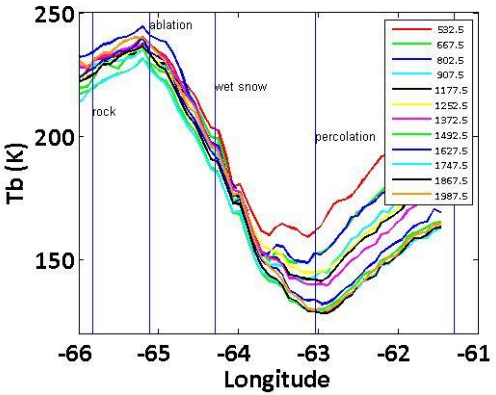

- Good correlation in T_b, σ & ice facies.

- Ice-lenses, ~10cm in diameter, cause backscatter

Jezek et al., 2017. 500-2000 MHz brightness temperature spectra of the Northwestern Greenland ice sheet, submitted to *IEEE TGRS*.

Brightness Temperatures Incorporating Volume Scattering From Ice Lens (Disks)

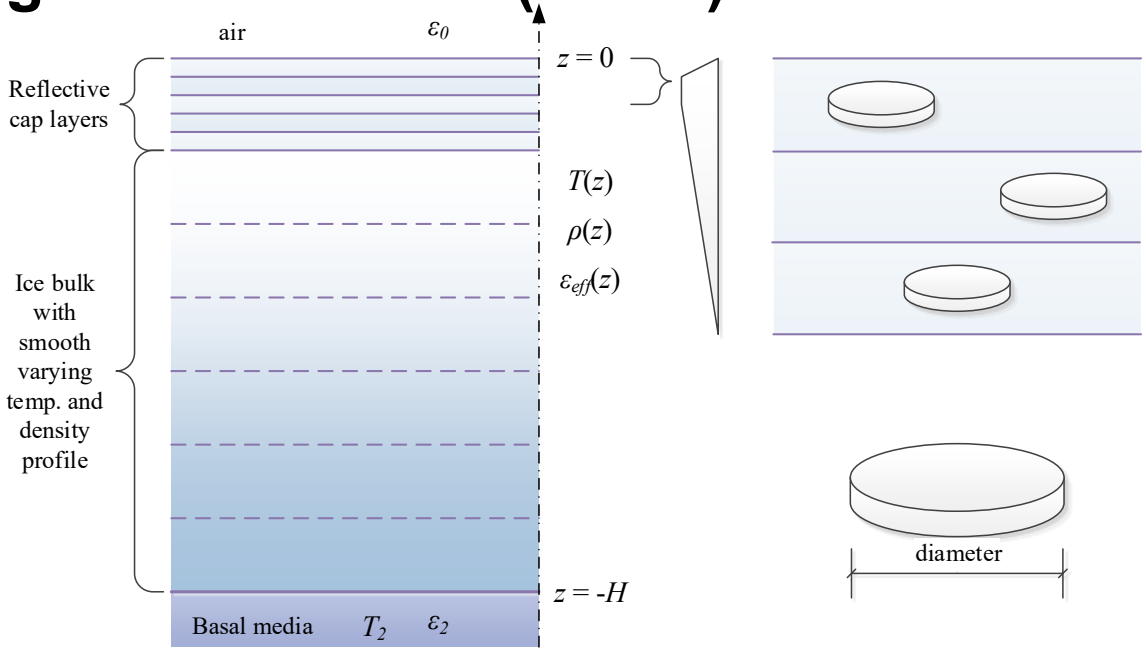

- Calculate Tb without ice lens (disks)
- Apply ice lens scattering corrections

$$T_b \approx T_b^{\text{cloud}}(1 - r)\exp(-\tau_s)$$

Tb Spectra in Various Facies: Model vs. Data

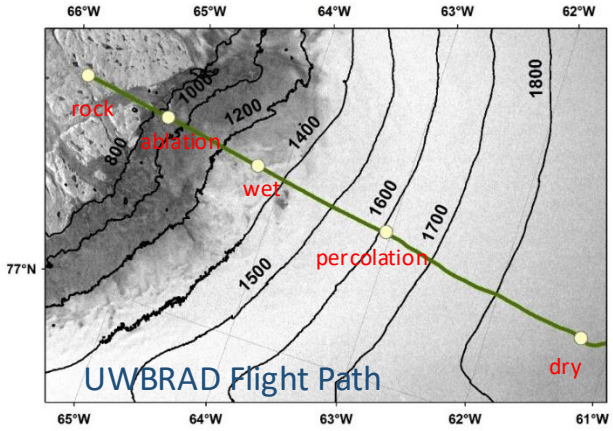

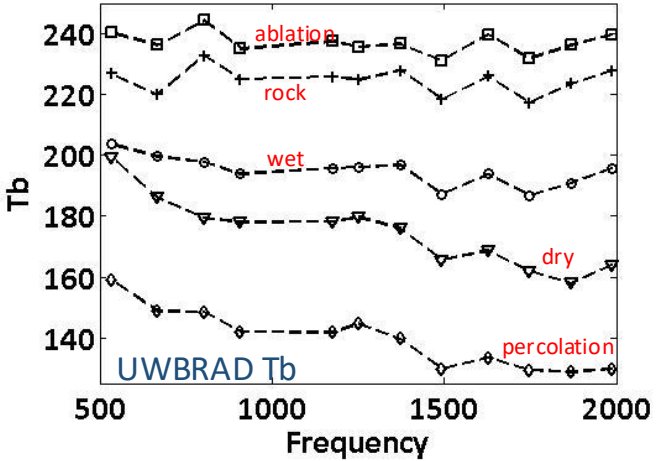

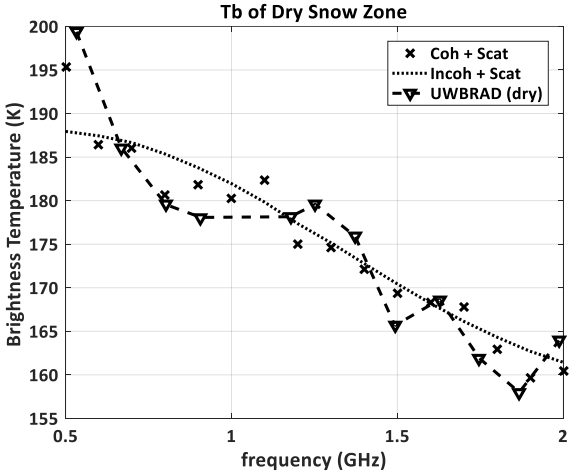

$\Delta = 0.080\text{gm/cm}^3$
$l = 15\text{cm}$
$\alpha = 75\text{m}$
$n_0 = 6/\text{m}^3$

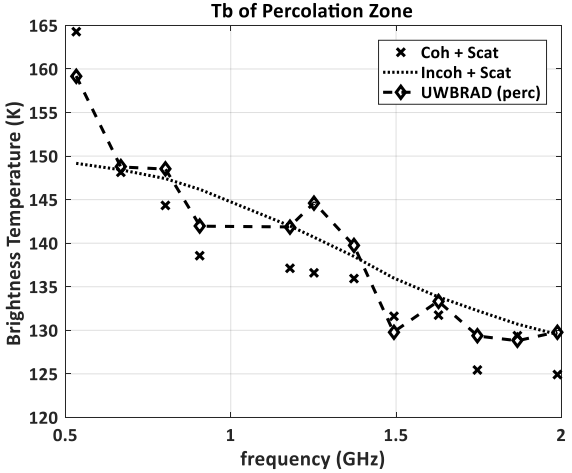

$\Delta = 0.13\text{gm/cm}^3$
$l = 12\text{cm}$
$\alpha = 50\text{m}$
$n_0 = 9/\text{m}^3$

Tb Spatial and Spectral Patterns: Model vs. Data

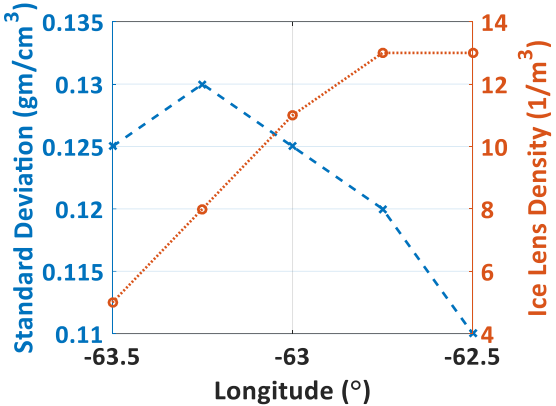

Δ affect mean Tb

n_0 affect spectral differences

n_0 estimated from T_b^{cloud}/T_b

Left: UWBRAD measurements

Right: Model Predictions

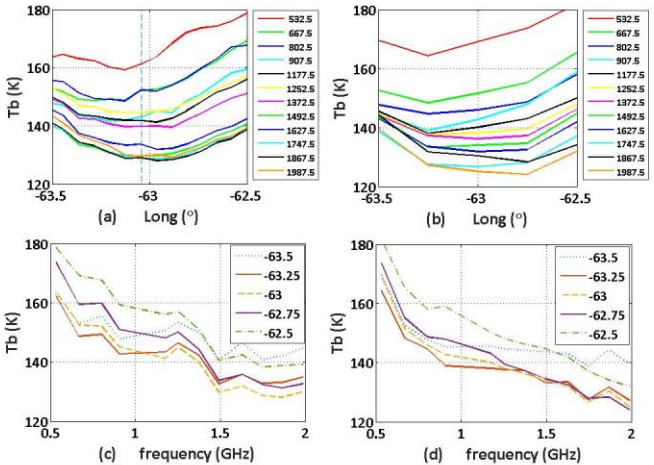

- Good agreement in Tb spatial and spectral patterns
- Interplay of density fluctuation and ice-lenses explains the shift in Tb minimum

Jezek et al., 2018. 500-2000 MHz brightness temperature spectra of the Northwestern Greenland ice sheet, *IEEE TGRS*. 56(3), 1485-1496.

Analysis of Ice Sheet Flight 2017

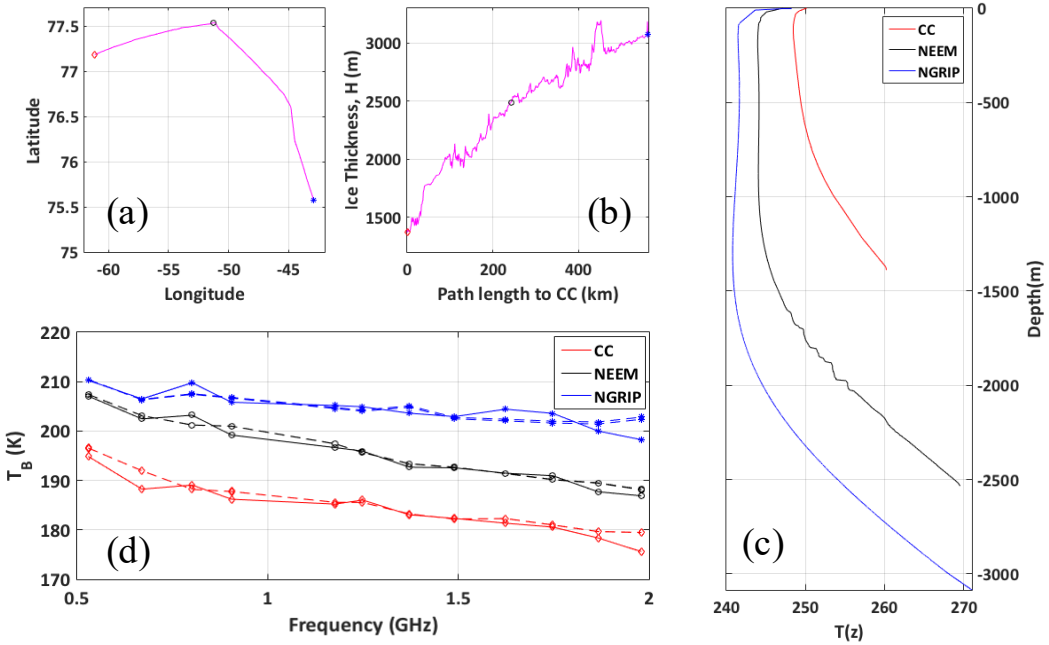

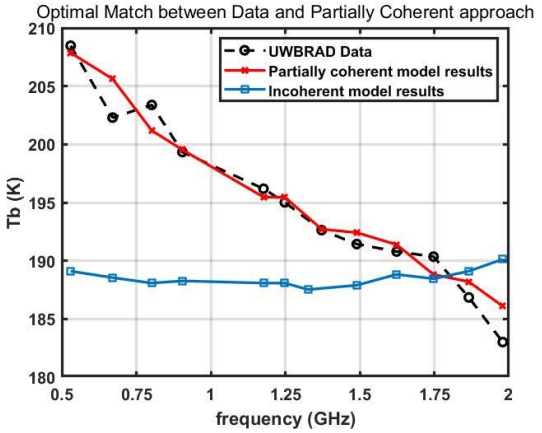

- Two-scale density fluctuation model assumed
- Coherent model captures the spectral difference

(a) Section of the flight path for Sept 14 flight starting at CC to NEEM, ending at NGRIP. (b) Ice thickness variation along CC-NEEM-NGRIP path. (c) Borehole data available at the 3 sites. (d) Measured brightness temperature vs. best fit after inversion at the 3 sites.

Greenland Ice Sheet Temperature Retrieval From UWBRAD 2017 Data

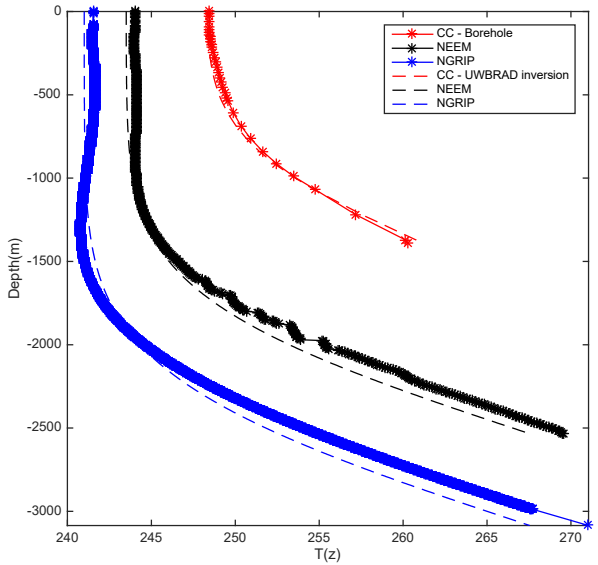

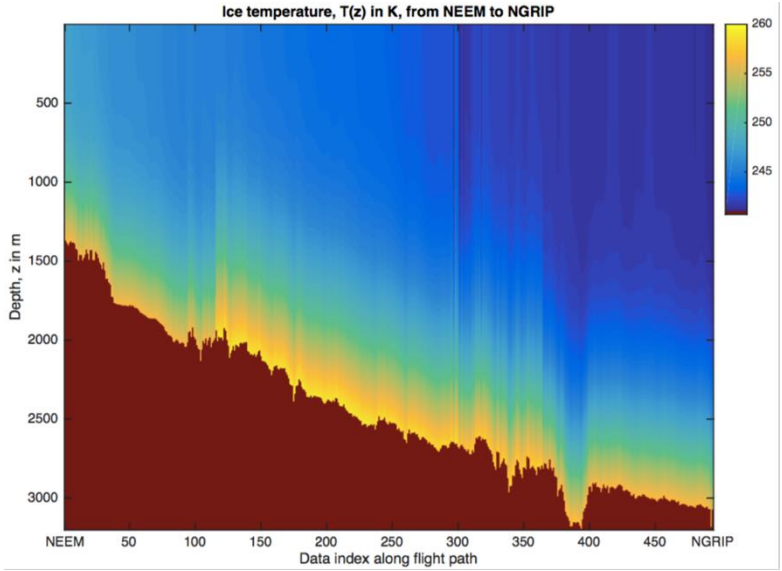

Other Possible Applications of UWBRAD

- Sea Ice thickness and salinity
- Ocean salinity
- Firn aquifer
- Permafrost
- Terrestrial Snow

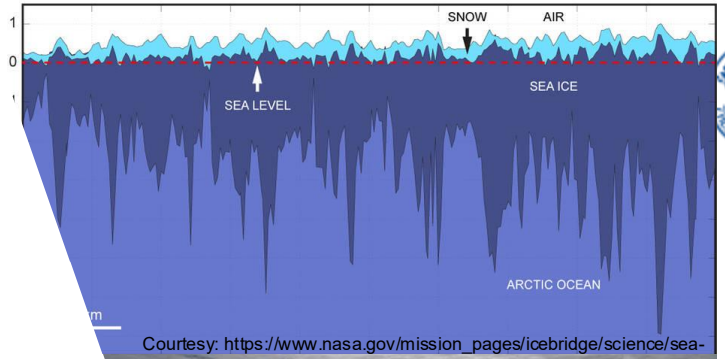

Courtesy: https://www.nasa.gov/mission_pages/icebridge/science/sea-ice.html

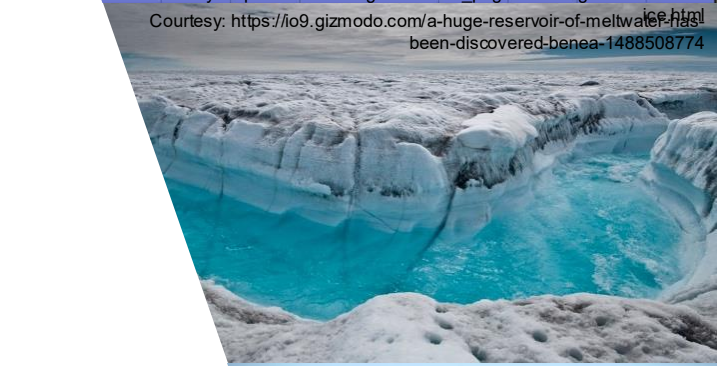

Courtesy: https://io9.gizmodo.com/a-huge-reservoir-of-meltwater-has-been-discovered-benea-1488508774

Courtesy: Nick Bonzey from Juneau, AK - The best part of the class, CC BY-SA 2.0, https://commons.wikimedia.org/w/index.php?curid=27720 14

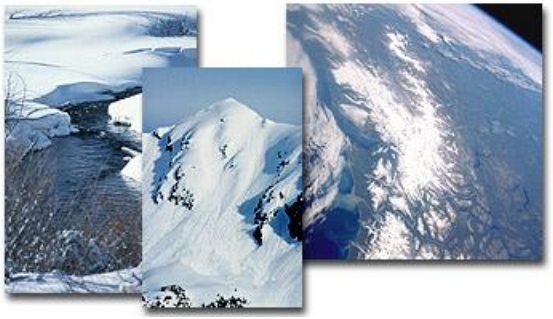

Scattering of Dense Random Media: Snow Covered Land

- Wet snow

Scattering from Structured Sparse Random Media: Vegetated Land

- Vegetation structure
- Volume surface coupling

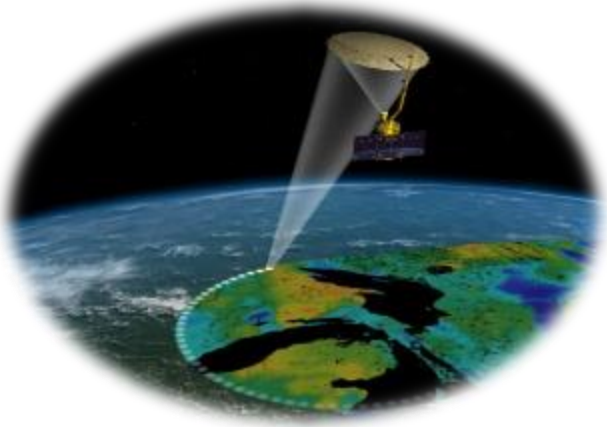

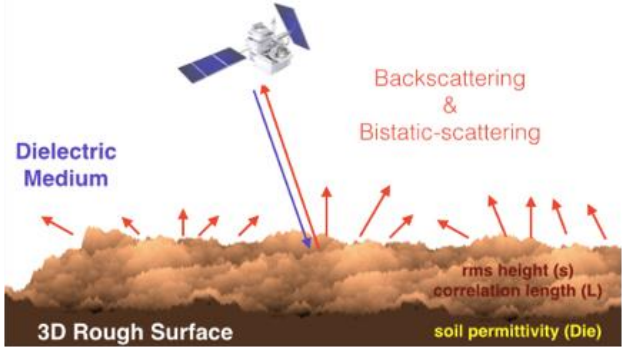

Scattering from Rough Surfaces: Bare Soil

- NMM3D-VIE: vertical soil inhomogeneity

Towards AI enabled efficient microwave modeling

Physics-Informed Neural Networks: DDA-NN

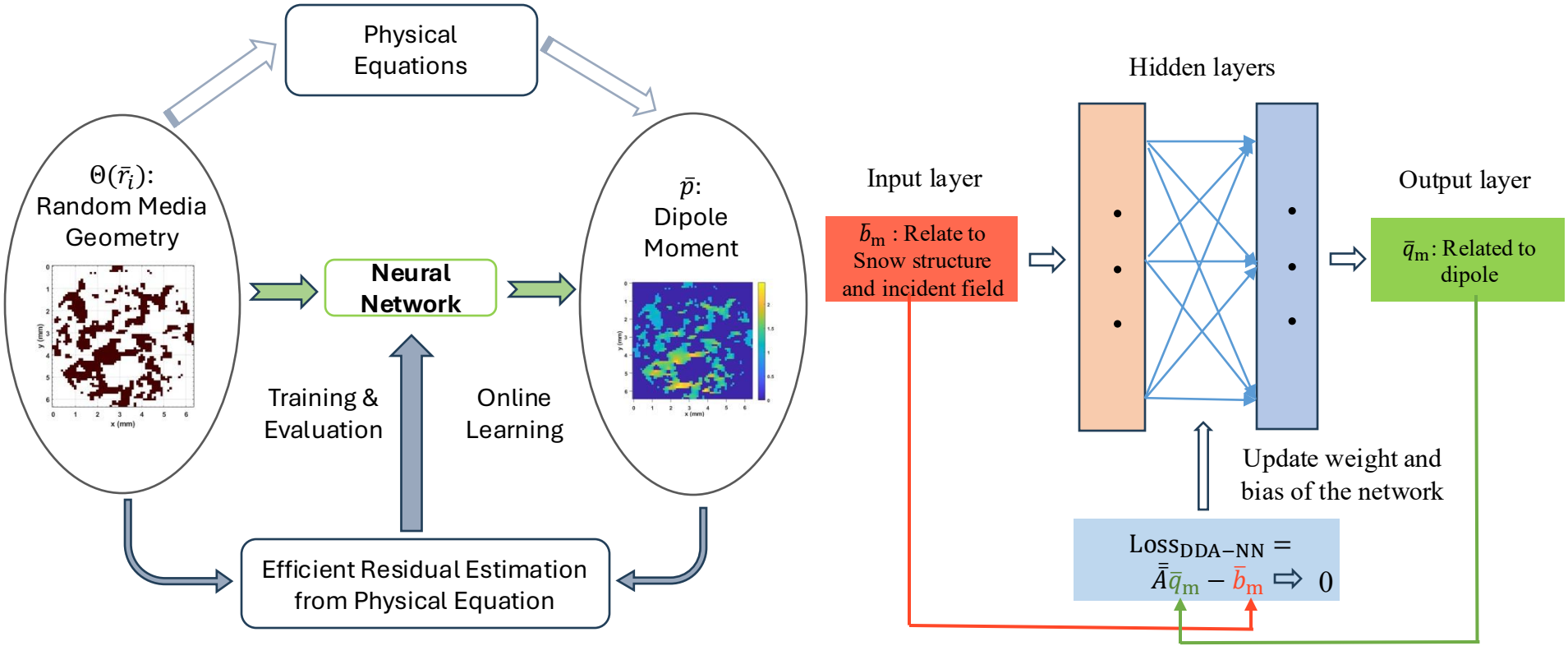

Jiayi Du, Yuanhao Cao, Chunzeng Luo, Gaoang Wang, and Shurun Tan, "Acceleration of Solving Volume Integral Equations through a Physics Driven Neural Network and Its Applications to Random Media Scattering," Progress In Electromagnetics Research, Vol. 183, 45-57, 2025. doi:10.2528/PIER25012103

Visualization of the predicted dipole and near field

ZJUI

- The model trained based on the samples with parameter of scenario 1, and then validated on samples with different structural parameter (scenario 2), and with different frequency (scenario 3)

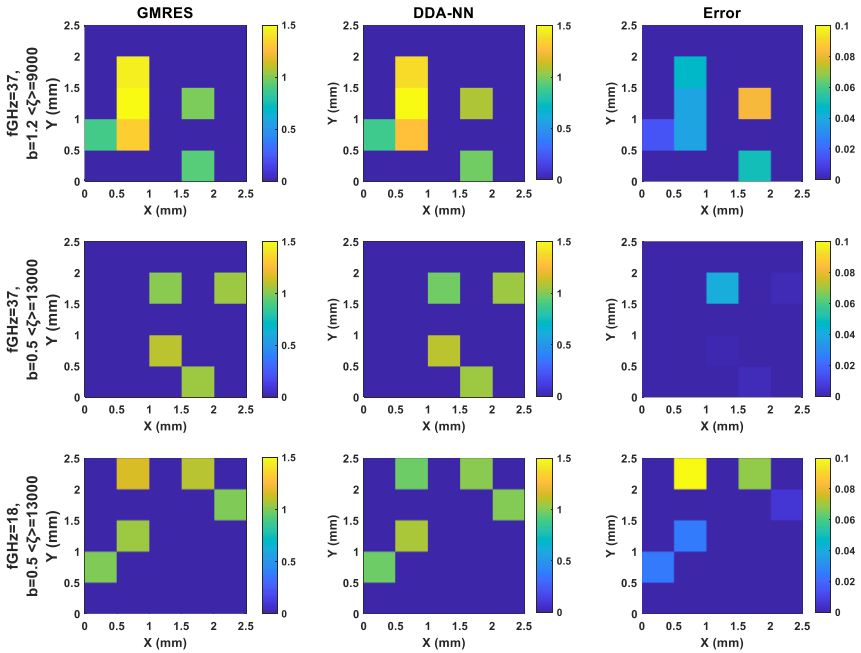

Figure 1. Results of $\bar{q}$ derived from DDA-NN compared with GMRES method. Each subplot represents a 5x5 data grid (the third layer of the voxel) for different scenarios.

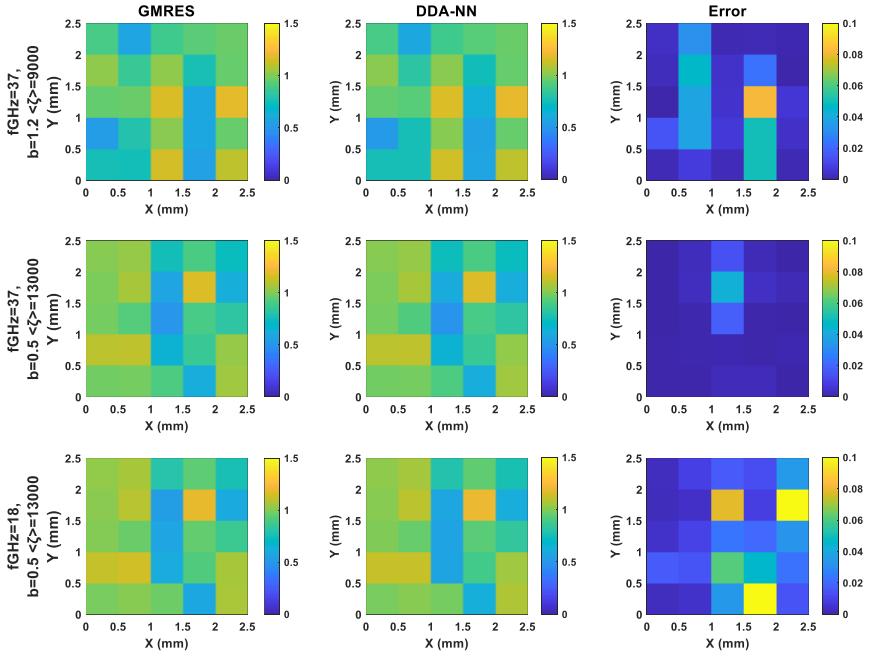

Figure 2. Results of near field derived from DDA-NN compared with GMRES method. Each subplot represents a 5x5 data grid (the third layer of the voxel) for different scenarios.

Prediction precision and efficiency

ZJUI

Table 1. RMSE comparison between $\bar{q}'$ and predicted $\bar{q}$ from two NNs for three scenarios.

Scenarios	RMSE (Data-NN)	RMSE (DDA-NN)
37GHz b=1.2, $\langle\zeta\rangle$=9000m^{-1} D=2.5mm, d=0.5mm	0.0675	0.0691
37GHz b=0.5 , $\langle\zeta\rangle$=13000m^{-1} D=2.5mm, d=0.5mm	0.0662	0.0675
18GHz b=0.5 , $\langle\zeta\rangle$=13000m^{-1} D=2.5mm, d=0.5mm	0.2219	0.2158

- The RMSE is calculated by the NNs predicted dipole and the GMRES derived dipole of different scenarios (1000 samples for each scenario)
- Both DDA-NN and Data-NN perform well on different scenarios

Table 2. CPU time record for solving deterministic and stochastic problems: GMRES vs. DDA-NN and Data-NN

Problem	Method	1 sample	100 samples	1000 samples	Training times
Deterministic	GMRES	0.036s	0.51s	4.95s	
	DDA-NN	9.87s	178.53s	not measured	
Stochastic	DDA-NN	0.00154 s	0.00205s	0.01278s	101091s
	Data-NN	0.00148 s	0.00223s	0.01319s	9895s

- DDA-NN and Data-NN exhibited around two orders of magnitudes efficiency improvement compared to GMRES in the inference stage (for stochastic problems) over 1000 random media samples

DDA-NN advantages

ZJUI

- Compared to traditional data driven NN, DDA-NN do **not require prepared data pairs** as model input and output

→ ✓ eliminates the need for extensive pre-computed datasets;

- **Generate random media** on demand, further enhancing its flexibility

→ ✓ reduces memory usage and self-check its prediction accuracy;

- **Loss function** is the function of frequency and random media structure

→ ✓ Generalization across a wide range of scattering scenarios.

Further improvements

✓ Combining DDA-NN and iterative algorithm

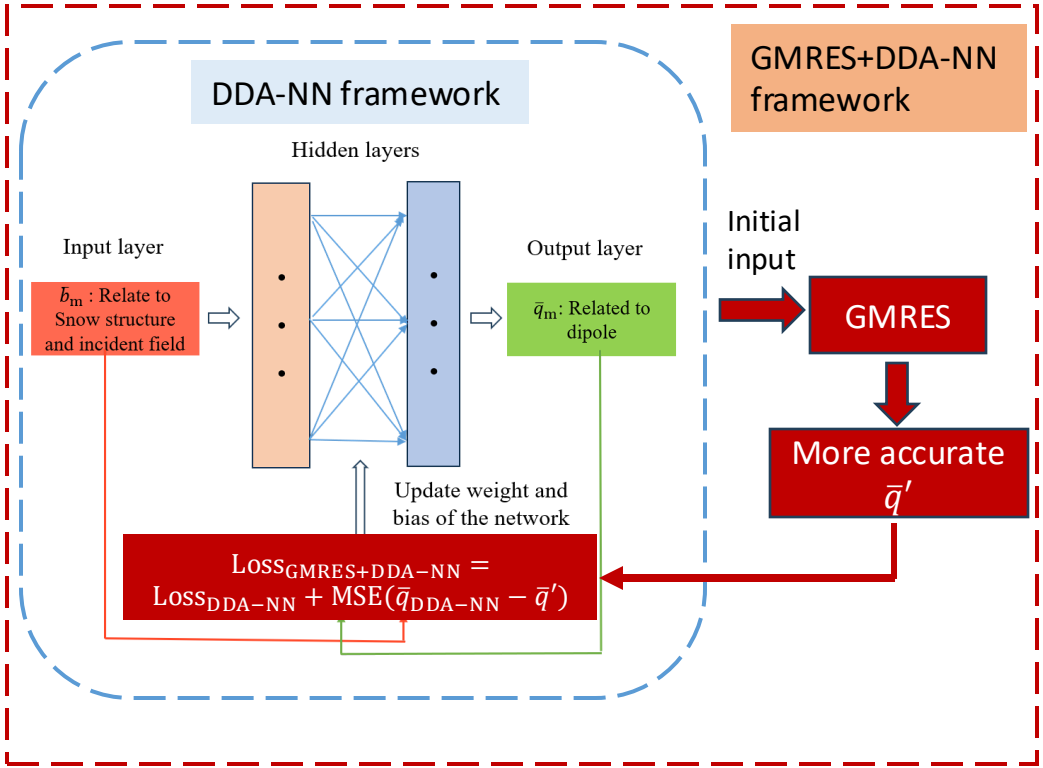

✓ Using advanced NN architectures, such convolutional neural networks (CNN) and complex-valued network:

- Handle larger data dimension
- Incorporate spatial features: trained on 2D images
- …

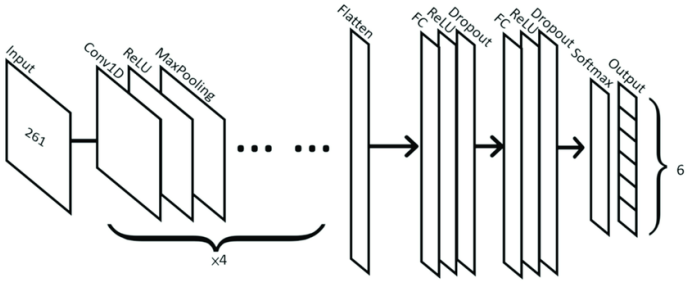

An example of CNN model

A Surrogate Neural Network for The Bicontinuous Media Model

ZJUI

Input

Snow microstate parameters (depth, density, grain size, snow temperature) & Numerical parameters in DDA

The Bicontinuous Media / DDA Model

Greens function calculation

Monte Carlo Simulation

- Radom media generation
- Solve DDA by GMRES
- Statistical average

Neural Network

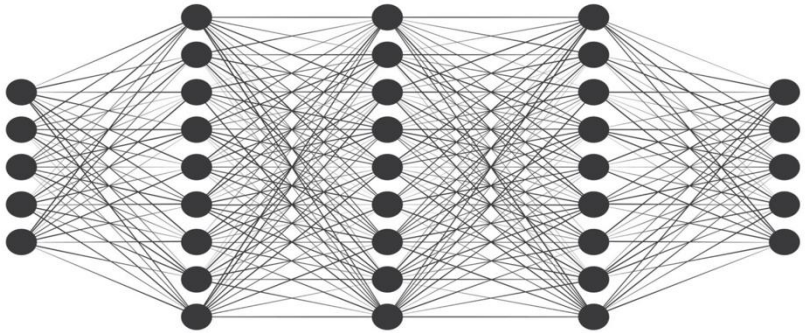

Output

Scattering coefficient & Absorption coefficient & Snow Permittivity & Phase Matrix

Key advantages:

- Requires less computing than building a fully sampled LUT
- High computational efficiency that interpolating a large LUT
- Low memory usage compared to storing a LUT

A ResMLP Neural Network for Improved Learning Performance

ZJUI

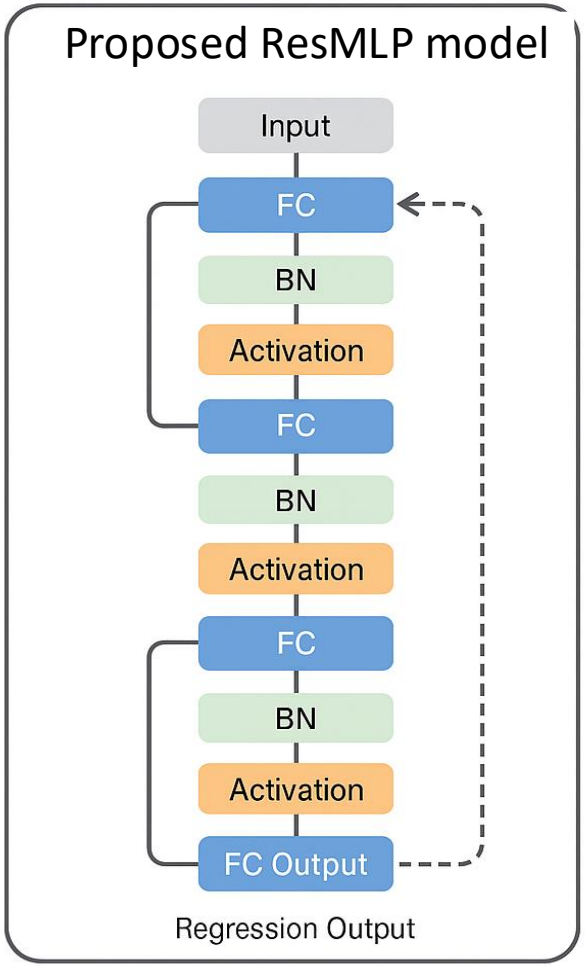

- Traditional **MLPs face gradient vanishing & performance bottlenecks** with high-dimensional outputs.
- **Residual blocks** (He et al., 2016) introduced to:
  - Improve gradient flow
  - Enhance feature learning
  - Boost accuracy and generalization

Preliminary κ_s results at C band

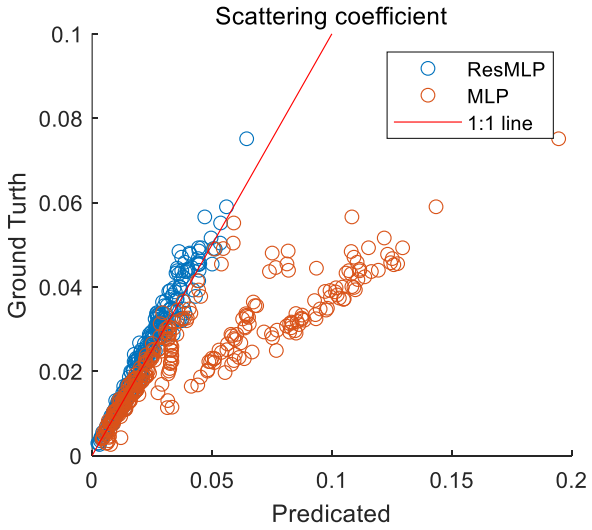

Reference: He, K., Zhang, X., Ren, S., & Sun, J. (2016). Deep residual learning for image recognition. In *Proceedings of the IEEE conference on computer vision and pattern recognition* (pp. 770-778).

A few attempts towards combing physical modeling and AI for intelligent microwave data interpretation

Combining The Representative Power of Physical Scattering Models and Artificial Intelligence for Multi-channel Observation Driven Multi-variable Retrieval

How could the versatility of forward modeling fully support retrieval algorithm?

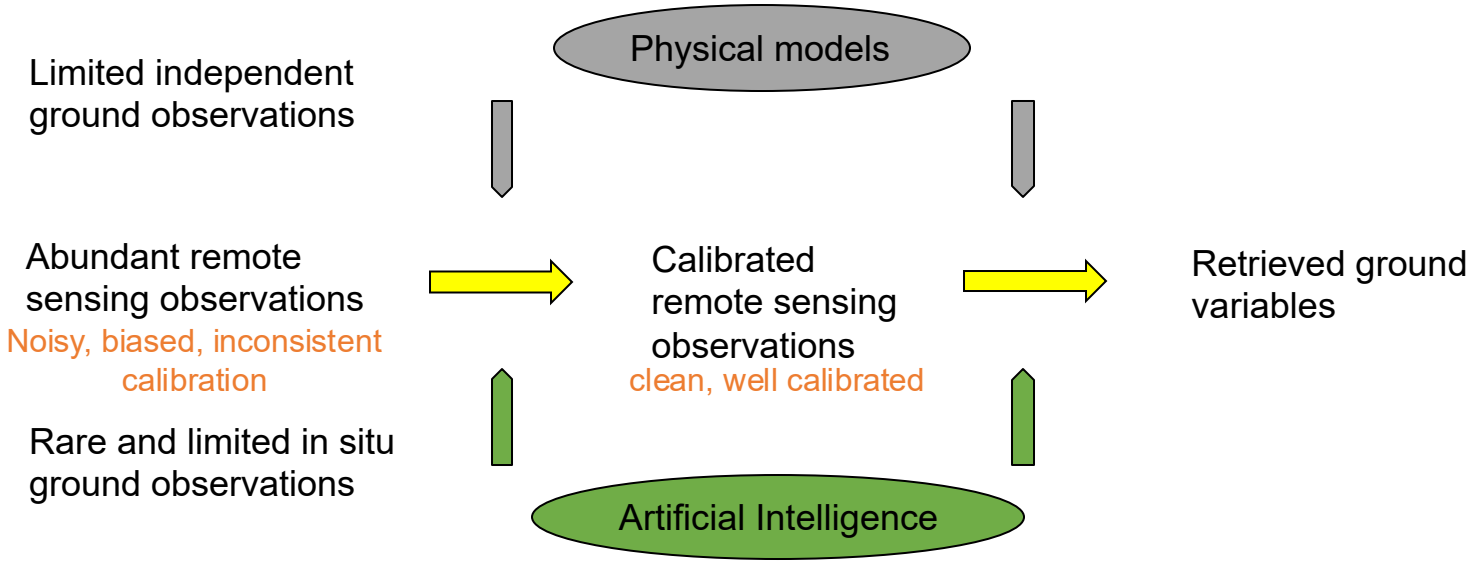

Forward physical models make it possible to:

- Analyze and make use of the inherent connections among multi-channel observations;
- Provide dataset and constraints on neural network training and effectively reduce the dimensionality of in situ observations;
- Support multi-channel observation driven multi-variable retrieval;

Physics embedded NN for inversion problem: Layered soil remote sensing

The layered-soil inversion problem

Physical Model

Multi-polarization, multi-angle, multi-frequency

Inversion algorithm

- Local optimization: local trapping
- Global optimization: slow
- Normal Neural network: Rely on experimental data, and hard to obtain consistent multi-channel observations.

Physics-Embedded Artificial Intelligence Framework (P-ANN) with Multichannel Passive Microwave Observations

X. Bai, S. Tan, "Layered Soil Remote Sensing with Multi-Channel Passive Microwave Observations Using A Physics Embedded Artificial Intelligence Framework: A Theoretical Study," IEEE TGRS, 2023

The PANN framework

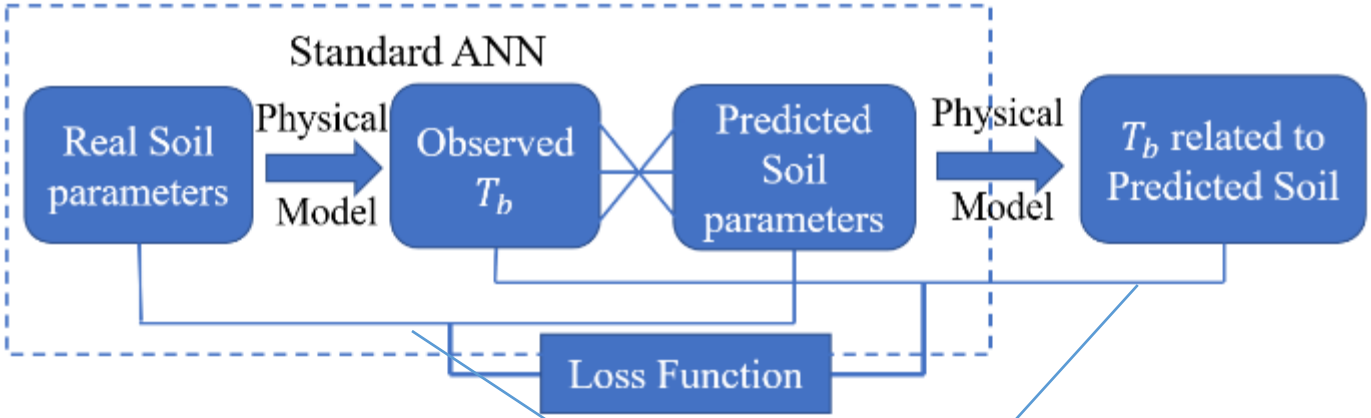

$$Loss_0 = \frac{1}{N_0}\sum_{i=1}^{N_0}\left(\left\|\overrightarrow{S_i^0} - \overrightarrow{\widetilde{S}_i^0}\right\|\right)$$

$$\text{Loss} = \text{Loss}_0 + \text{Loss}_p$$

$$Loss_p = \frac{1}{N_0}\sum_{i=1}^{N_0}\left(\left\|\overrightarrow{T_{bi}^0} - \overrightarrow{\widetilde{T}_{bi}^0}\right\|\right)$$

The PANN framework

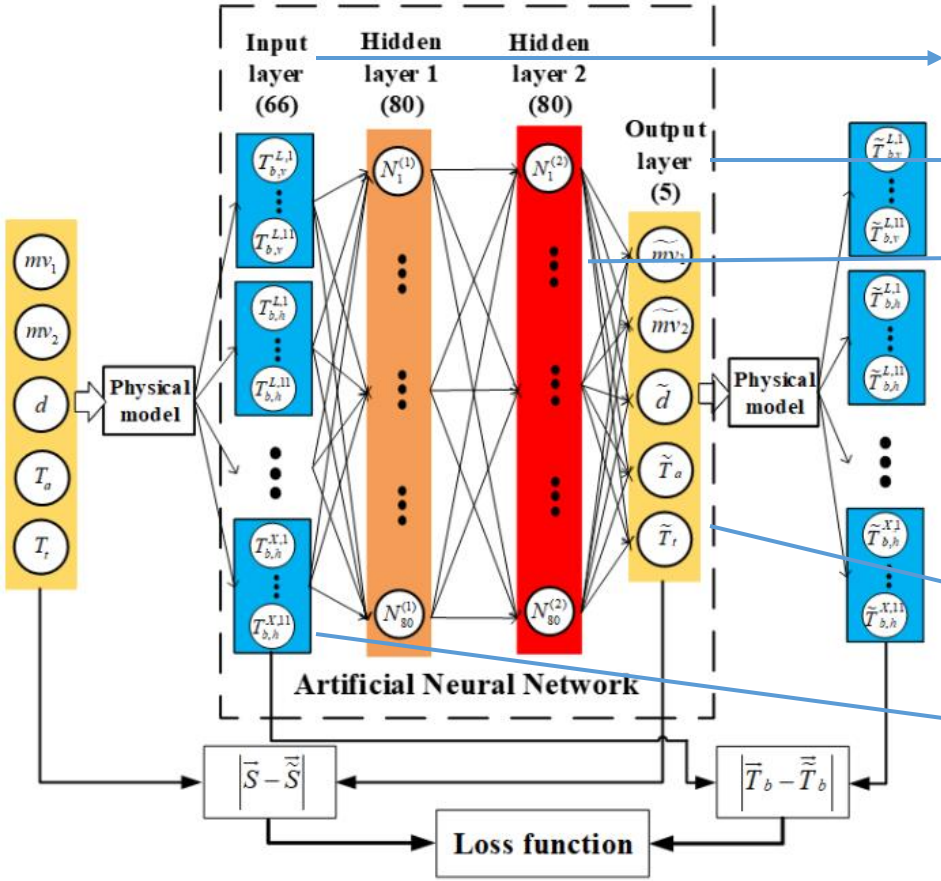

Input layer: Multi-channel Tb

Output: soil parameters

Hidden layer: 80 ×80

$$y = f(\sum_{i=1}^{n} \omega_i \cdot x_i + b)$$

Activation function: **relu**

Normalization when training:

$$T_b^0 = \frac{T_b - 200}{100} \qquad s^0 = \frac{s - s_{low}}{s_{up} - s_{low}}$$

The soil structure and scattering model

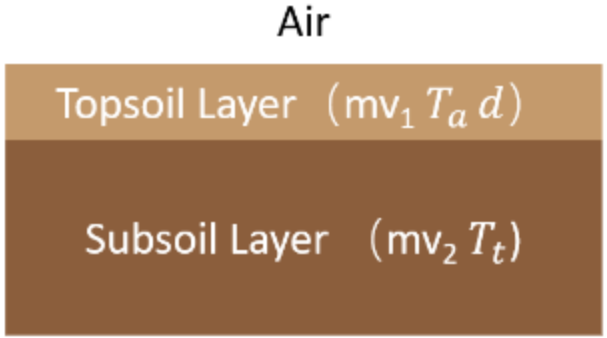

RANGE OF SOIL PARAMETERS

mv_1 /(m^3/m^3)	mv_2 /(m^3/m^3)	d/m	T_a/K	T_t/K
0.03-0.06	0.07-0.10	0.04-0.06	280-300	280-300

Coherent model

$$
\begin{aligned}
T_{bv}(\theta_0) = & \frac{k}{\cos\theta_0}\frac{\varepsilon_1'' T_1}{2\varepsilon_0}\frac{|k_{1z}|^2 + k_x^2}{|k_1|^2} \\
& \times \left\{ \frac{|C_1|^2}{k_{1z}''} e^{2k_{1z}'' d} - \frac{|D_1|^2}{k_{1z}''} e^{-2k_{1z}'' d} \right. \\
& \left. + \frac{|k_{1z}|^2 - k_x^2}{|k_{1z}|^2 + k_x^2} \cdot 2\mathrm{Re}\left(\frac{C_1 D_1^*}{ik_{1z}'} e^{-i2k_{1z}' d} \right) \right\} \\
& + \frac{k}{\cos\theta_0}\frac{\varepsilon_t'' T_t}{2\varepsilon_0}\frac{|k_{tz}|^2 + k_x^2}{k_{tz}''|k_t|^2} |T^{TM}|^2 e^{-2k_{tz}''}
\end{aligned}
$$

$$
\begin{aligned}
T_{bh}(\theta_0) = & \frac{k}{\cos\theta_0}\frac{\varepsilon_1'' T_1}{2\varepsilon_0} \times \left\{ \frac{A_1}{k_{1z}''} e^{2k_{1z}'' d} \right. \\
& - \frac{B_1}{k_{1z}''} e^{-2k_{1z}'' d} \\
& \left. + 2\mathrm{Re}\left(\frac{iA_1 B_1^*}{k_{1z}'} e^{-i2k_{1z}' d} \right) \right\} \\
& + \frac{k}{\cos\theta_0}\frac{\varepsilon_t'' T_t}{2\varepsilon_0}\frac{|T^{TE}|^2}{k_{tz}''} e^{-2k_{tz}'' d}.
\end{aligned}
$$

Training and testing results

Training data: **5000** groups of **soil parameters** with their **corresponding simulated Tb.**

Validation Data: **11 points are evenly** sampled for each parameter, and **all the possible combinations** are investigated (**N=11^5**). The validation set is evaluated every 200 iterations.

Testing Data:

21 points are evenly sampled for each parameter, and **all the possible combinations** are investigated (**N=21^5**) as the Testing Data.

Training process

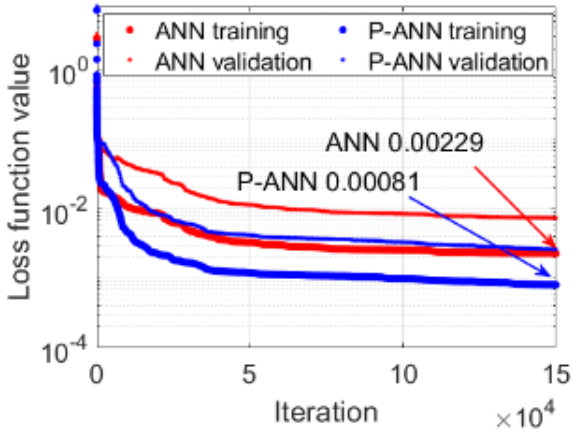

Training and testing results

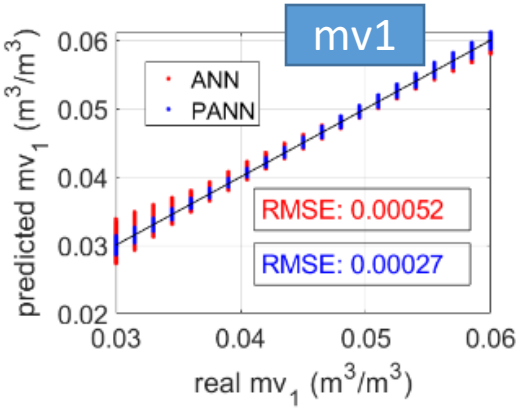

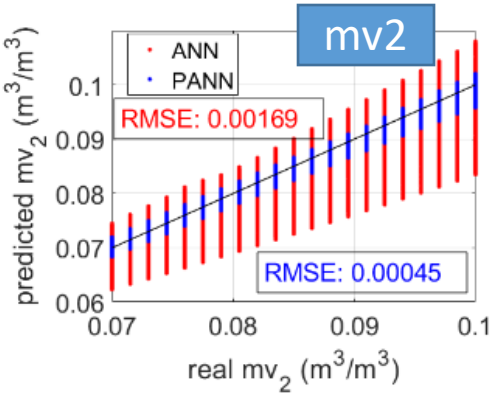

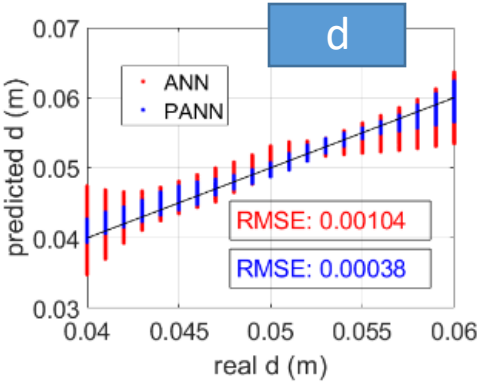

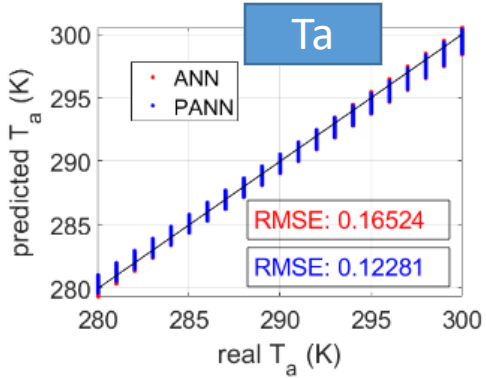

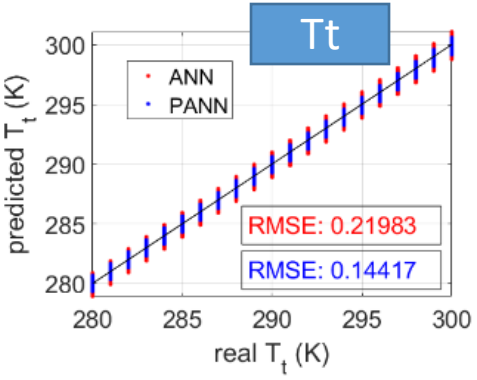

P-ANN exhibited superior inversion outcomes compared to ANN, particularly with regards to the retrieval of subsoil moisture and soil depth.

Testing for different soil ranges

Good results in small-range soil and relatively low soil moisture.

Ranges	mv_1 /(m^3/m^3)	mv_2 /(m^3/m^3)	d/m	T_a/K	T_l/K	RMSE
ran1	0.03-0.06	0.07-0.10	0.04-0.06	280-300	280-300	0.0112
ran2	0.13-0.16	0.17-0.20	0.04-0.06	280-300	280-300	0.0241
ran3	0.23-0.26	0.27-0.30	0.04-0.06	280-300	280-300	0.0254
ran4	0.33-0.36	0.37-0.40	0.04-0.06	280-300	280-300	0.0821
ran5	0.43-0.46	0.47-0.50	0.04-0.06	280-300	280-300	0.1003
ran6	0.02-0.06	0.06-0.10	0.03-0.06	280-300	280-300	0.0287
ran7	0.02-0.08	0.08-0.16	0.02-0.08	280-300	280-300	0.0851

A divide-and-conquer technique can be used to effectively combine the prediction from multiple small scale neural networks to consider a large-scale soil inversion.

The divide-and-conquer technique for large-scope soil

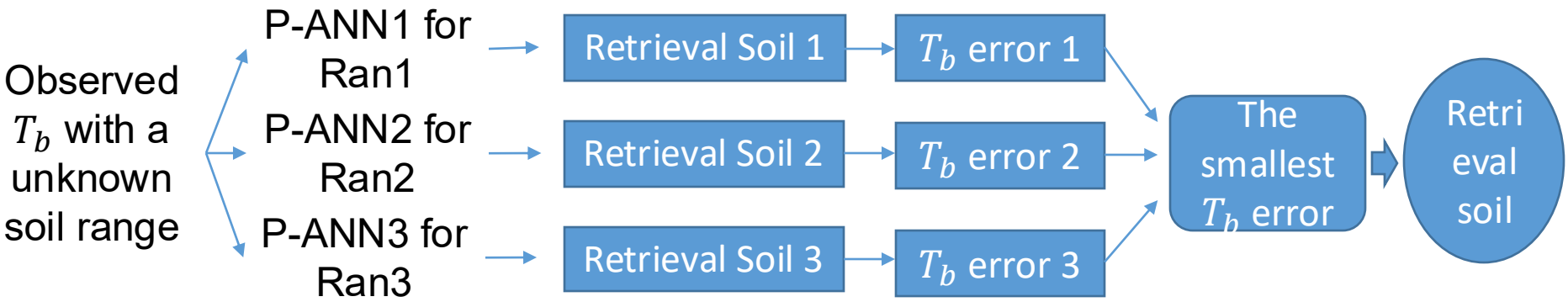

An inversion test for the example soil with P-ANN for different ranges.

	mv_1 /(m^3/m^3)	mv_2 /(m^3/m^3)	d/m	T_a/K	T_t/K	RMSE soil	RMSE T_b/K
Ground truth (in ran2)	0.150	0.180	0.050	290.00	290.00	-	-
Outcomes from P-ANN for different ranges							
ran1	0.123	0.134	0.055	292.32	286.42	0.598	2.287
ran2	0.167	0.186	0.052	288.25	287.27	0.220	1.139
ran3	0.263	0.271	0.054	305.998	305.02	1.702	3.273

Local optimization algorithm with initialization from P-ANN

Model structure

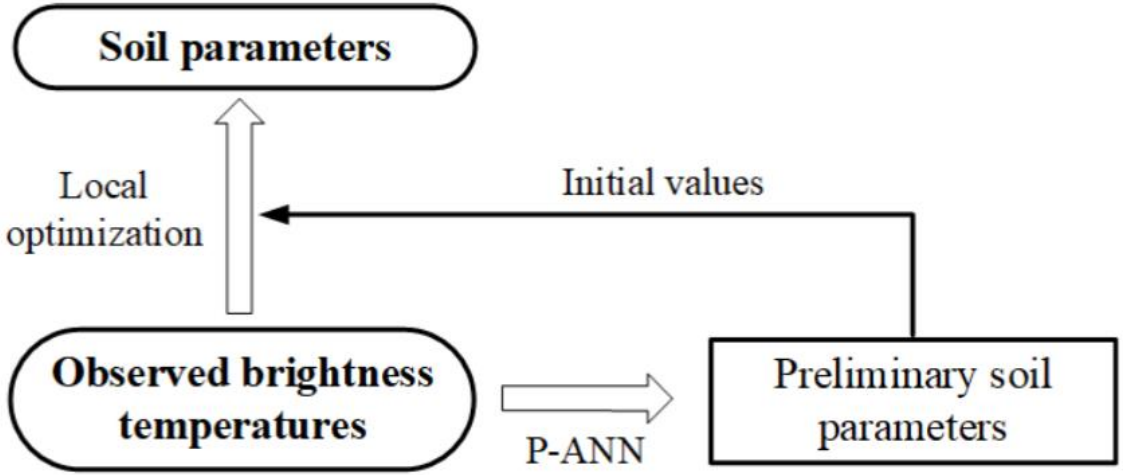

X. Bai, S. Tan, “Layered Soil Remote Sensing with Multi-Channel Passive Microwave Observations Using A Physics Embedded Artificial Intelligence Framework: A Theoretical Study,” IEEE TGRS, 2023

Local optimization algorithm with initialization from P-ANN

Testing results

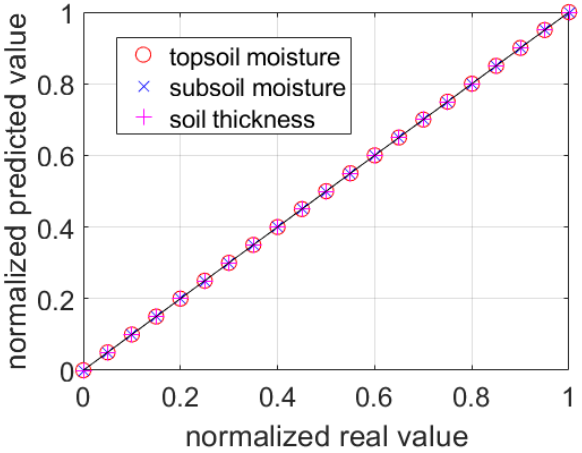

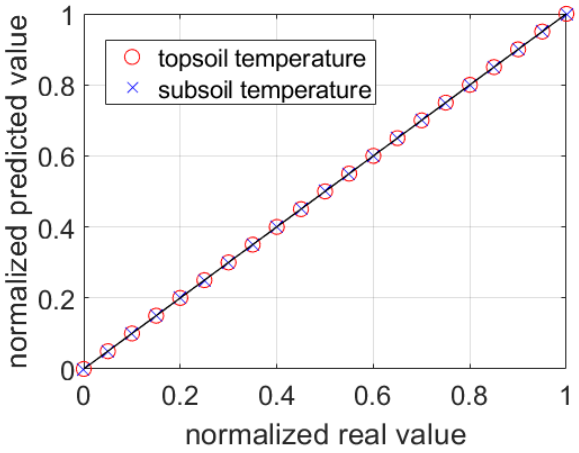

Average retrieval time & RMSE:

P-ANN: 0.0015s
RMSE: 0.0126

Local opt + P-ANN: 0.1020s
RMSE: 0.0000

The P-ANN driven localized optimization algorithm further enhances the inversion accuracy but introduces additional inversion time.

Reliability Analysis for P-ANN

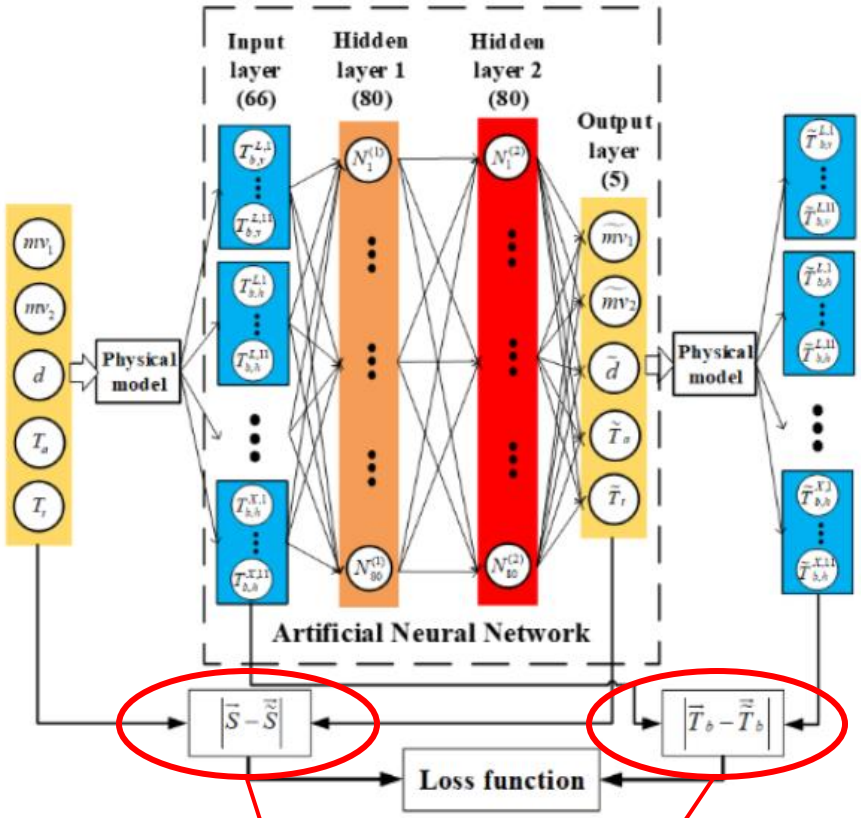

Retrieval process

Measured Tb

P-ANN

Retrieval soil parameters

Calculate corresponding Tb

Error of Soil parameters

$S_{pdf} = f(e_{T_b})$

Obtained relations of the soil error and Tb error for P-ANN

$$S_{pdf} = f(e_{T_b})$$

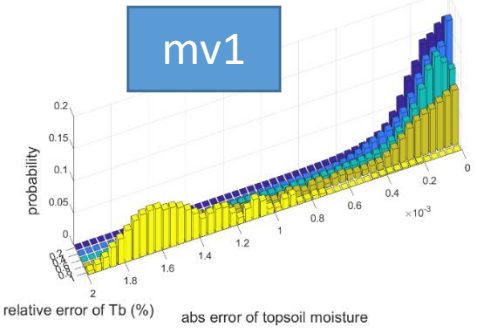

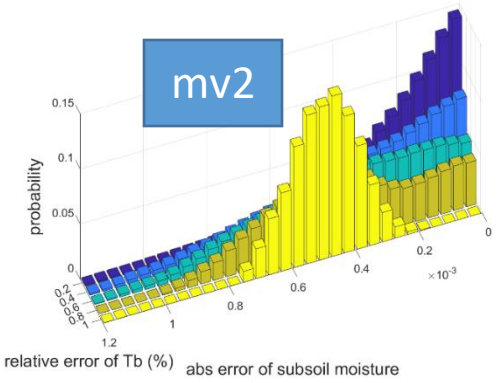

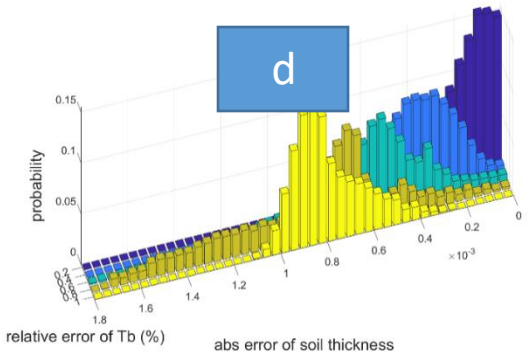

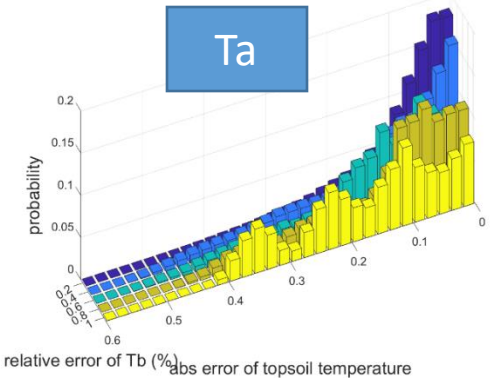

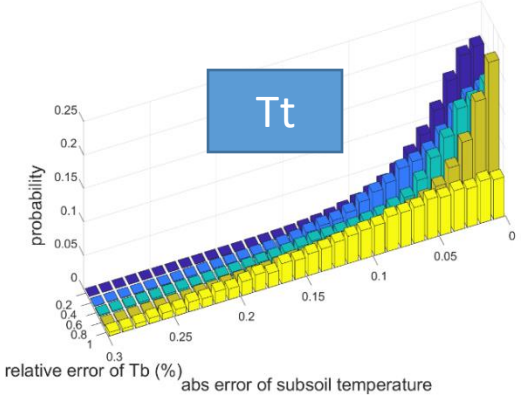

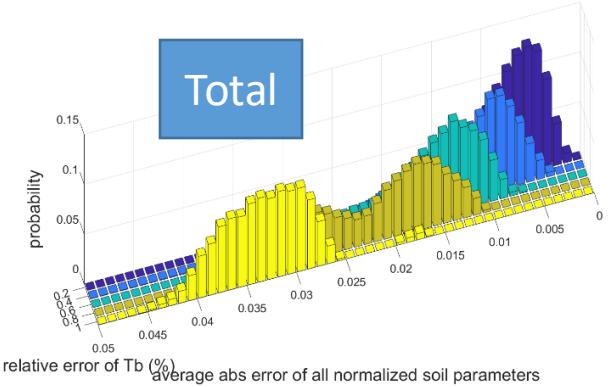

As the increases of Tb error, the distribution of soil error tends to align more closely with larger values.

The maximum error with 95% confidence

Estimated Maximum Error of each soil parameters with 95% confidence level under different Tb error ranges

Error of T_b	mv_1 $/10^{-3}$ (m^3/m^3)	mv_2 $/10^{-3}$ (m^3/m^3)	d $/10^{-3}$ m	T_a/K	T_t/K	Average
0-0.1%	0.447	0.662	0.299	0.147	0.164	0.010
0.1-0.2%	0.509	0.828	0.656	0.238	0.305	0.014
0.2-0.3%	0.562	1.006	1.157	0.356	0.421	0.020
0.3-0.4%	0.675	1.141	1.398	0.423	0.423	0.025
0.4-0.5%	0.708	1.335	1.466	0.458	0.348	0.028
0.5-0.6%	0.751	2.173	1.480	0.445	0.373	0.035

Robustness to noisy observations

Add noise to the testing Tb

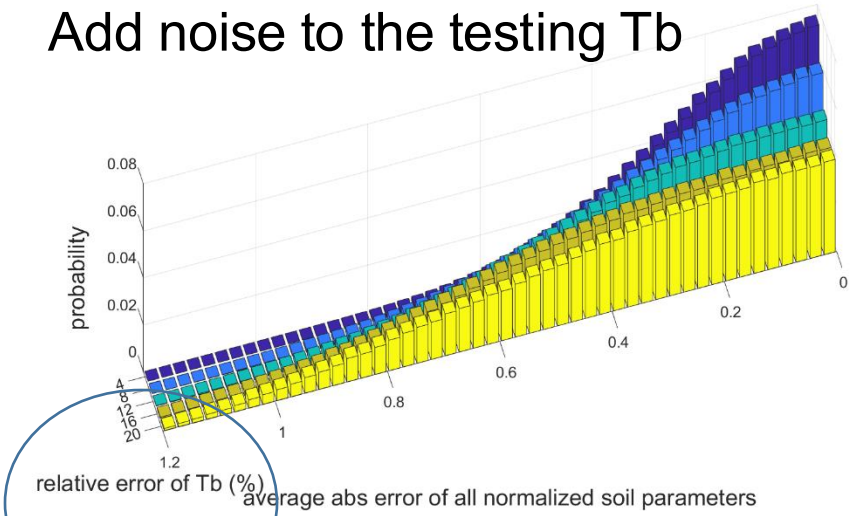

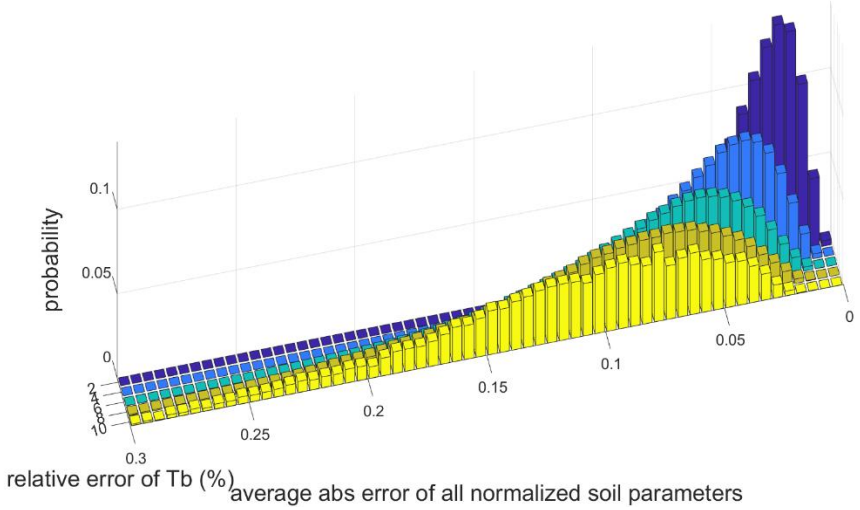

P-ANN

Local optimization algorithm with P-ANN

Too large

The proposed local optimization algorithm with P-ANN has a certain level of anti-noise capability.

Summary of the Physics Driven Retrieval Net

- Physical model driven retrieval net with improved training efficiency, retrieval performance, and reliability analysis
- Performance gain and improved anti-noise capability when cascading the retrieval net with a local optimization algorithm
- Potential to develop an adaptive calibration net to deal with noisy and uncalibrated microwave observation data making use of limited in situ ground observations and the sparsity embedded in high dimension observation data

X. Bai, S. Tan, “Layered Soil Remote Sensing with Multichannel Passive Microwave Observations Using A Physics-Embedded Artificial Intelligence Framework: A Theoretical Study,” IEEE TGRS, 2023

LLM heuristic logic and domain-specific-knowledge driven human out-of-loop intelligent microwave data analysis

Why LLMs for Microwave data analysis?

• Automates setup and analysis • Suggests parameters • Natural language interaction

Chatbot

Please calibrate/ parameterize the DMRT-QMS model so that the absolute error of TB is less than 5 K.

Snow.txt

Reasoning from the document…
The client wants to choose reasonable parameters of DMRT-QMS for the given snowpack. Continue choose parameters until absolute error of modeled TB is less 5 K.

COZE

Model Bank

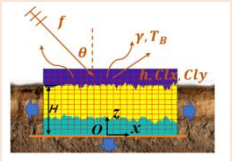

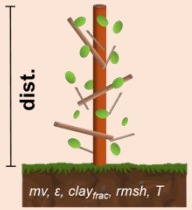

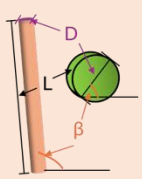

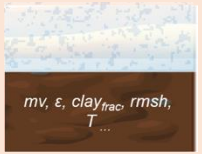

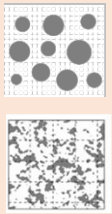

Tasks

- Interpret inputs
- Choose the tool to fulfil the request
- Verify the results that it meets physical constraints and clients' needs
- Return outputs to the clients

Tools

- Physical models and rules
- Optimization algorithms
- Generative guesses

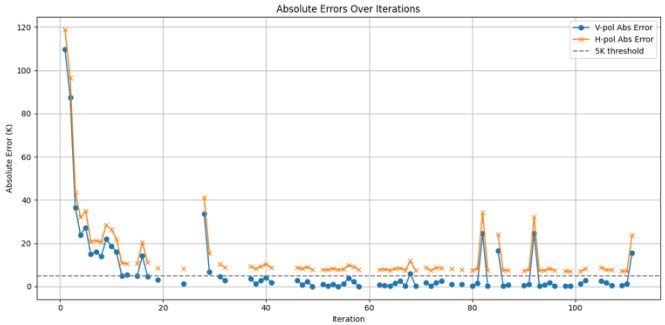

Trends in Remote Sensing Research

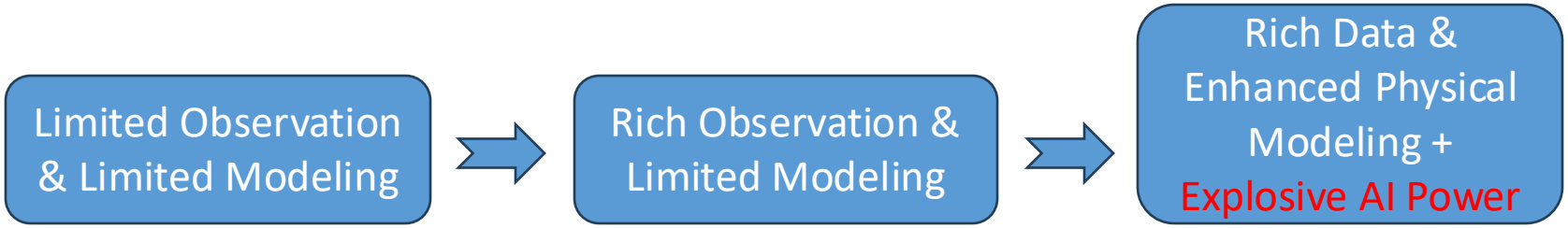

- Empirical model and simple physics driven retrieval algorithm dominate.
- Observable parameters are quite limited.

- Data driven retrieval algorithms gain attention.
- Observable parameters are still limited due to sparsity of ground truth observations.

- AI, data and physical models join forces for improved performance and efficiency in retrieval.
- Retrievable parameters are significantly enriched.
- Multi-channel observations are seamlessly fused together.

Forward modeling and AI acceleration for microwave interactions with various scenarios

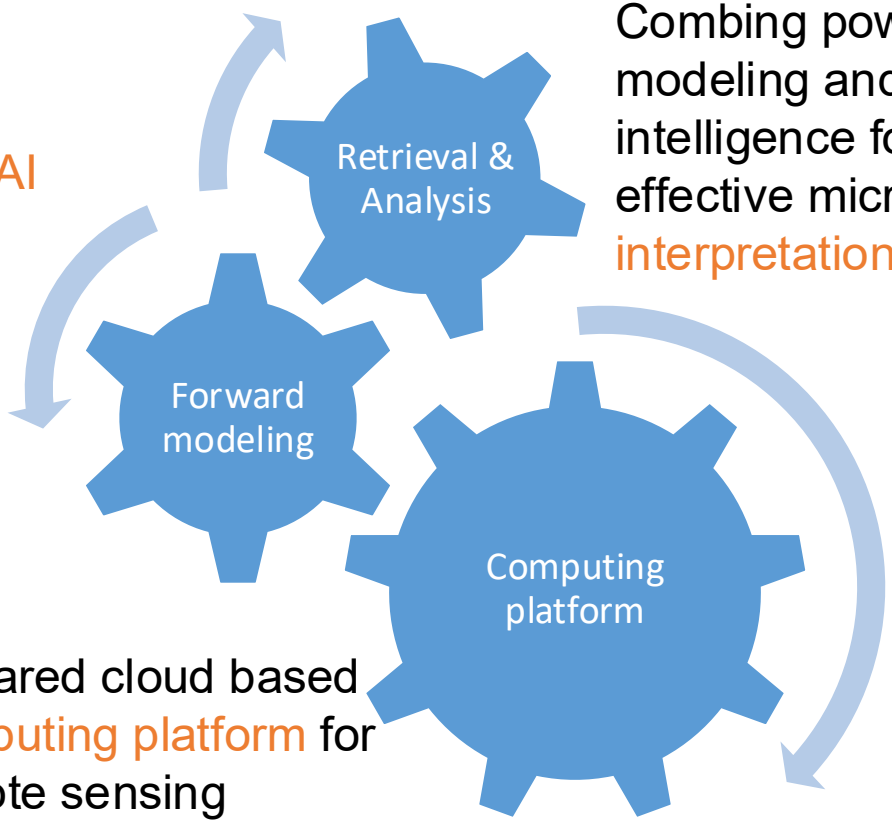

Combing power from physical modeling and artificial intelligence for efficient and effective microwave data interpretation

A shared cloud based computing platform for remote sensing community

Remote Sensing Hub (RSHub): A Shared Computing Platform for Remote Sensing Community

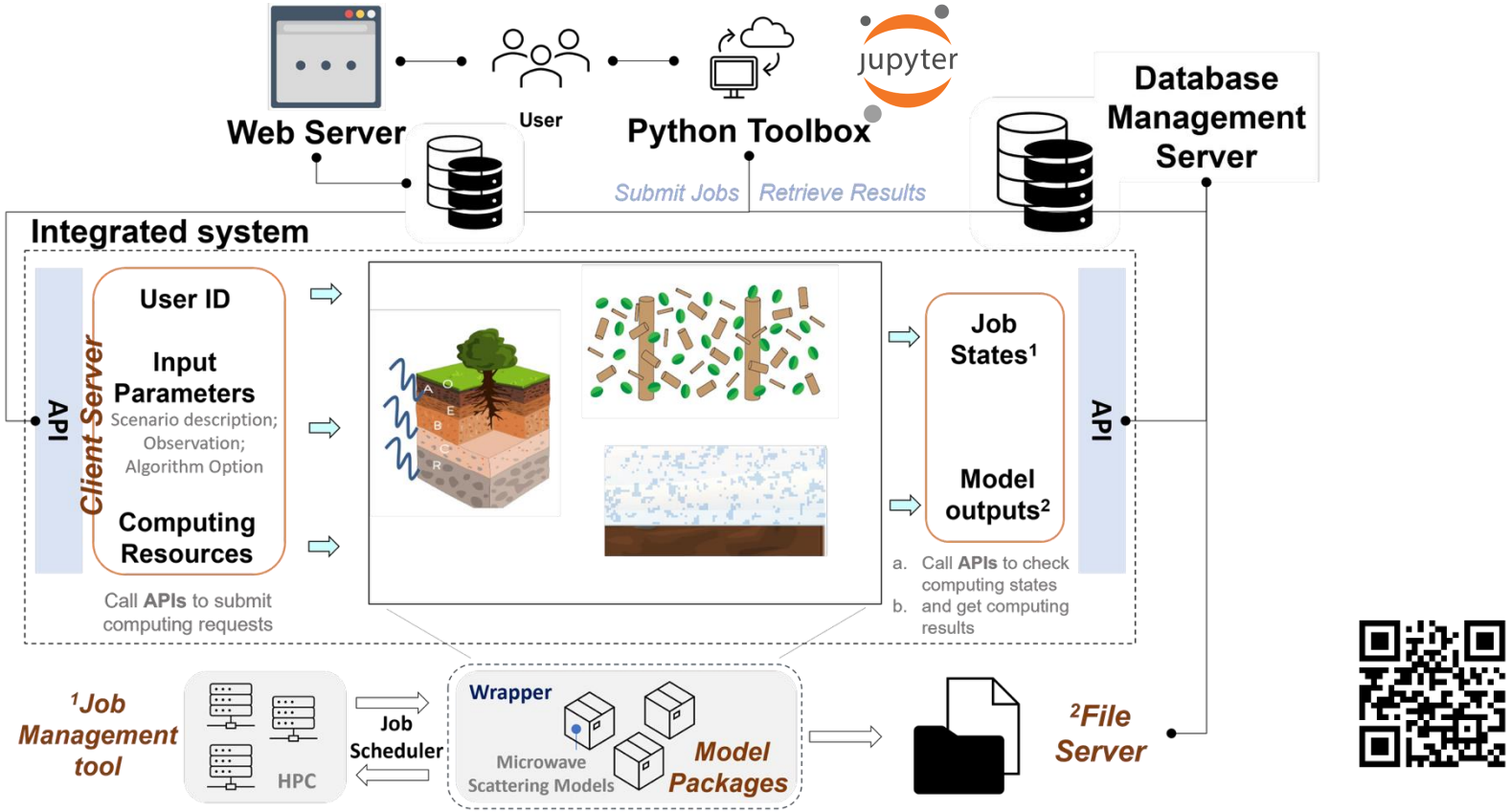

Fang, … & Tan, 2025. RSHub: A Remote Sensing Hub for geophysical microwave scattering modeling. Accepted by *Geoscience and Remote Sensing Magazine*.

Rationale for Such Shared Computing Platform

Advanced scattering models and retrieval algorithms are rarely available to researchers and practioners in remote sensing.

Lack of expertise to optimize parameters and to tune the code

I don't know how to use the code.

Difficult to configure a working computing environment

I cannot run the code.

Difficult to reimplement a published work

I have no code.

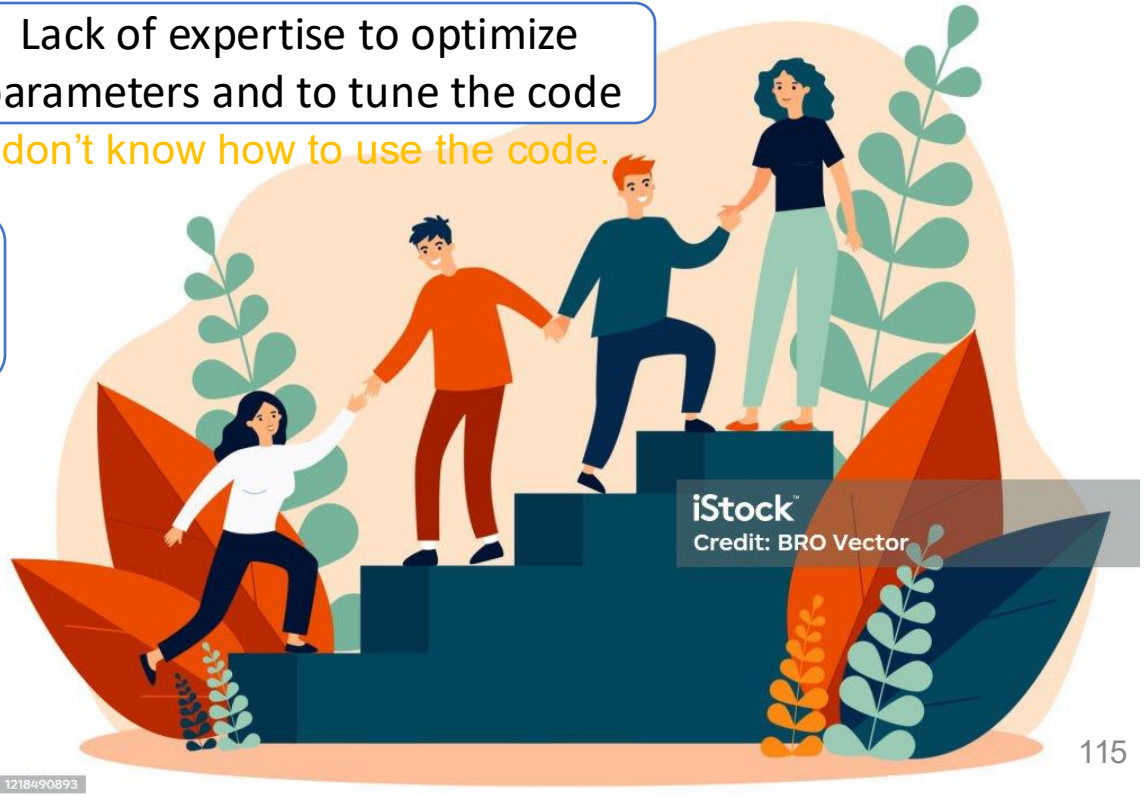

Key Features and Supporting Scenarios

Soil

- NMM3D-VIE-DDA
- NMM3D-SIE
- AIEM
- …

Snow

- DMRT-QMS
- DMRT-BIC
- DMRT-TRI
- …

Vegetation

- VRT
- …

- A python based coding interface through jupyter notebook
- Enriched profiling capability and multi-functionality to facilitate interpretation of results
- Unified user interface supporting multi-purpose simulation on scalable Cloud
- Continued model development and update

A demo to compute brightness temperature using the RSHub

0. Register on RSHub to get a token

1. Define types of scenarios

2. Define observation configurations
   - Observation Angle
   - Frequency
   - Active or Passive Sensor

3. Choose your algorithms

4. Describe your scenario

5. Submit a job

```
result1=submit_jobs.run(data)
```

6. Retrieve and analyze results

Radiometer

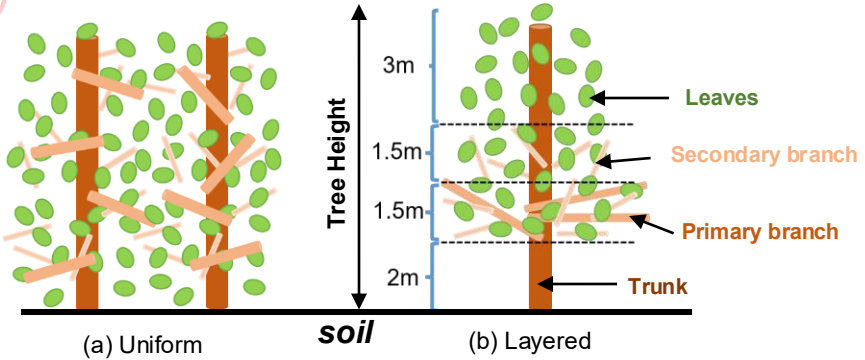

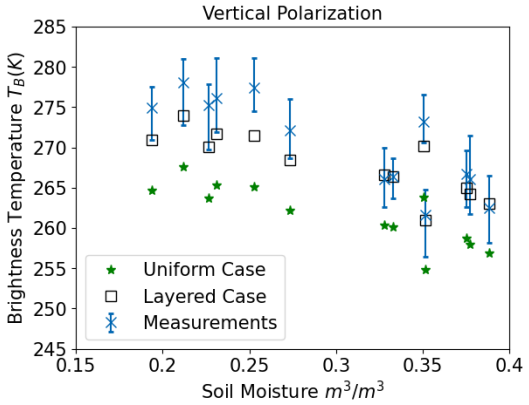

Features and Continued Development of RSHub

High-fidelity physics-based models: RSHub is mostly consisted of full-wave based microwave models and radiative transfer models that could resemble physical experiments
Towards an intelligent computing system: LLM-assisted tools are being added to streamline the process of parameters optimization, model running, and results analysis.

Features

In Development

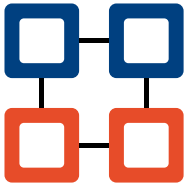

Modulization
- Output useful variables at intermedia step
- Enable flexible combination of algorithms for each scenario

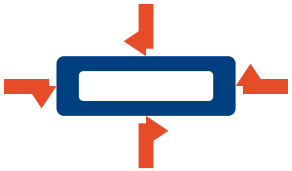

Expansion
- Embed additional scenarios including ice scenario
- Add new models to each scenario

ML-powered model
- Upgrade traditional look up tables by machine learning models

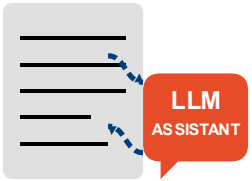

LLM-assisted tool
- Enable LLM-based Chatbot to generate script, run, and analyze results


Thank you & Welcome

ZJU-UIUC INSTITUTE

Zhejiang University/University of Illinois at Urbana-Champaign Institute